Lawrence Berkeley National Laboratory

Recent Work

Title

RECOIL RANGE STUDIES OF HEAVY PRODUCTS OF MULTINUCLEON TRANSFER FROM l8O TO 245 Cm AND 249Cf

Permalink

https://escholarship.org/uc/item/80f03261

Authors

McFarland, R.M.
Ghiorso, A.
Seaborg, G.T.

Publication Date

1983-02-01

eScholarship.org Powered by the California Digital Library
University of California

LBL-15529
Preprint

Lawrence Berkeley Laboratory
UNIVERSITY OF CALIFORNIA

RECEIVED
BERKELEY LABORATORY
MAR 21 1983
LIBRARY AND
DOCUMENTS SECTION

Submitted to Physical Review C

RECOIL RANGE STUDIES OF HEAVY PRODUCTS OF MULTINUCLEON TRANSFER FROM ^{18}O TO ^{245}Cm AND ^{249}Cf

Rose Marie McFarland, Albert Ghiorso,
and Glenn T. Seaborg

February 1983

TWO-WEEK LOAN COPY

This is a Library Circulating Copy which may be borrowed for two weeks. For a personal retention copy, call Tech. Info. Division, Ext. 6782.

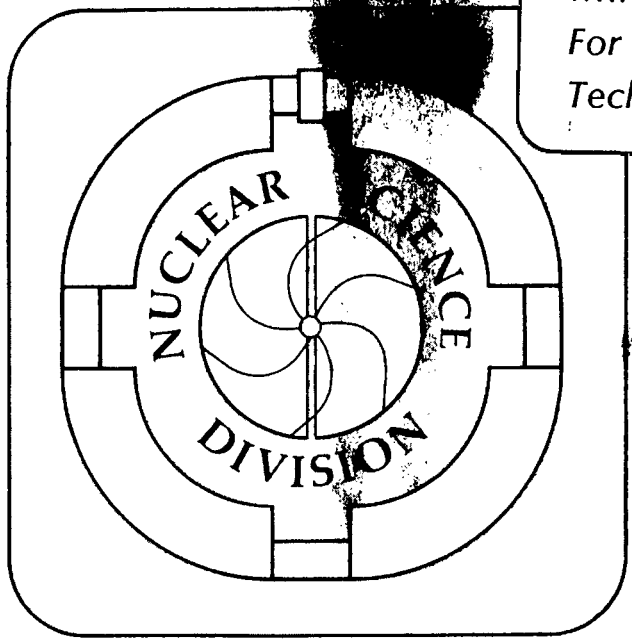

Prepared for the U.S. Department of Energy under Contract DE-AC03-76SF00098

LBL-15529 c2

DISCLAIMER

This document was prepared as an account of work sponsored by the United States Government. While this document is believed to contain correct information, neither the United States Government nor any agency thereof, nor the Regents of the University of California, nor any of their employees, makes any warranty, express or implied, or assumes any legal responsibility for the accuracy, completeness, or usefulness of any information, apparatus, product, or process disclosed, or represents that its use would not infringe privately owned rights. Reference herein to any specific commercial product, process, or service by its trade name, trademark, manufacturer, or otherwise, does not necessarily constitute or imply its endorsement, recommendation, or favoring by the United States Government or any agency thereof, or the Regents of the University of California. The views and opinions of authors expressed herein do not necessarily state or reflect those of the United States Government or any agency thereof or the Regents of the University of California.

LBL-15529

Recoil Range Studies of Heavy Products of Multinucleon Transfer from ^{18}O to ^{245}Cm and ^{249}Cf

by

Rose Marie McFarland, Albert Ghiorso and Glenn T. Seaborg

Nuclear Science Division
Lawrence Berkeley Laboratory
University of California
Berkeley, CA 94720

This work was supported by the Director, Office of Energy Research, Division of Nuclear Physics of the Office of High Energy and Nuclear Physics of the U.S. Department of Energy under Contract DE-AC03-76SF00098.

Recoil Range Studies of Heavy Products of Multinucleon Transfer from ^{18}O to ^{245}Cm and ^{249}Cf

by

Rose Marie McFarland, Albert Ghiorso and Glenn T. Seaborg

ABSTRACT

Recoil range distributions were measured for alpha and spontaneous fission activities made in the bombardment of ^{245}Cm and ^{249}Cf with ^{18}O from 6.20 MeV/nucleon down to the interaction barrier. The shape of the distributions indicates that transfers of up to four protons take place via a combination of quasi-elastic (QET) and deep inelastic (DIT) mechanisms, rather than complete fusion-de-excitation (CF) or massive transfer (MT). Angular distributions constructed from recoil range distributions, assuming QET/DIT, indicate that the QET component contributes more significantly to the heavy product residue cross section than the DIT, even though primary cross sections are expected to be higher for DIT than for QET. This may be explained qualitatively as a result of the high excitation energies associated with DIT; the very negative Q_{gg} of projectile stripping for these systems combined with the lower expected optimal Q_{rxn} of QET compared to DIT can give QET products comparatively low excitation.

INTRODUCTION

Multinucleon transfer from light heavy ions (LHI) ($4 < A \leq 40$) to actinide targets is a useful mechanism for making actinides of Z and A between those of the target and compound nucleus. Transfers are possible which carry less excitation than the equivalent fusion reaction, limiting the number of particles evaporated and the chance of fission during de-excitation of target-like fragments. If, in addition to producing little excitation, a transfer is neutron-rich, actinide residues may be accessible which would not be made in complete fusion.

Extensive measurements of angular distributions, energy spectra, and isotopic distributions of projectile-like products of LHI and heavy targets, including actinides, have shown that two separate mechanisms contribute to multinucleon transfer.[1-9] Quasi-elastic transfer (QET) is characterized by an angular distribution peaked at a side-angle, near the classical Rutherford grazing angle θ_{gr}, and an optimal exit channel kinetic energy E^{f}_{opt} determined by entrance-to-exit channel trajectory matching conditions. In reactions with high projectile-target asymmetry and bombardment energy E^{i}_{lab} not too far above the interaction barrier, in which the bulk of the close collisions lead to fusion, deep inelastic transfer (DIT) occurs via a long-lived dinuclear complex.[10-12] The angular distribution peaks at or near 0° and decreases exponentially. In some cases a $1/\sin\theta$ component is present. The separation energy is equal

to the exit channel coulomb repulsion energy E_C^f. A third mechanism, massive transfer (MT), has been recently described.[13-18] It is thought to take place in two steps.[15] The projectile first breaks up in the field of the target. Subsequently, one of the fragments may fuse with the target while the other continues at its original velocity. Ref. 16 is a review of MT models and experimental investigations.

Off-line radioanalytic measurements of the target-like products of LHI + actinide transfer reactions have been done; for example Hahn, et. al.,[19] have compared recoil range and angular distributions of Cf from $^{238}U(^{12}C,xn)^{244,245}Cf$ and $^{239}Pu(^{12}C,\alpha xn)^{244,245}Cf$. A comprehensive series of bombardments is in progress for which radiochemical separation techniques are used in measuring excitation functions of actinide products of LHI + actinide reactions.[20,21] It is hoped that some information on product excitation can be gleaned and that a systematic way of estimating cross sections for unknown nuclides will emerge from these data.

The purpose of this study is to use recoil range distributions of target-like products of multinucleon transfer from ^{18}O to ^{245}Cm and ^{249}Cf to deduce information on the subclass of transfer reactions that lead to actinide nuclides.

EXPERIMENTAL

All bombardments were done with $^{18}O^{+4}$ accelerated at the 88-inch cyclotron at Lawrence Berkeley Laboratory. Beam current

was between 1 and 3 μAe. Targets were supplied by Ron Lougheed and E. K. Hulet of Lawrence Livermore National Laboratory. They were made by vacuum deposition of a 6 mm diameter disk of the actinide trifluoride on a 2.5 mg/cm^2 Be foil. The CmF_3 target contained 0.240 mg $^{245}Cm/cm^2$ and the CfF_3 target contained 0.520 mg $^{249}Cf/cm^2$.

During a bombardment, the target was mounted facing downstream in a water-cooled copper block which also held a 1.8 mg/cm^2 Havar "beam window" foil upstream of the target backing. Nitrogen cooling gas flowed at 50 standard ft^3/min between the window and target. In some bombardments a 1.92 mg/cm^2 Havar foil and/or a 2.3 mg/cm^2 Be foil were mounted immediately upstream of the beam window to serve as beam energy degraders.

Recoiling heavy products were stopped in a stack of ten 2.54 cm diameter 0.1 mg/cm^2 thick aluminum catcher foils mounted coaxially with and 0.3 cm downstream from the target face in a chamber through which He cooling gas flowed at a pressure of 4 torr. The foils were mounted on brass rings which were indented so that the foils were held apart, allowing the He to flow across every surface. After bombardment the foils were sprayed on one side to give added strength so that they could be handled more readily during sample changes. The stack varied in length from 1.7 to 1.8 cm. Figure 1 is a sketch of the target holder and recoil chamber configuration.

Four bombardments of ^{249}Cf were done, at 111.6, 99.8, 89.2, and 83 MeV (lab), and three bombardments of ^{245}Cm were done, at 111.6, 99.6 and 93 MeV (lab). Beam energies were calculated at the center of the target using the Northcliffe and Schilling electronic stopping power tables.[22] The Ni table was used for Havar, the thickness of the N_2 layer was taken to be 0.3 mg/cm^2, and the stopping powers of Cm and Cf were estimated by linear extrapolation by Z from the tables for Au and U.

Following bombardment the catcher stack was disassembled and each foil was placed over one of ten 1.2 cm diameter Ortec Si(Au) surface barrier detectors. The amplified alpha and fission event signals were sent through a pulse-height analyzer to a PDP-15 computer which tagged each event by energy, time, and detector and wrote the information to magnetic tape for future analysis. Spectra were collected continuously for one to two weeks, and periodically afterwards for up to six months after the end of bombardment. Spectra were collected for each individual foil, and a total stack spectrum was constructed by the computer by summing the individual foil spectra.

DATA COLLECTION AND ANALYSIS

The decay curve of SF events and of each observed peak in each total stack alpha spectrum were fit via an error-weighted least-squares analysis using the code FUTILE.[23] SF activities were identified by half-life and alpha activities were identified by E_α and half-life. A_o's were found by refitting decay curves with the half-lives of identified components held fixed at the values given in the Table of Isotopes[24] (See Table I).

The A_o's for the individual foil spectra were found by fitting their decay curves using the half-lives of activities identified in the total stack spectra. The recoil range distribution for each nuclide was calculated from the cross-sections in all the foils, obtained from these A_o's and corrected for feeding during bombardment from any parents observed. Figures 2 - 19 show observed recoil range distributions.

Tables II and III list total cross sections measured for ^{249}Cf and ^{245}Cm bombardments, respectively.

All error bars are standard deviations and include statistical uncertainties from decay rates and the least-squares decay curve analyses and the uncertainty in detector efficiency.

Cross sections presented here for ^{249}Cf bombardments should be compared with those reported in the radiochemical analyses of Ref. 21 which were designed especially for cross section measurements. In most cases agreement between the two measurements is acceptable; where extreme discrepancy appears, as for ^{253}Es, the Ref. 21 value should be accepted as the more accurate, and the recoil range distribution rejected.

RESULTS AND DISCUSSION

Recoil Range Distributions

Axial recoil range is a function of both exit channel separation energy and angle:

$$v_{T'}\cos\phi_{T'} = V_{T'}\cos\theta_{T'} + v_{cm} \qquad (1)$$

where $v_{T'}$ and $\phi_{T'}$ are the lab velocity and recoil angle of the target-like fragment, $V_{T'}$ and $\theta_{T'}$ are the center-of-mass velocity and angle, and v_{cm} is the velocity of the center of mass. The expression on the left side of the equation is a direct measure of the recoil range.

The shape of a recoil range distribution of a nuclide is determined by the mechanism by which it is formed. The lab angle and kinetic energy of recoil of a compound nucleus are

restricted to 0° and E^{i}_{lab} $(A_P)/(A_P + A_T)$, where A_P and A_T are the masses of the projectile and target, respectively. Therefore, the peak range corresponds to the allowed value and the distribution is narrow. A massive transfer product distribution would also be expected to show a compound nucleus-like shape with a peak located at the range appropriate for the fusion of the fraction of the projectile with the target.

A wide range of V_T, and Θ_T, are allowed for QET and DIT. The recoil range distributions of heavy products peak at a projected range corresponding to the maximum in the angular distribution and the most probable separation energy, Θ_{gr} and E^{f}_{opt} for QET, or 0° (c.m.s.) and E^{f}_{C} for DIT. The activity drops off quite gradually at higher and lower ranges. The recoil range peak for QET moves rapidly to lower ranges with increasing bombardment energy near the coulomb barrier reflecting a rapid decrease in Θ_{gr}.

The distributions presented in this study show features that can be related to the QET/DIT mechanism. There is usually one peak which moves to shorter ranges with increasing bombardment energy, the projection of the QET component. A DIT component would be seen as a very short range peak, relatively insensitive to bombardment energy. The heavy fragment peaks at 180° (c.m.s.), relative to the beam axis. This subtraction of the separation velocity from the velocity of the center of mass results in a very low lab velocity, which could be negative at lower v_{cm}. Therefore, the peak of a DIT component might be trapped in the target and not seen in inspection of a recoil range distribution.

These distributions fall off gradually on both sides of the peak, reflecting the broad energy and angular distributions characteristic of both mechanisms.

A study of Ref. 19 shows the correlation of angular distribution, and mechanism, with recoil range distribution shape. The lower energy ^{239}Pu bombardments show angular distributions of the transfer products $^{244,245}Cf$ that agree with measurements of projectile-like products. The side angle corresponds to θ_{gr}, assuming separation energy equal to E^{f}_{opt}, and there is a second maximum near 0° (c.m.s.). The corresponding recoil range distribution shapes are very broad and the peak decreases in range with increasing bombardment energy. These distributions are quite distinct from those from compound nucleus and from the higher energy transfer reactions. The angular distributions for the latter also change, losing the side peak. These are probably due to massive transfer. The recoil range distribution is sharp and insensitive to initial kinetic energy and peaks at a position appropriate for ^{8}Be fusing with ^{239}Pu at the beam velocity.

Angular Distributions

Axial range alone is not sufficient to determine separation energy and angle of a binary reaction. The following assumptions were used with the code RECOILS to construct angular distributions from recoil range distributions:

1) Only QET and DIT contribute to the reaction, and therefore
   a) The angular distribution $P(\theta)$ is a linear combination of a gaussian centered at some side angle θ_{max} with

some width σ plus a component peaked at 0^{o} that decreases exponentially with increasing angle with some half-angle $\theta_{\frac{1}{2}}$:

$$P(\theta) = PE \times \theta/\theta_{\frac{1}{2}} + PG \times (\theta - \theta_{max})^2/(2\sigma^2) \qquad (2)$$

$$= PREX + PRGAUS$$

PE and PG are constants.

b) the energy of separation, E^f_{sepn}, at each angle is a weighted average of E^f_C and E^f_{opt}:

$$E^f_{sepn} = PREX\ (E^f_C) + PRGAUS\ (E^f_{opt}) \qquad (3)$$

where

$$E^f_C = \frac{Z_P, Z_T, e^2}{R},$$

$$E^f_{opt} = E^i_{cms} \frac{Z_P . Z_T,}{Z_P\ Z_T} \times \frac{[1 - (m_x R_P,/m_P R)]}{[(M_T,/M_T) + (m_x R_P,)/M_T, R)]} \qquad (4)$$

(Ref. 25),

$$R_i = 1.12A_i^{1/3} - .94A_i^{-1/3}\ fm \qquad (5)$$

$$R = R_P + R_T + 3\ fm = \text{internuclear grazing separation} \qquad (6)$$

(Ref. 26), and

m_i = mass of particle i

x = transferred cluster .

2) A first approximation to the angular distribution was made by

a) assuming $E^f_{sepn} = E^f_C$ at all c.m.s. angles and calculating the c.m.s. angle intervals subtended by each foil. The Northcliffe and Schilling range tables were used to transform velocity to range for the target-like fragments. The accuracy of these tables for these velocities, which were on the order of .02 - .03 MeV/nucleon, was verified using the range of elastically scattered target nuclei and the range distributions of the products of complete fusion in Ref. 19.

b) using these intervals to transform the recoil range distribution to an angular distribution and graphically resolving the latter into an exponential and a gaussian component; i.e. values for PE, $\theta_{\frac{1}{2}}$, PG, θ_{max}, and σ were estimated. This angular distribution was constructed assuming exit channel energies of separation characteristic of DIT. However, the distribution itself generally turned out to have a gaussian shape, indicating that QET was the dominant mechanism. Therefore:

3) This first-guess angular distribution was used to recalculate the angle intervals represented by each foil, this time using the angle dependent E^f_{sepn} (Eqn. 5). This foil-to-angle transformation was used to construct a second approximation to the angular distribution. Integration of projected range over all angles gave a predicted recoil range distribution.

Further attempts at refinement did not improve the agreement between predicted and experimental range distributions or change the foil-to-angle transformation by more than a few percent.

Angular distributions obtained in this way are shown in Figures 20 - 31. Except for ^{252}Fm from ^{245}Cm bombardments, these are all products of projectile-stripping of one or two protons and some neutrons. In angular distributions of projectile-like products the forward-peaked DIT component is comparable in importance to QET for such transfers. The QET contribution decreases with increasing number of transferred protons; for example the side peak disappears from angular distributions of products of transfer of four or more protons from ^{22}Ne to ^{232}Th. However, in only one of the angular distributions constructed in this study, ^{252}Fm made in the highest energy ^{245}Cm bombardment, which would be expected to have the strongest DIT contribution of all measured products, can the case be made for the existence of a forward-peaked component. This result can be interpreted as an effect of looking at the target-like residues. These products will be depleted by fission to an extent dependent upon the excitation. DIT is accompanied by higher excitation than QET, particularly at low bombardment energies, so it is reasonable that QET is the predominant contributor to the formation of actinide target-like residues.

In the case of the ^{249}Cf bombardments, the excitation function clearly shows that the interaction barrier is near

83 MeV(lab) from Eqn. (7).

$$\theta_{gr} = 2\sin^{-1} \frac{E_C}{2E^i_{cms} - E_C} \qquad (7)$$

where $E_C = \frac{Z_P Z_T e^2}{R}$

This value for E_C corresponds to c.m.s. grazing angles of 107, 89, and 59 degrees for the 111.6, 99.8, and 89.2 MeV(lab), respectively. These values agree well with the centroids of the angular distribution. In the case of the ^{245}Cm experiments, the lowest energy of bombardment is still well above the barrier, so the grazing angle was estimated to be 117.5^0 from the angular distribution of ^{248}Cf from the 111.6 MeV bombardment. This value corresponds to E_C = 4.24 MeV/amu (Eqn.7), which predicts grazing angles of 103° and 92° for the 93. and 99.6 MeV bombardments respectively.

PREDICTIONS OF RECOIL EFFICIENCY

Recoil catcher experiments depend upon the bulk of the product escaping the target. In fusion it is a straightforward problem. A high enough bombardment energy will "kick" the product free. The problem is more complex for transfer products.

Consider the reaction ^{249}Cf (^{18}O,^{14}C) ^{253}Fm, a reasonable channel for Fm production for 111.6 MeV(lab) bombardment energy. The most probable recoil range of ^{253}Fm from a QET channel, assuming $E^f_{sepn} = E^f_{opt}$ and $\theta = \theta_{gr}$ is predicted to be 0.32 mg Al/cm^2 which corresponds to the third foil in the 111.6 MeV ^{18}O + ^{249}Cf bombardment, allowing for the target thickness, in agreement with experiment. The calculation which fits the recoil range distribution also predicts that less than 0.05 of the heavy products would

remain in the target. At 160 MeV (lab), the most probable recoil range is predicted to be 0.13 mg Al/cm^2, less than 0.1 mg Al/cm^2 longer than half the target thickness. This is a marginally low range in view of the breadth of the range distribution.

It is possible that MT or DIT take over the bulk of the cross section at this higher energy. The DIT product would have a lower c.m.s. separation energy than the QET product, at least partially compensating for separation angle of 180° with respect to the beam direction. At 160 MeV (lab) initial energy, the most probable axial range is predicted to be 0.13 mg Al/cm^2. This is a lower limit, so an appreciable fraction of product should escape the target. The MT product would have a most probable axial range of 0.12 mg Al/cm^2, but virtually all the activity would be concentrated near this range, which is also longer than target thickness. Either mechanism would deposit about 100 MeV excitation energy into the target-like fragment.

CONCLUSION

Recoil range distribution shapes can be used to distinguish between complete fusion, massive transfer, and quasi-elastic-plus deep-inelastic transfer. Angular distributions derived from recoil range distributions imply that while the DIT contribution is expected to be significant, it is strongly depleted relative to QET. Massive transfer does not appear to be important for ^{18}O bombardments at these energies.

It would be interesting to do higher energy bombardments

to look for an increase in the relative contribution of DIT and the onset of MT. It would be extremely valuable to actually measure angular distributions of heavy fragments. Complementary light-fragment experiments would be useful in separating the primary cross-section and de-excitation factors in residue cross-section measurements.

The decrease in cross-section at higher energies observed in Ref. 21 may be caused by the increase of E^{f}_{opt} and the loss of QET as a low excitation energy reaction path.

ACKNOWLEDGEMENTS

We would like to thank Darleane Hoffman, Diana Lee, and J. B. Wilhelmy for helpful discussions and Gary Shen for his technical assistance. This report is based on the Ph. D. thesis (LBL-15027) of Rose Marie McFarland.

This work was supported by the Director, Office of Energy Research, Division of Nuclear Physics of the Office of High Energy and Nuclear Physics of the U. S. Department of Energy under Contract DE-AC03-76SF00098.

REFERENCES

1. Galin, J., D. Guerreau, M. Lefort, J. Peter, and X. Tarrago. Nucl. Phys. A159 (1970) 461-480.

2. Artyukh, A. G., J. Wilczynski, V. V. Volkov, G. F. Gridnev, and V. L. Mikheev. Sov. J. Nucl. Phys. 17 (1973) 586-589.

3. Artyukh, A. G., G. F. Gridnev, V. L. Mikheev, V. V. Volkov, and J. Wilczynski. Nucl. Phys. A215 (1973) 91-108.

4. Jacmart, J. C., P. Colombani, H. Doubre, N. Frascaria, N. Poffe, M. Riou, J. C. Roynette, and C. Stèphan. Nucl. Phys. A242 (1975) 175-188.

5. Oganesyan, Yu. Ts., Yu. E. Penionzhkevich, and A. O. Shamsutdinov. Sov. J. Nucl. Phys. 14 (1972) 31-36.

6. Gardes, D., R. Bimbot, J. Maison, M. F. Rivet, A. Fleury, F. Hubert, and G. Llabador. Phys. Rev. C 21 (1980) 2447 - 2466.

7. Hubert, F., H. Delagrange, and A. Fleury. Nucl. Phys. A228 (1974) 415-431.

8. Colombani, P., N. Franscaria, J. C. Jacmart, M. Riou, C. Stèphan, H. Doubre, N. Poffe, and J. C. Roynette, Phys. Lett. 55B (1975) 45-48.

9. Strudler, P. M., I. L. Preiss, and Richard Wolfgang, Phys. Rev. 154 (1967) 1126-1135.

10. Moretto, L. G. and R. Schmitt, J. de Phys. (Paris) C5 (1976) 109-140.

11. Galin, Joel. J. de Phys. (Paris) C5 (1976) 83-105.

12. Lefort, M. and Ch. Ngo. Ann, Phys. 3 (1978).

13. Inamura, T., M. Ishihara, T. Fukuda, T. Shimoda, and H. Hiruta. Phys. Lett. 68B (1977) 51-54.

14. Zolnowski, D. R., H. Yamada, S. E. Cala, A. C. Kahler, and T. T. Sugihara. Phys. Rev. Lett. 41 (1978) 92-95.

15. Udagawa, T. and T. Tamura. Phys. Rev. Lett. 45 (1980) 1311-1314.

16. Sugihara, T. T. Phys. Scripta. 24 (1981) 108-112.

17. Barker, J. H., J. R. Beene, M. L. Halbert, D. C. Hensley, M. Jaaskelainen, D. G. Sarantites, and R. Woodward. Phys. Rev. Lett. 45 (1980) 424-427.

18. Geoffroy, K. A., D. G. Sarantites, M. L. Halbert, D. C. Hensley, R. A. Dayras, and J. H. Barker. Phys. Rev. Lett. 43 (1979) 1303-1306.

19. Hahn, R. L., P. F. Dittner, K. S. Toth, and O. L. Keller. Phys. Rev. C 10 (1974) 1889-1903.

20. Lee, Diana, Hans von Gunten, Barbara Jacak, Matti Nurmia, Yuan-fang Liu, Cheng Luo, Glenn T. Seaborg, and Darleane Hoffman. Phys. Rev. C 25 (1982) 286-292.

21. Lee, Diana, Kenton Moody, Matti Murmia, Glenn T. Seaborg, Hans R. von Gunten, and Darleane Hoffman. Excitation functions for production of heavy actinides from interactions of ^{18}O with ^{248}Cm and ^{249}Cf. To be published.

22. Northcliffe, L. C. and R. F. Schilling. Nuclear Data Tables A7 (1970) 233-463.

23. Moody, Kenton J. Private communication (1980).

24. Table of Isotopes, 7th ed. Edited by C. M. Lederer, and V. S. Shirley. Wiley (New York 1978).

25. Toepffer, C. Z. Phys. 253 (1972) 78-88.

26. Bass, Reiner. Nuclear Reactions with Heavy Ions Springer-Verlag (New York 1980).

Table I. Decay Properties of Observed Nuclides (Ref. 24).

NUCLIDE	decay mode (abundance)	half-life	principal E_α (MeV)
^{250}Fm	α (1.0)	30 min.	7.42
^{251}Fm	α (.018)	5.3 hr.	6.834
^{252}Fm	α (1.0)	25.4 hr.	7.04
^{253}Fm	α (.12)	3.0 days	6.943,6.674
^{254}Fm	α (1.0)	3.240 hr.	7.187
^{256}Fm	SF (.919)	2.63 hr.	
^{251}Es	α (.005)	33 hr.	6.492
^{252}Es	α (.78)	472 days	6.632
^{253}Es	α (1.0)	20.47 days	6.633
^{254m}Es	β, to ^{254}Fm (.9959)	39.3 hr.	7.187
^{245}Cf	α (.3)	44 min.	7.137
^{246}Cf	α (1.0)	35.7 hr.	6.758,6.719
^{248}Cf	α (1.0)	333 days	6.26
^{250}Cf	α (1.0)	13.1 yr	6.031.5.989
^{242}Cm	α (1.0)	162.8 days	6.113,6.070

TABLE II. Cross sections in microbarns for products of ^{18}O + ^{249}Cf

	BOMBARDMENT ENERGY (LAB) (MeV)			
PRODUCT	111.6	99.8	89.2	83.
^{250}Fm	74. ± 3.6	15.4 ± .75	.22 ± .012	.05 ± .18
^{251}Fm	1080. ± 57.	790. ± 40.	28. ± 1.5	.3 ± .12
^{252}Fm	870. ± 43.	1530. ± 74.	530. ± 28.	.069 ± .0062
^{253}Fm	250. ± 13.	430. ± 21.	260. ± 14.	.01 ± .20
^{254}Fm	43. ± 2.1	61. ± 3.0	10.9 ± .58	.008 ± .0022
^{256}Fm	0. ± .038	.07 ± .033	.047 ± .0080	.0004 ± .00018
^{251}Es	5000. ± 250.	4000. ± 200.	390. ± 23.	12. ± .1.3
^{252}Es	660. ± 35.	1270. ± 62.	650. ± 42.	.6 ± .25
^{253}Es	300. ± 17.	580. ± 29.	90. ± 5.1	.08 ± .021
^{254m}Es	.38 ± .028	.40 ± .021	.22 ± .014	.037 ± .0050
^{246}Cf	146. ± 8.2	53. ± 3.1	1.8 ± .13	.36 ± .173
^{248}Cf	14300. ± 700.	15200. ± 740.	2500. ± 130.	540. ± 31.
^{250}Cf	23000. ± 1200.	27000. ± 1300.	9900. ± 580.	0. ± 33.

TABLE III. Cross sections in microbarns for products of ^{18}O + ^{245}Cm

	BOMBARDMENT ENERGY (LAB) (MeV)		
PRODUCT	111.6	99.6	93.
^{252}Fm	1.71 ± .088	2.3 ± .12	2.6 ± .13
^{252}Es	0. ± 24.	6.3 ± 2.7	6.9 ± 2.5
^{253}Es	1.1 ± .24	.57 ± .22	.25 ± .17
^{245}Cf	2.7 ± .16		.02 ± .140
^{246}Cf	154. ± 7.5	85. ± 4.1	37. ± 1.8
^{248}Cf	1650. ± 81.	2020. ± 99.	2500. ± 120.
^{242}Cm	280. ± 14.	153. ± 7.8	

FIGURE CAPTIONS

Figure 1. Target and recoil catcher foil chamber

Figure 2. Recoil range distributions of Fm isotopes from ^{18}O (111.6 MeV) + ^{249}Cf

Figure 3. Recoil range distributions of Es isotopes from ^{18}O (111.6 MeV) + ^{249}Cf

Figure 4. Recoil range distributions of Cf isotopes from ^{18}O (111.6 MeV) + ^{249}Cf

Figure 5. Recoil range distributions of Fm isotopes from ^{18}O (99.8 MeV) + ^{249}Cf

Figure 6. Recoil range distributions of Es isotopes from ^{18}O (99.8 MeV) + ^{249}Cf

Figure 7. Recoil range distributions of Cf isotopes from ^{18}O (99.8 MeV) + ^{249}Cf

Figure 8. Recoil range distributions of Fm isotopes from ^{18}O (89.2 MeV) + ^{249}Cf.

Figure 9 Recoil range distributions of Es isotopes from ^{18}O (89.2 MeV) + ^{249}Cf

Figure 10 Recoil range distributions of Cf isotopes from ^{18}O (89.2 MeV) + ^{249}Cf

Figure 11 Recoil range distribution of ^{252}Fm from ^{18}O (111.6 MeV) + ^{245}Cm.

Figure 12 Recoil range distributions of Cf isotopes from ^{18}O (111.6 MeV) + ^{245}Cm.

Figure 13 Recoil range distributions of Cm isotopes from ^{18}O (111.6 MeV) + ^{245}Cm.

Figure 14 Recoil range distributions of ^{252}Fm from ^{18}O (99.6 MeV) + ^{245}Cm

Figure 15 Recoil range distributions of Cf isotopes from ^{18}O (99.6 MeV) + ^{245}Cm

Figure 16 Recoil range distributions of Cm isotopes from ^{18}O (99.6 MeV) + ^{245}Cm

Figure 17 Recoil range distributions of ^{252}Fm from ^{18}O (93. MeV) + ^{245}Cm

Figure 18 Recoil range distributions of Cf isotopes from ^{18}O (93. MeV) + ^{245}Cm

Figure 19 Recoil range distributions of Cm isotopes from ^{18}O (93. MeV) + ^{245}Cm

Figure 20 Fm angular distributions for ^{18}O (111.6 MeV) + ^{249}Cf extracted from recoil range data (see text)

Figure 21 Es angular distributions for ^{18}O (111.6 MeV) + ^{249}Cf extracted from recoil range data

Figure 22 Cf angular distributions for ^{18}O (111.6 MeV) + ^{249}Cf extracted from recoil range data

Figure 23 Fm angular distributions for ^{18}O (99.8 MeV) + ^{249}Cf extracted from recoil range data

Figure 24 Es angular distributions for ^{18}O (99.8 MeV) + ^{249}Cf extracted from recoil range data

Figure 25 Cf angular distributions for ^{18}O (99.8 MeV) + ^{249}Cf extracted from recoil range data

Figure 26 Fm angular distributions for ^{18}O (89.2 MeV) + ^{249}Cf extracted from recoil range data

Figure 27 Es angular distributions for ^{18}O (89.2 MeV) + ^{249}Cf extracted from recoil range data

Figure 28 Cf angular distributions for ^{18}O (89.2 MeV) + ^{249}Cf extracted from recoil range data.

Figure 29 ^{252}Fm angular distributions for ^{18}O (111.6, 99.6, 93. MeV) + ^{245}Cm, or OCm - III, - II, and I, respectively, extracted from recoil range distributions.

Figure 30 ^{248}Cf angular distributions for ^{18}O (111.6, 99.6, 93. MeV) + ^{245}Cm, or OCm - II, - II, and - I, respectively, extracted from recoil range distributions.

Figure 31 ^{246}Cf angular distributions for ^{18}O (111.6, 99.6, 93. MeV) + ^{245}Cm, or OCm - III, - II, and - I, respectively, extracted from recoil range distributions.

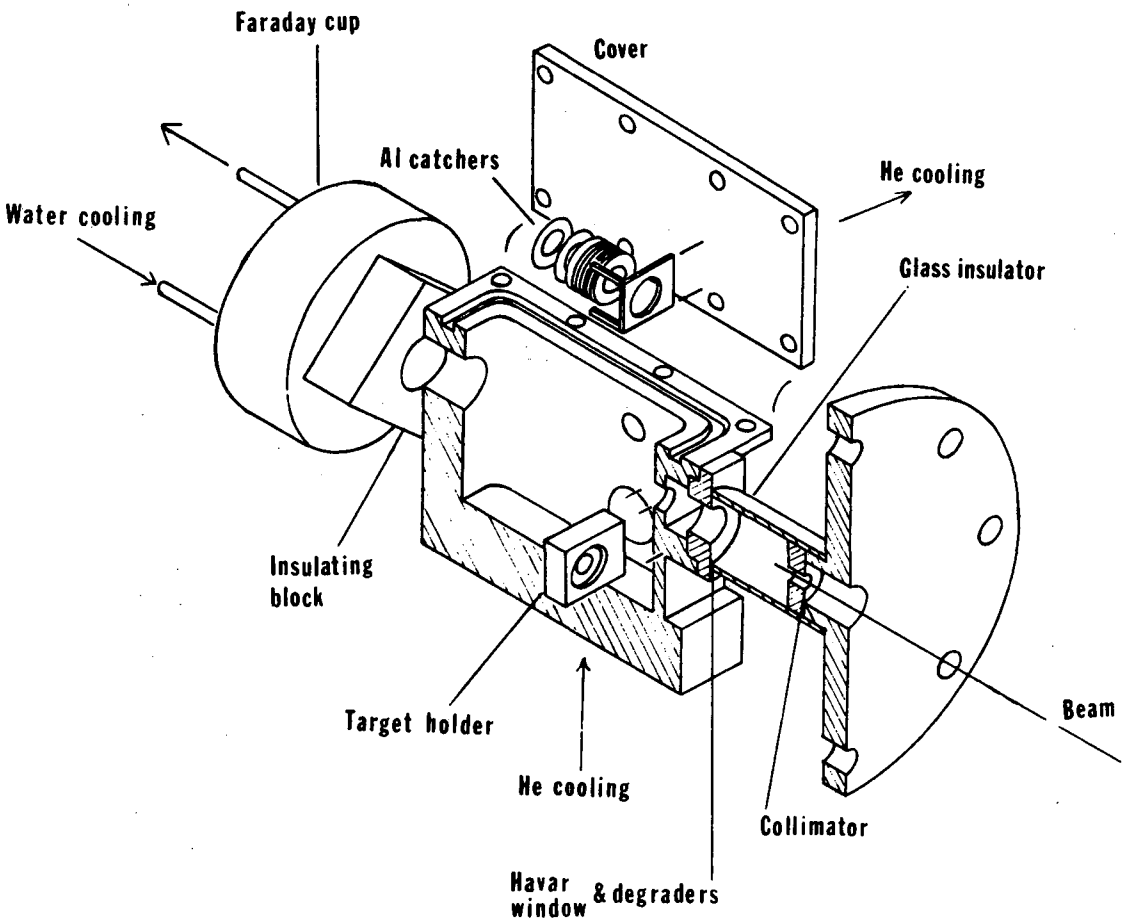

XBL 828-9568

Fig. 1

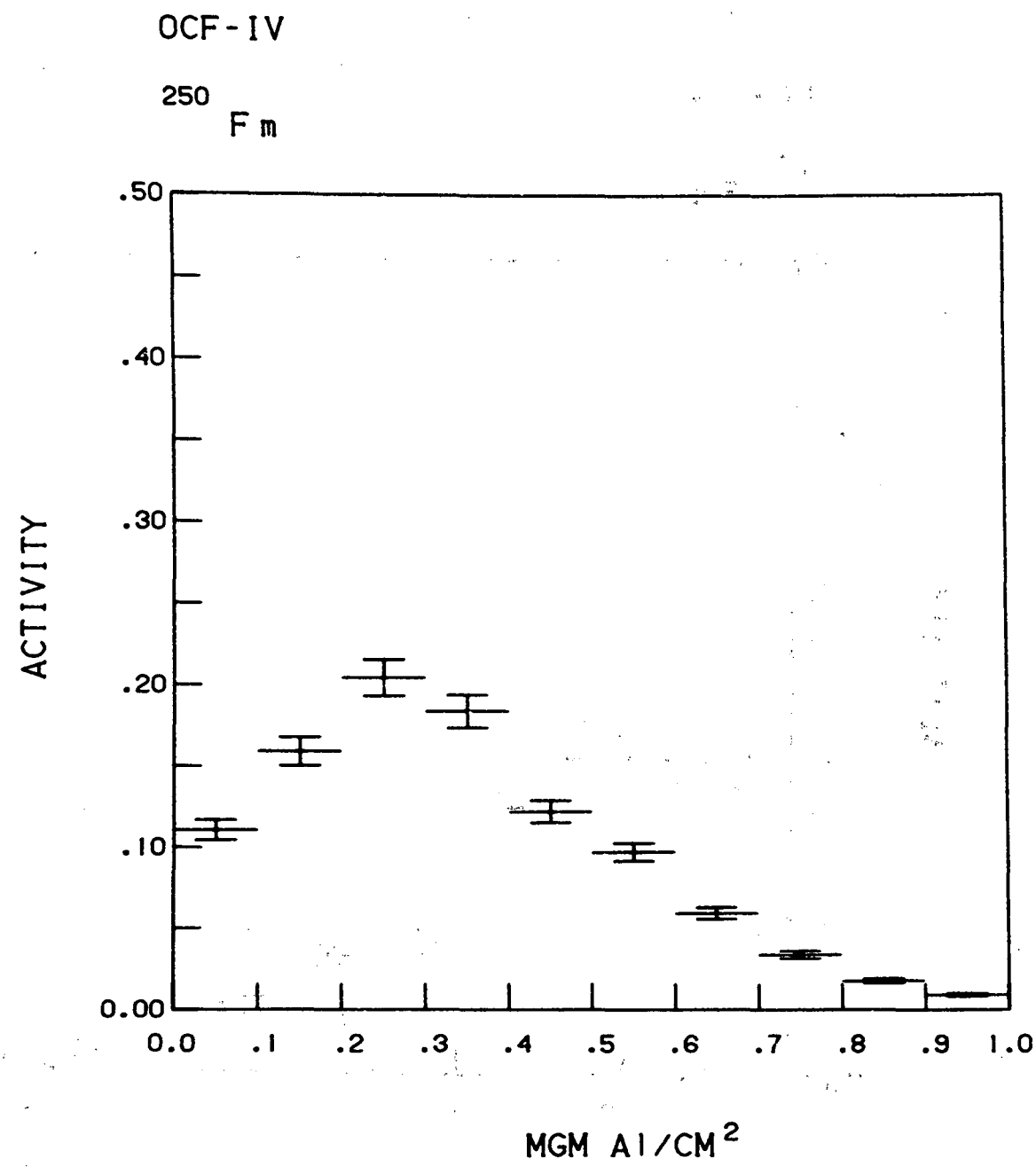
OCF-IV
250
Fm
ACTIVITY
.50
.40
.30
.20
.10
0.00
0.0
.1
.2
.3
.4
.5
.6
.7
.8
.9
1.0
MGM Al/CM 2
XBL 823-9503

Fig. 2a

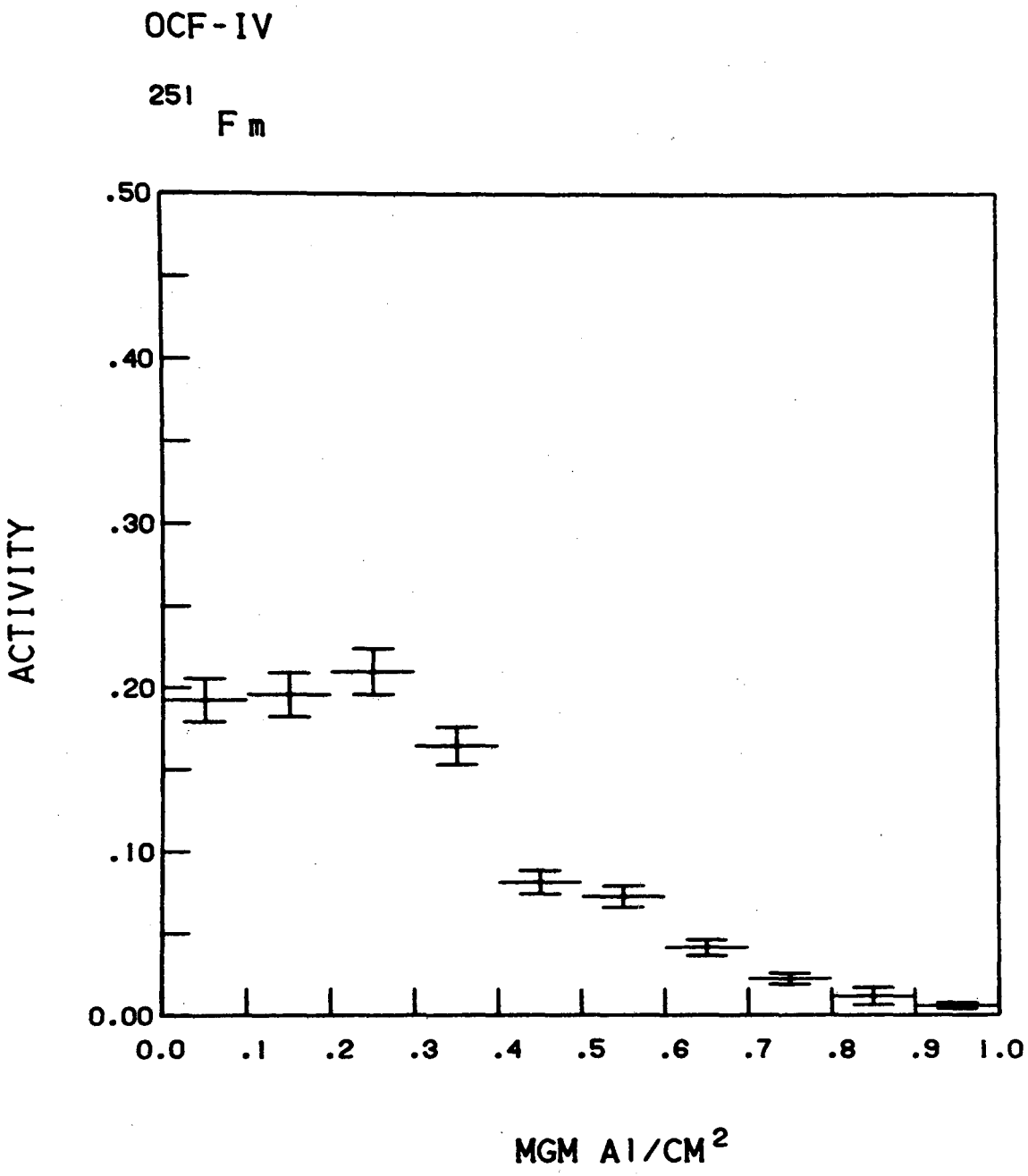
OCF-IV
251
Fm
.50
.40
.30
.20
.10
0.00
ACTIVITY
0.0
.1
.2
.3
.4
.5
.6
.7
.8
.9
1.0
MGM Al/CM2
XBL 823-9509

Fig. 2b

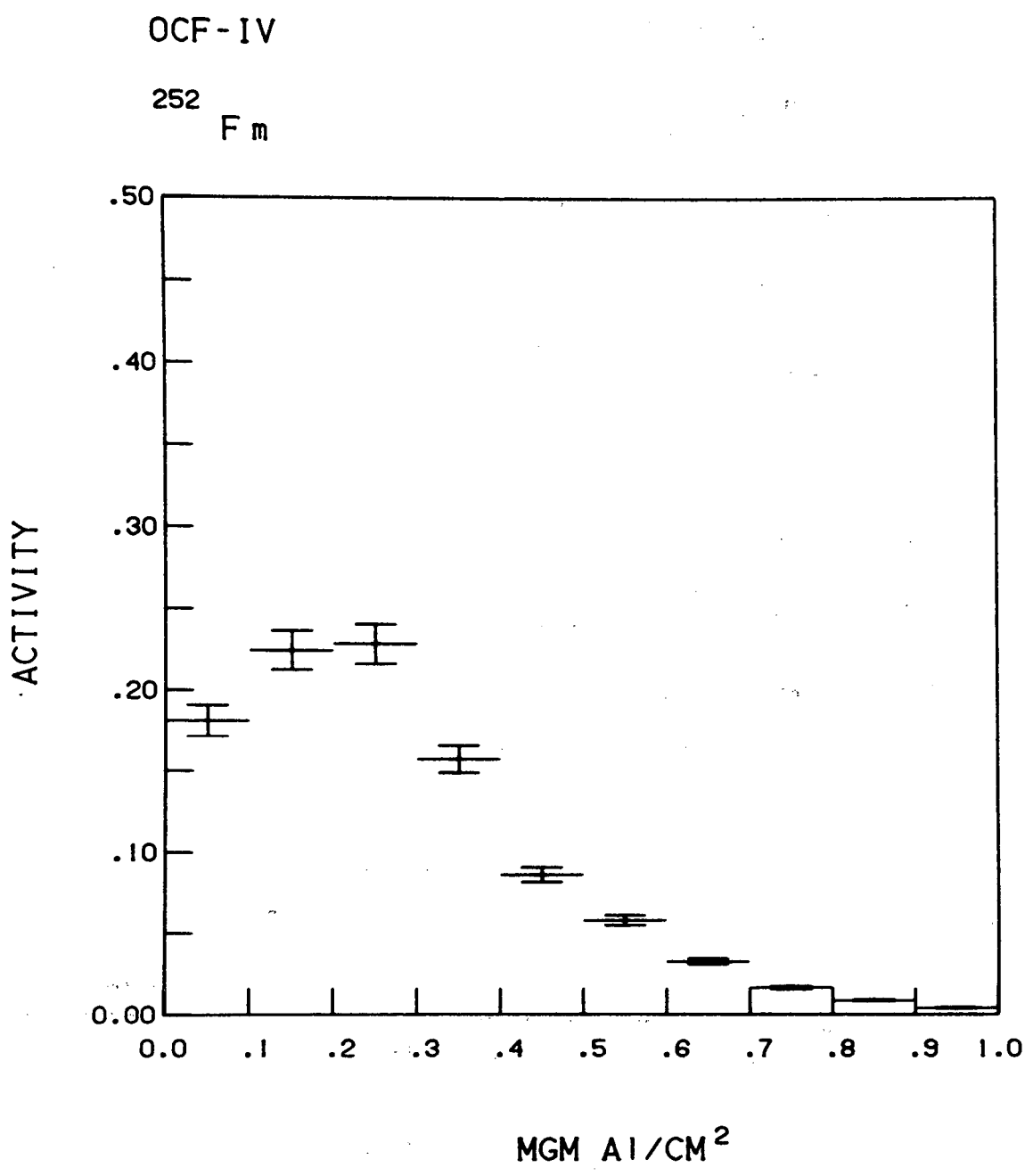
OCF-IV
252
Fm
ACTIVITY
.50
.40
.30
.20
.10
0.00
0.0
.1
.2
.3
.4
.5
.6
.7
.8
.9
1.0
MGM Al/CM 2
XBL 823-9501

Fig. 2c

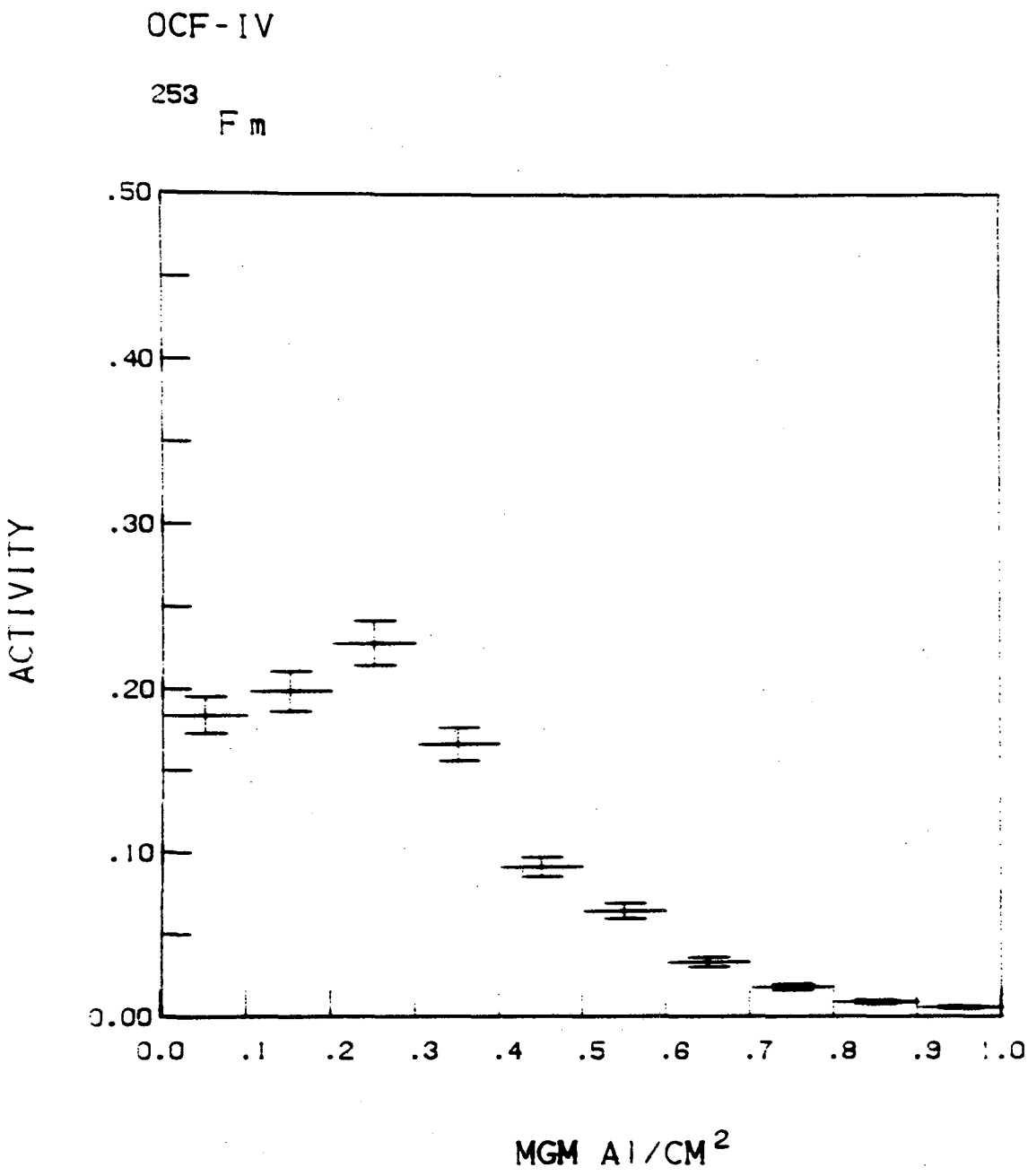
OCF-IV
253 Fm
ACTIVITY
.50
.40
.30
.20
.10
0.00
0.0
.1
.2
.3
.4
.5
.6
.7
.8
.9
1.0
MGM Al/CM 2
XBL 823-9502

Fig. 2d

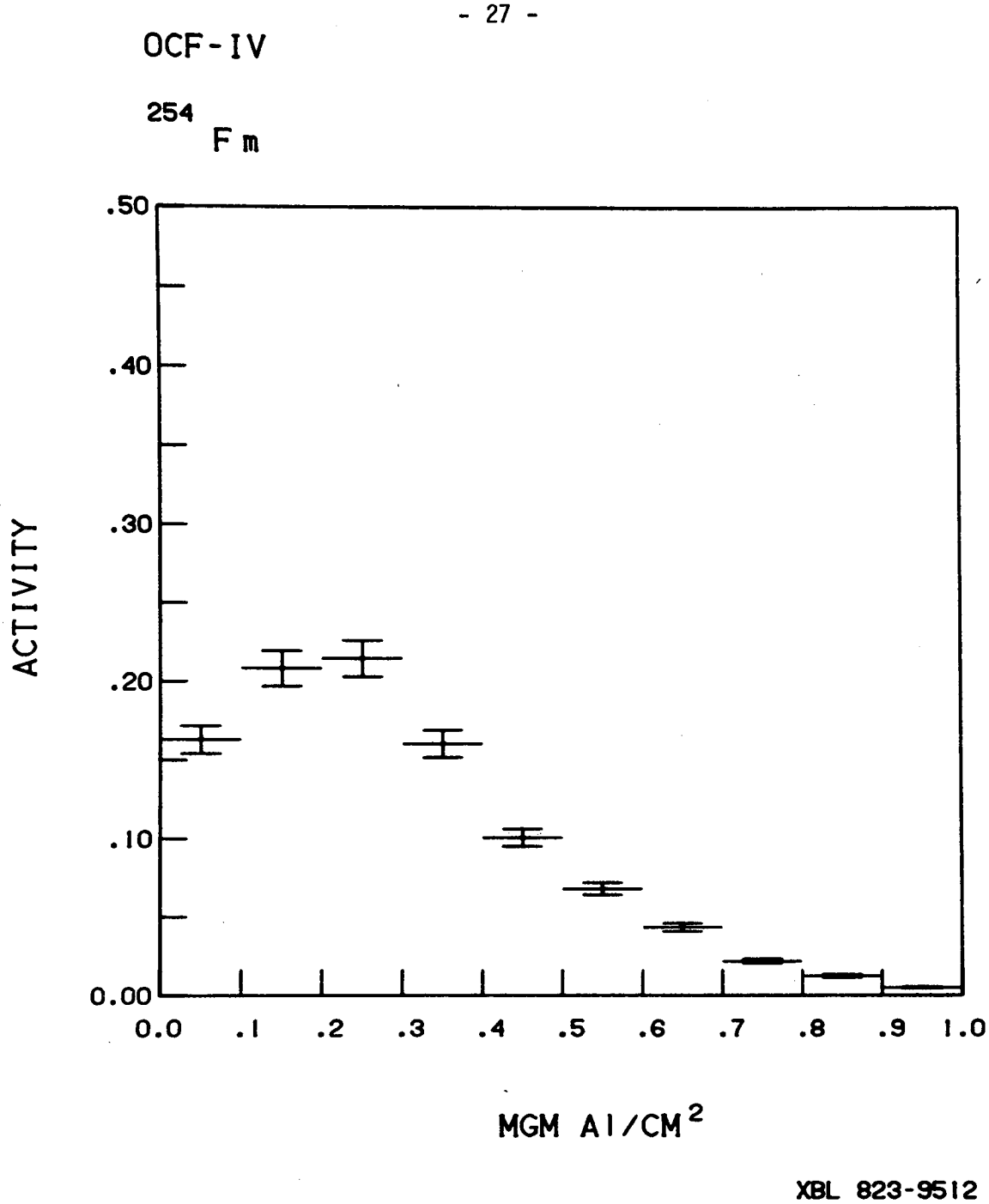
OCF-IV
254
Fm
.50
.40
.30
.20
.10
0.00
ACTIVITY
0.0
.1
.2
.3
.4
.5
.6
.7
.8
.9
1.0
MGM Al/CM 2
XBL 823-9512

Fig. 2e

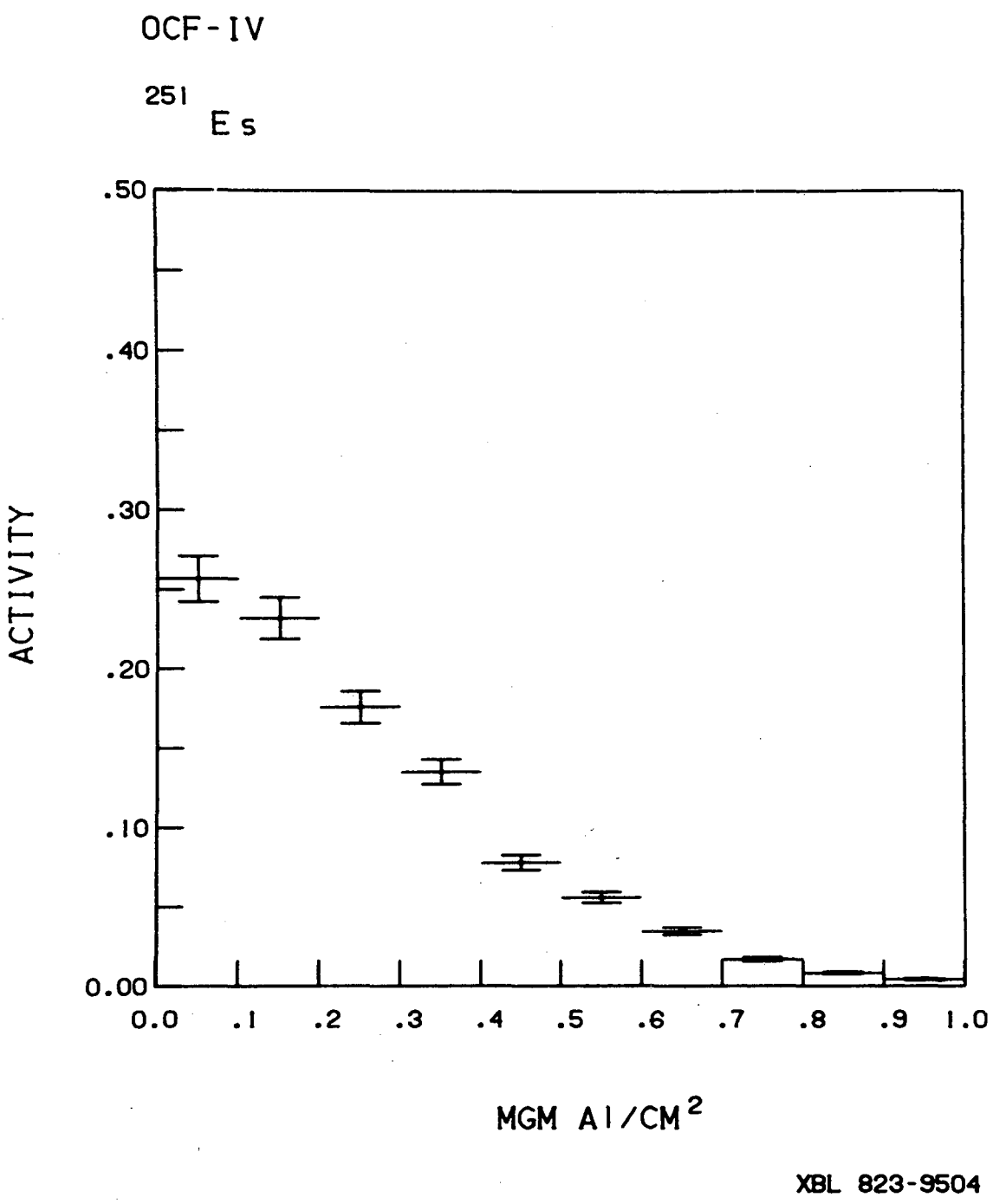
OCF-IV
251
Es
.50
.40
.30
.20
.10
0.00
ACTIVITY
0.0
.1
.2
.3
.4
.5
.6
.7
.8
.9
1.0
MGM Al/CM 2
XBL 823-9504

Fig. 3a

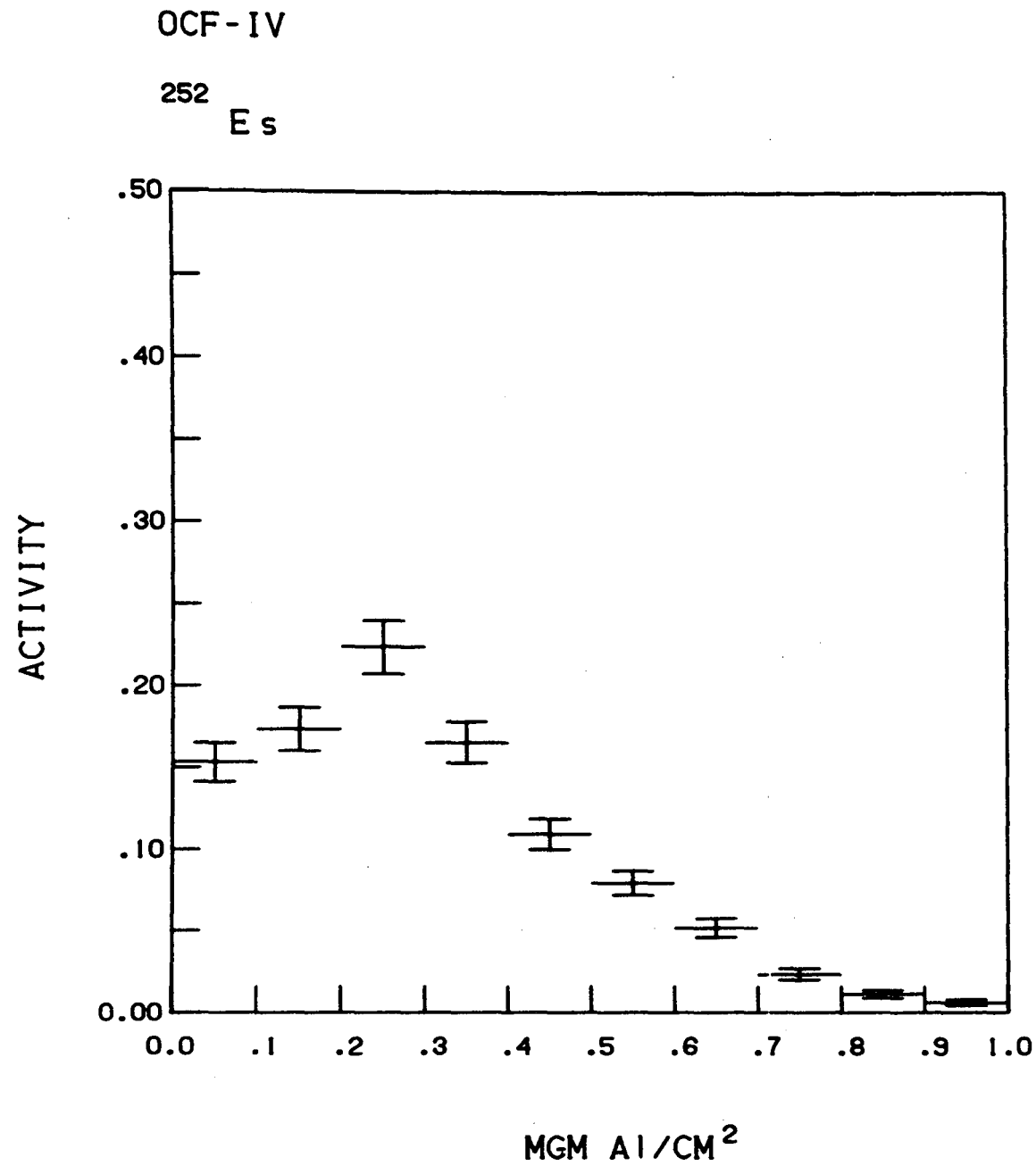
OCF-IV
252
Es
ACTIVITY
.50
.40
.30
.20
.10
0.00
0.0
.1
.2
.3
.4
.5
.6
.7
.8
.9
1.0
MGM Al/CM 2
XBL 823-9510

Fig. 3b

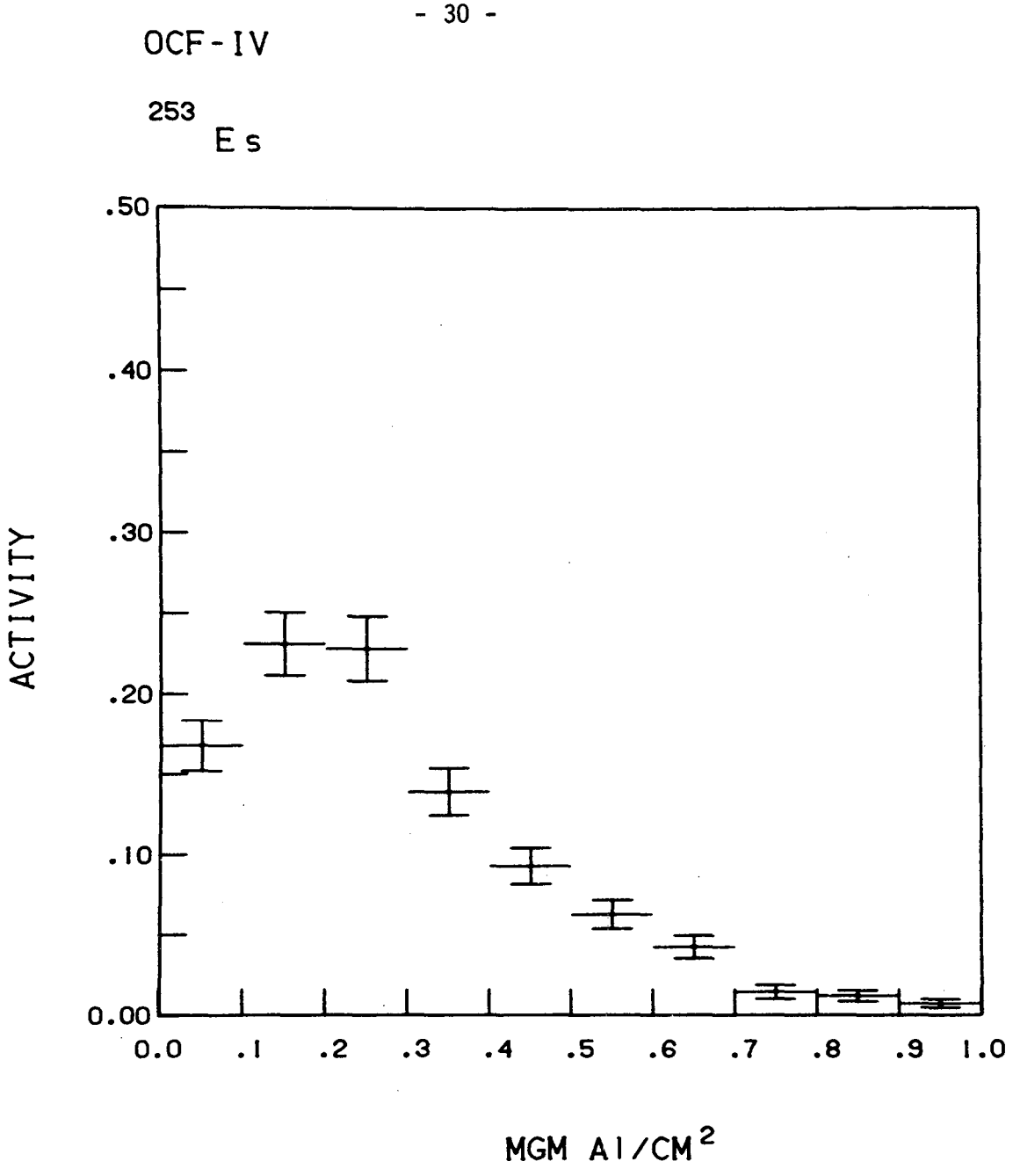
OCF-IV
253
Es
ACTIVITY
.50
.40
.30
.20
.10
0.00
0.0
.1
.2
.3
.4
.5
.6
.7
.8
.9
1.0
MGM Al/CM 2
XBL 823-9505

Fig. 3c

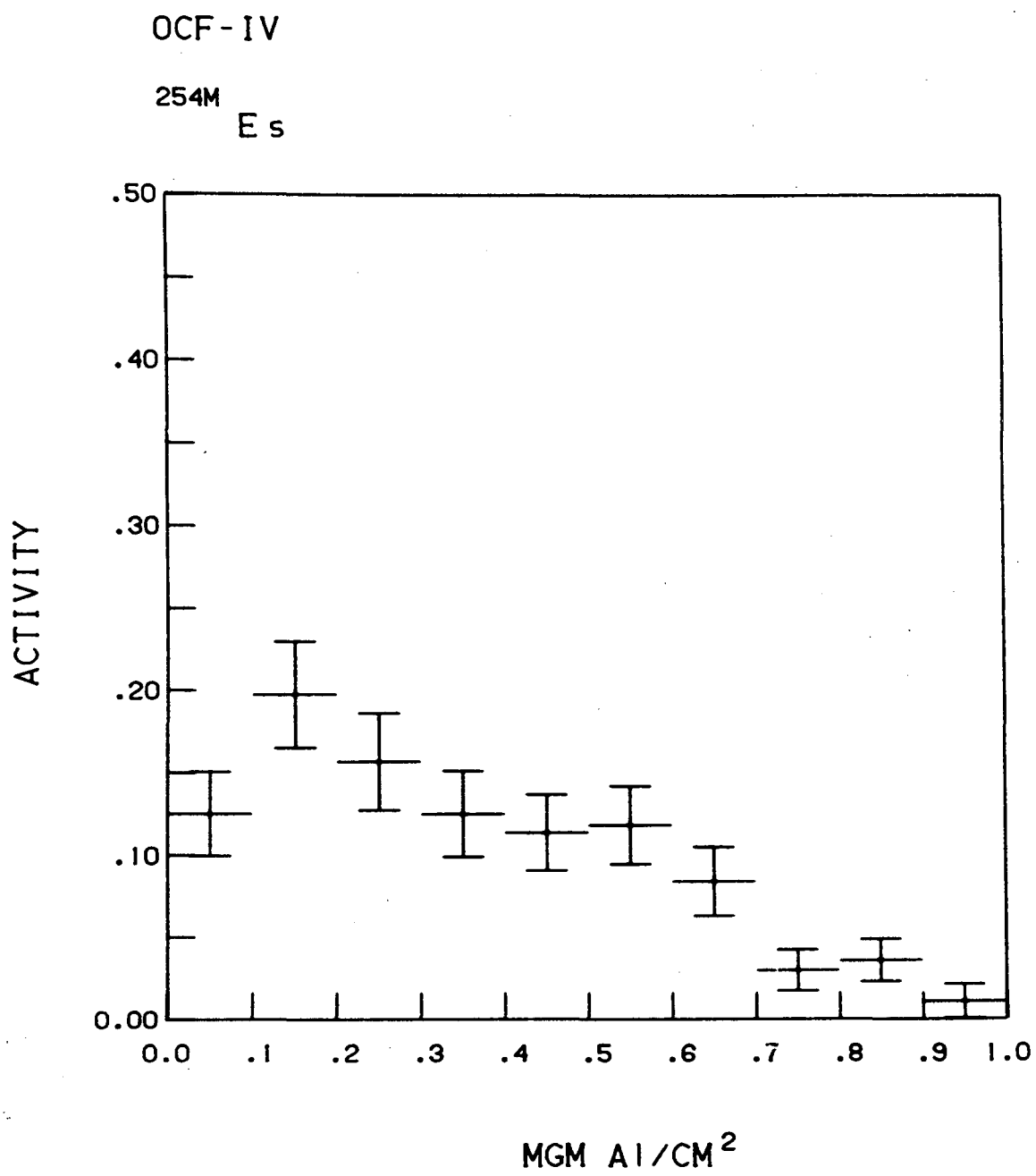
OCF-IV
254M
Es
.50
.40
.30
.20
.10
0.00
ACTIVITY
0.0
.1
.2
.3
.4
.5
.6
.7
.8
.9
1.0
MGM Al/CM 2
XBL 823-9500

Fig. 3d

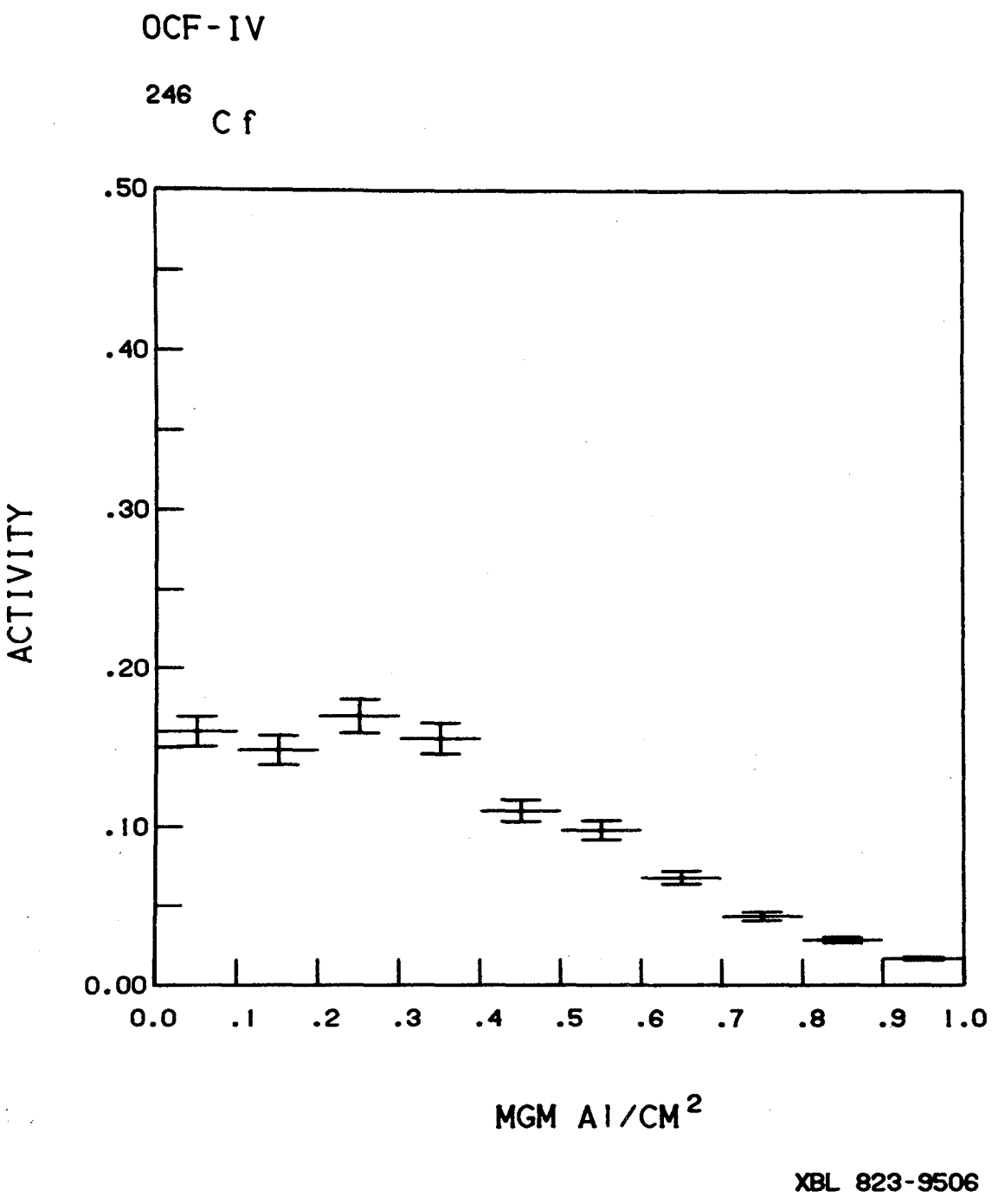
OCF-IV
246 Cf
ACTIVITY
.50
.40
.30
.20
.10
0.00
0.0
.1
.2
.3
.4
.5
.6
.7
.8
.9
1.0
MGM Al/CM 2
XBL 823-9506

Fig. 4a

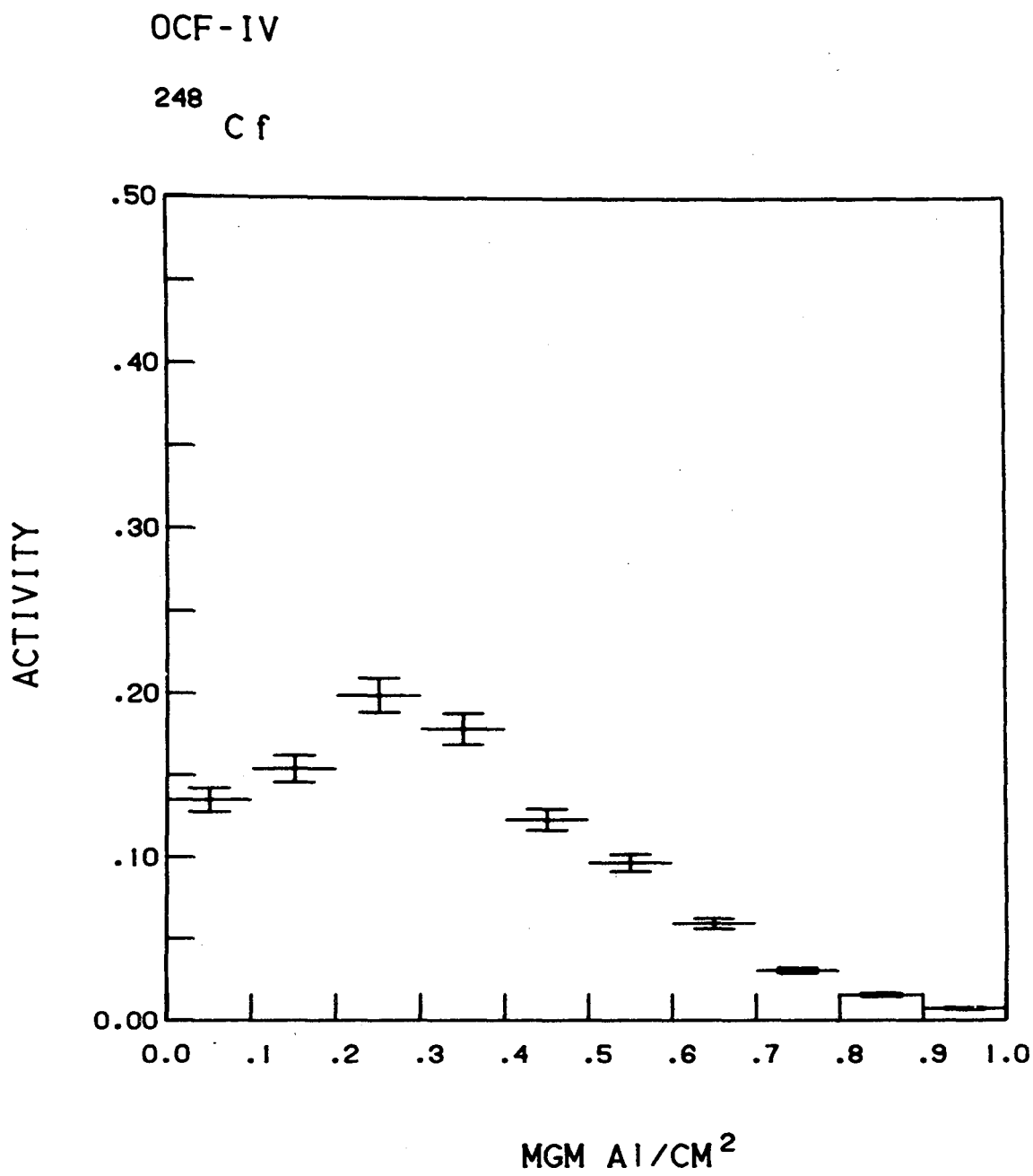
OCF-IV
248 Cf
.50
.40
.30
.20
.10
0.00
ACTIVITY
0.0
.1
.2
.3
.4
.5
.6
.7
.8
.9
1.0
MGM Al/CM 2
XBL 823-9507

Fig. 4b

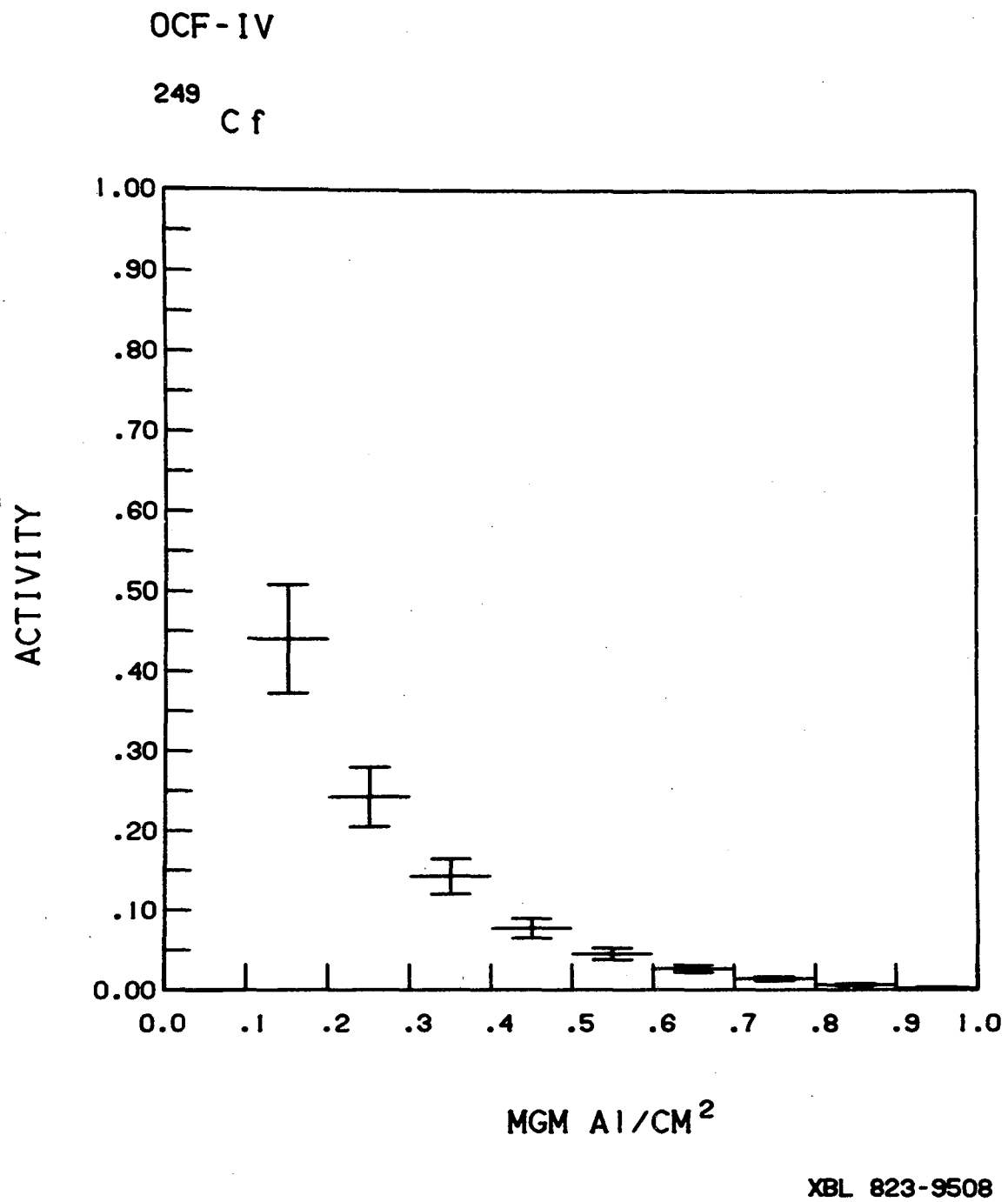
OCF-IV
249 Cf
ACTIVITY
1.00
.90
.80
.70
.60
.50
.40
.30
.20
.10
0.00
0.0
.1
.2
.3
.4
.5
.6
.7
.8
.9
1.0
MGM Al/CM 2
XBL 823-9508

Fig. 4c

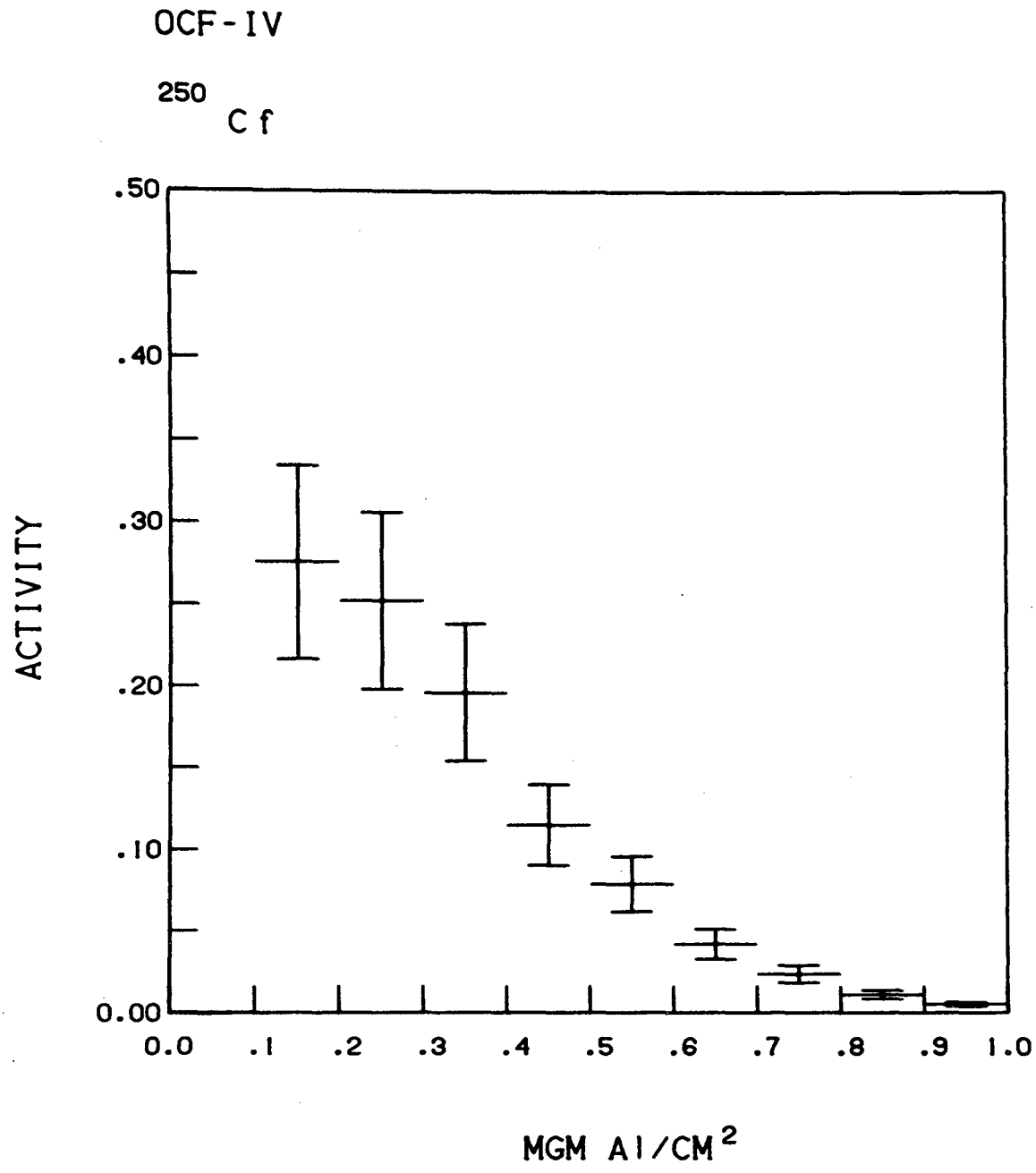
OCF-IV
250 Cf
.50
.40
.30
.20
.10
0.00
ACTIVITY
0.0
.1
.2
.3
.4
.5
.6
.7
.8
.9
1.0
MGM Al/CM 2
XBL 823-9511

Fig. 4d

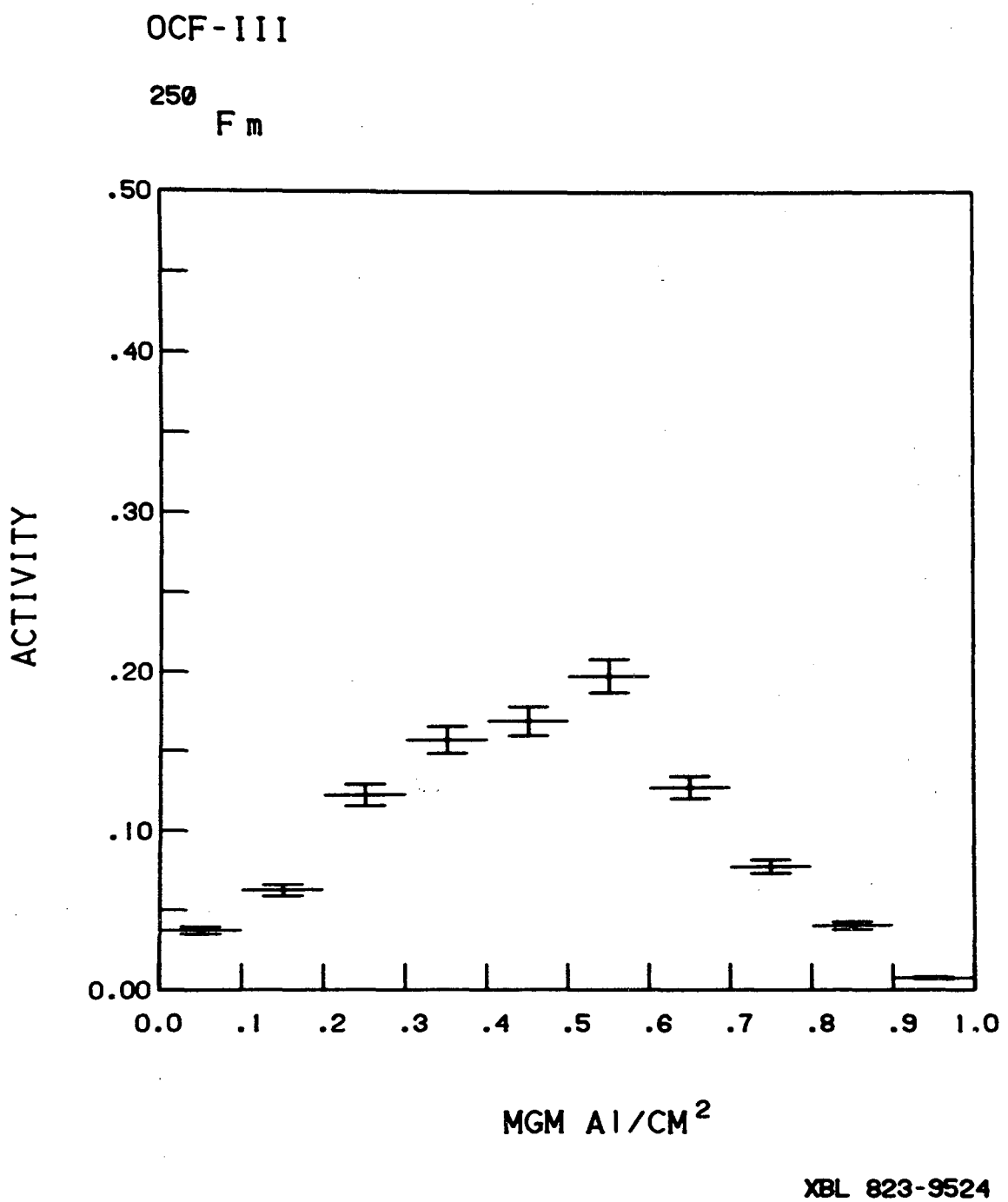
OCF-III
250
Fm
.50
.40
.30
.20
.10
0.00
ACTIVITY
0.0
.1
.2
.3
.4
.5
.6
.7
.8
.9
1.0
MGM Al/CM 2
XBL 823-9524

Fig. 5a

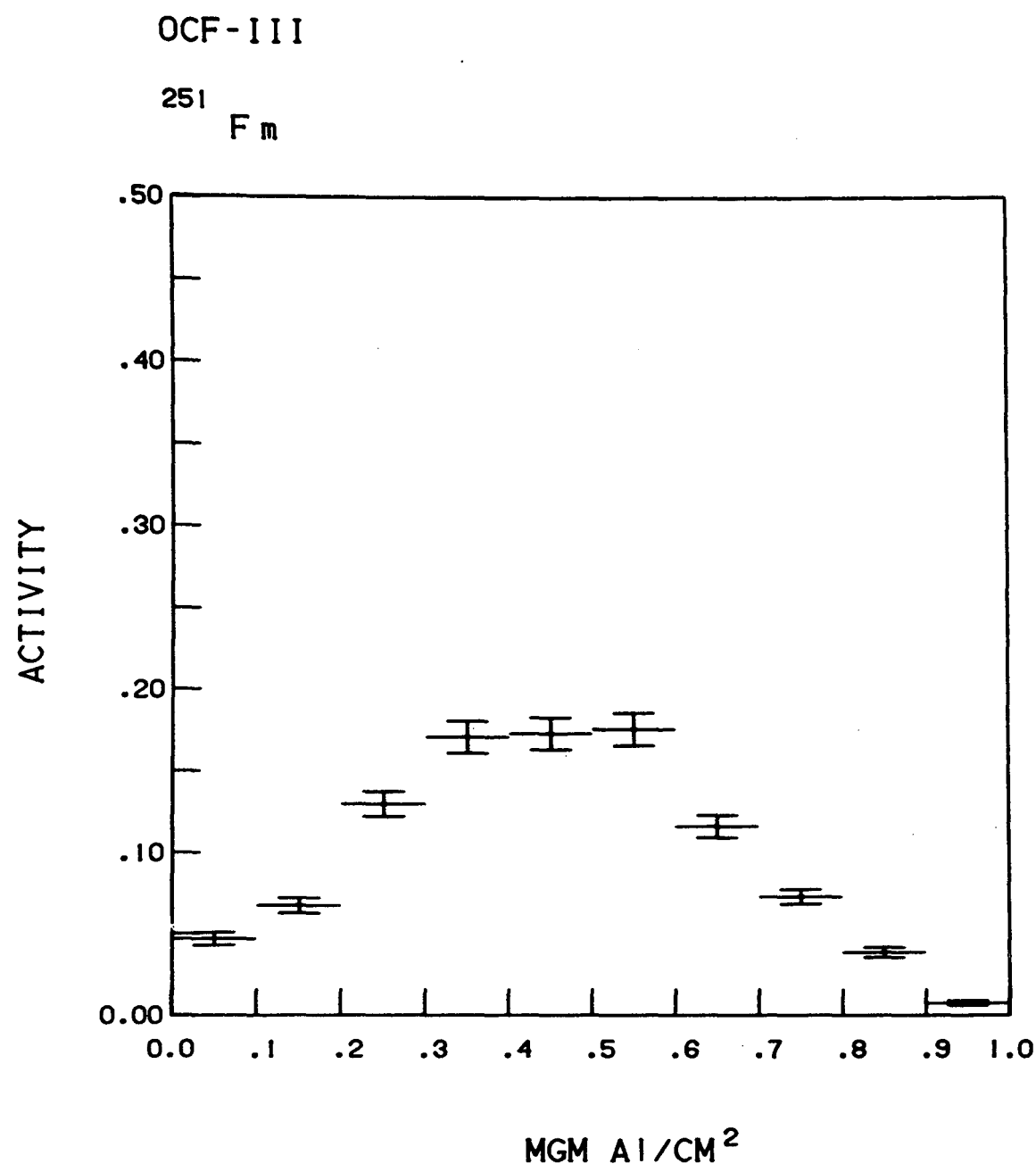
OCF-III
251
Fm
ACTIVITY
.50
.40
.30
.20
.10
0.00
0.0
.1
.2
.3
.4
.5
.6
.7
.8
.9
1.0
MGM Al/CM 2
XBL 823-9527

Fig. 5b

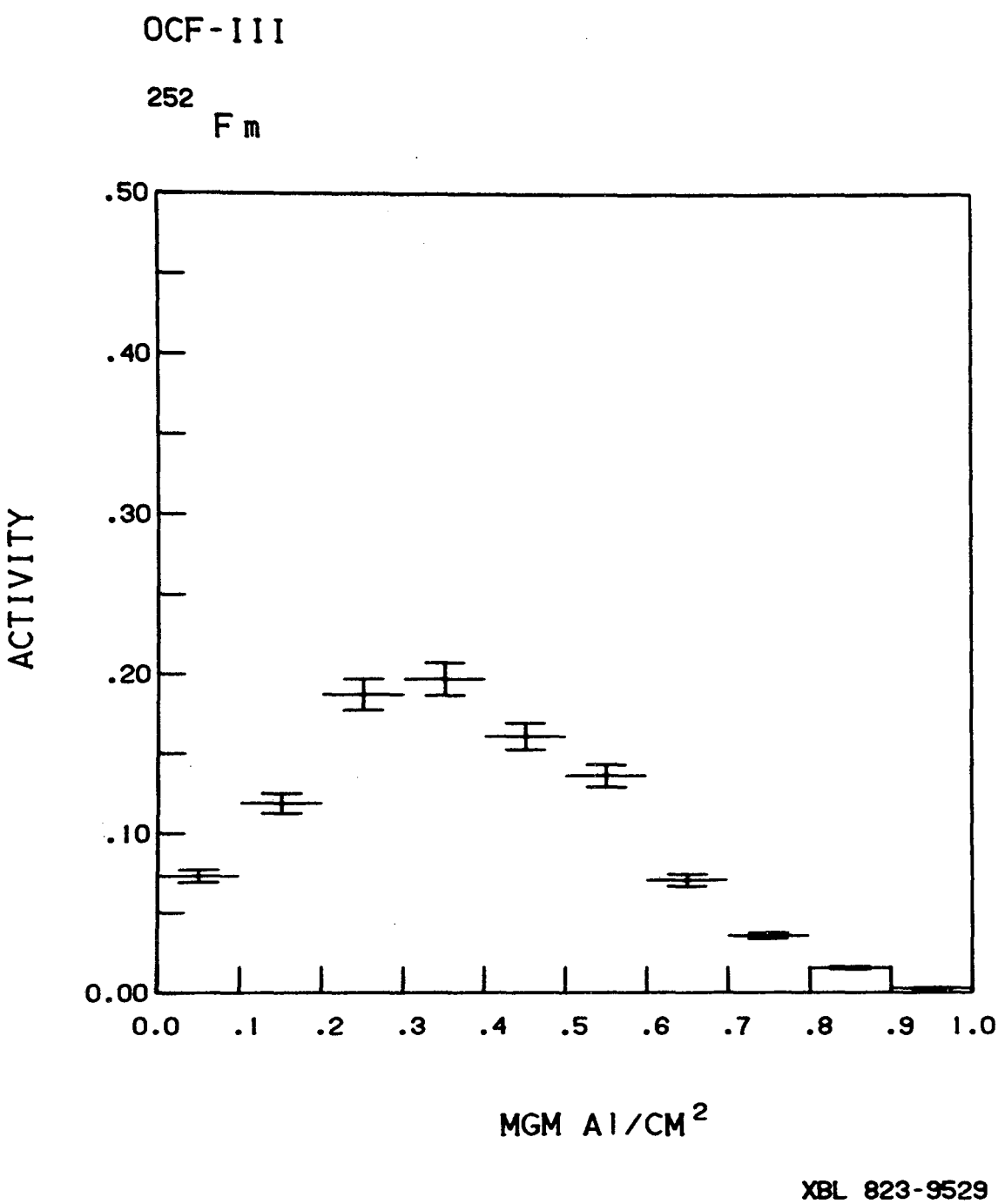
OCF-III
252
Fm
ACTIVITY
.50
.40
.30
.20
.10
0.00
0.0
.1
.2
.3
.4
.5
.6
.7
.8
.9
1.0
MGM Al/CM2
XBL 823-9529

Fig. 5c

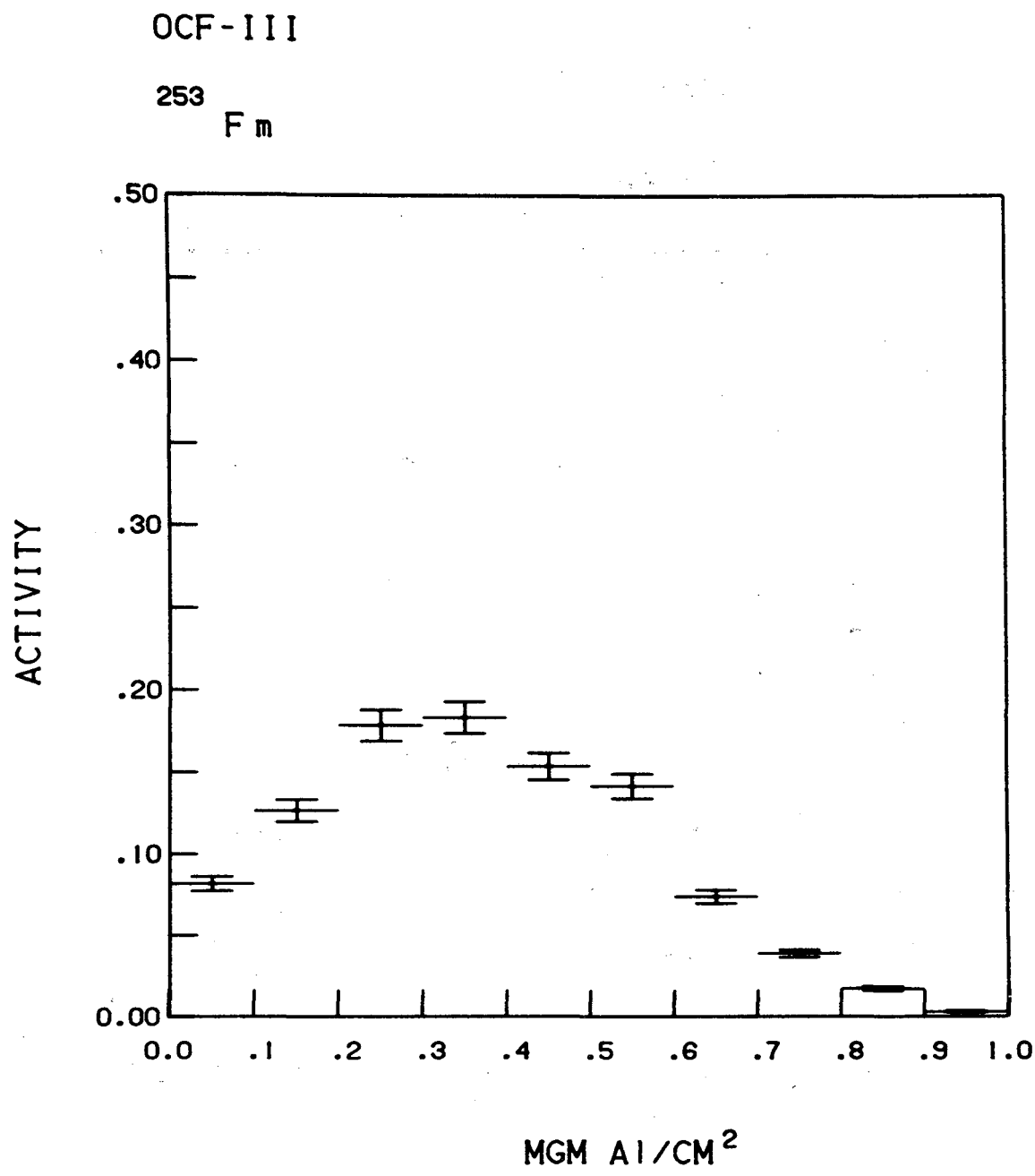
OCF-III
253
Fm
ACTIVITY
.50
.40
.30
.20
.10
0.00
0.0
.1
.2
.3
.4
.5
.6
.7
.8
.9
1.0
MGM Al/CM 2
XBL 823-9531

Fig. 5d

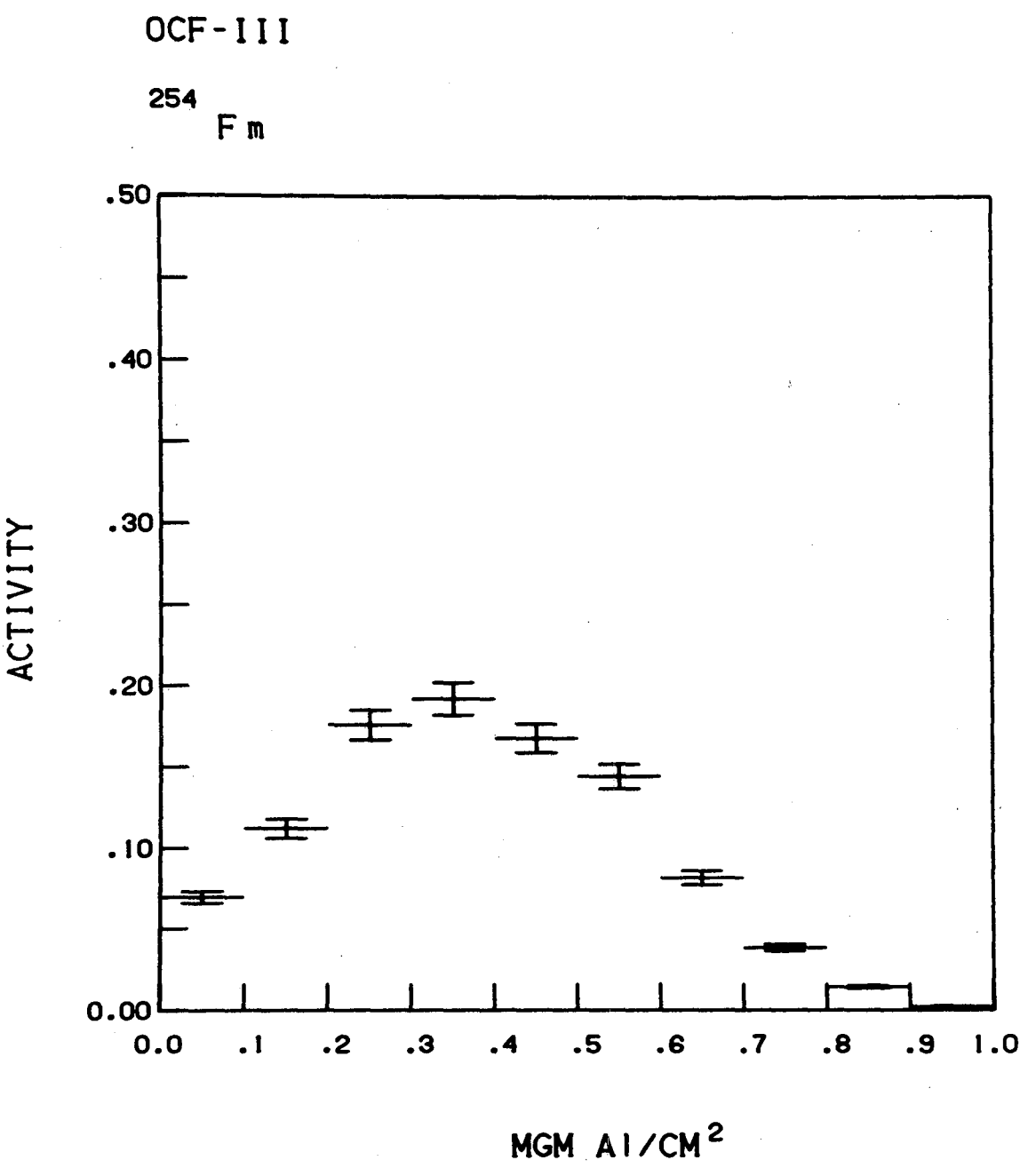
OCF-III
254
Fm
ACTIVITY
.50
.40
.30
.20
.10
0.00
0.0
.1
.2
.3
.4
.5
.6
.7
.8
.9
1.0
MGM Al/CM2
XBL 823-9526

Fig. 5e

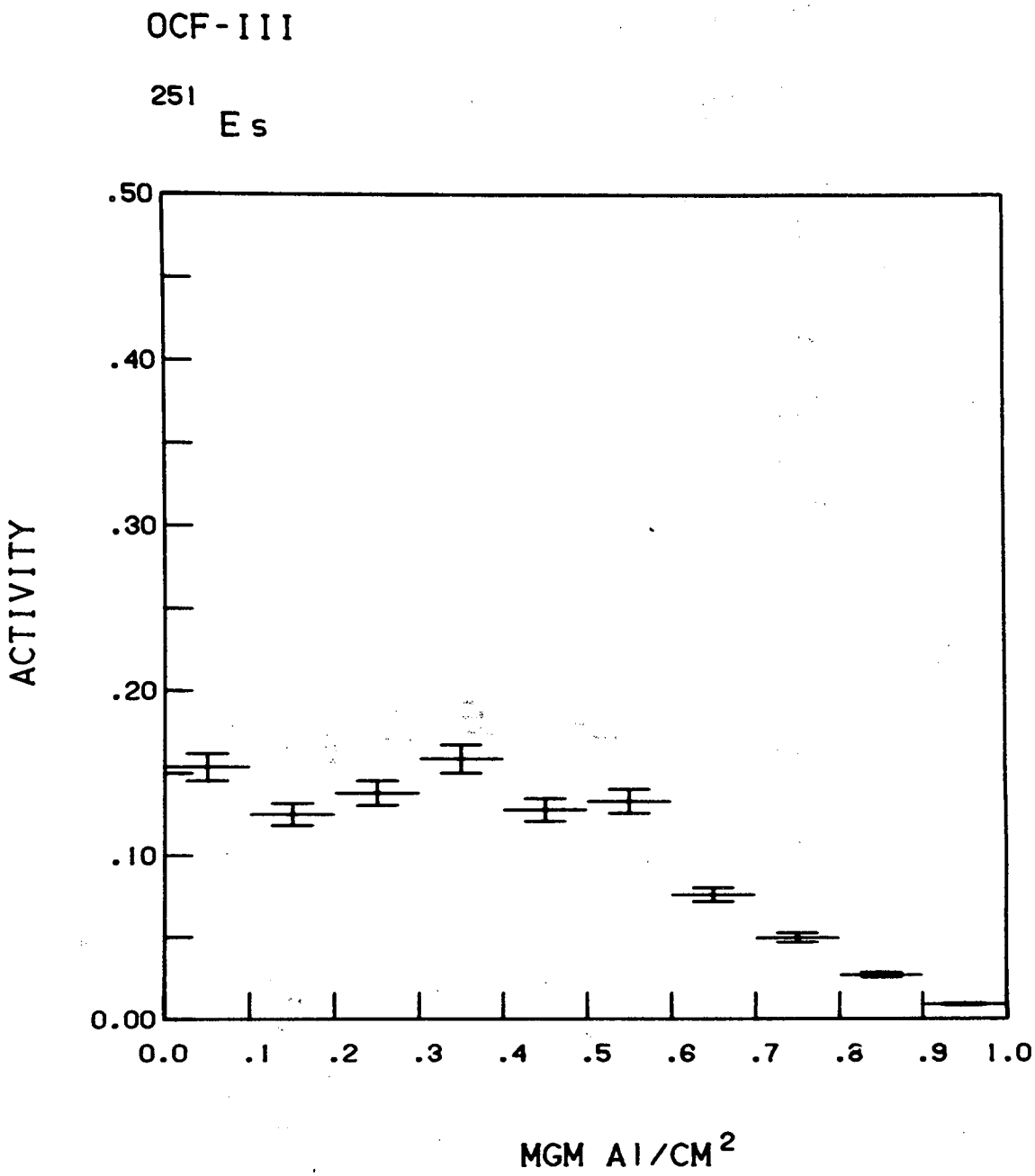
OCF-III
251 Es
ACTIVITY
.50
.40
.30
.20
.10
0.00
0.0
.1
.2
.3
.4
.5
.6
.7
.8
.9
1.0
MGM Al/CM 2
XBL 823-9528

Fig. 6a

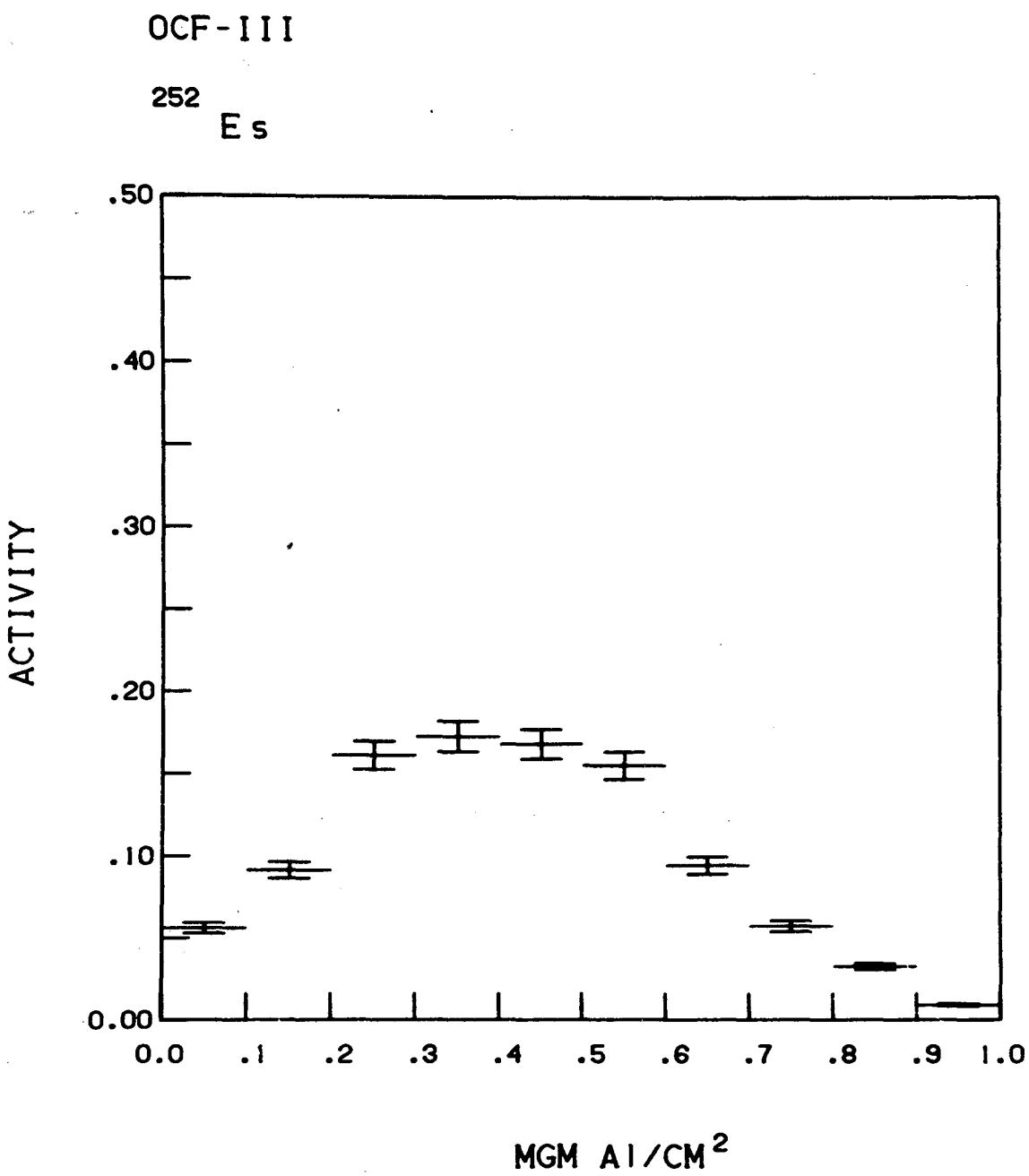
OCF-III
252
Es
.50
.40
.30
.20
.10
0.00
ACTIVITY
0.0
.1
.2
.3
.4
.5
.6
.7
.8
.9
1.0
MGM Al/CM 2
XBL 823-9532

Fig. 6b

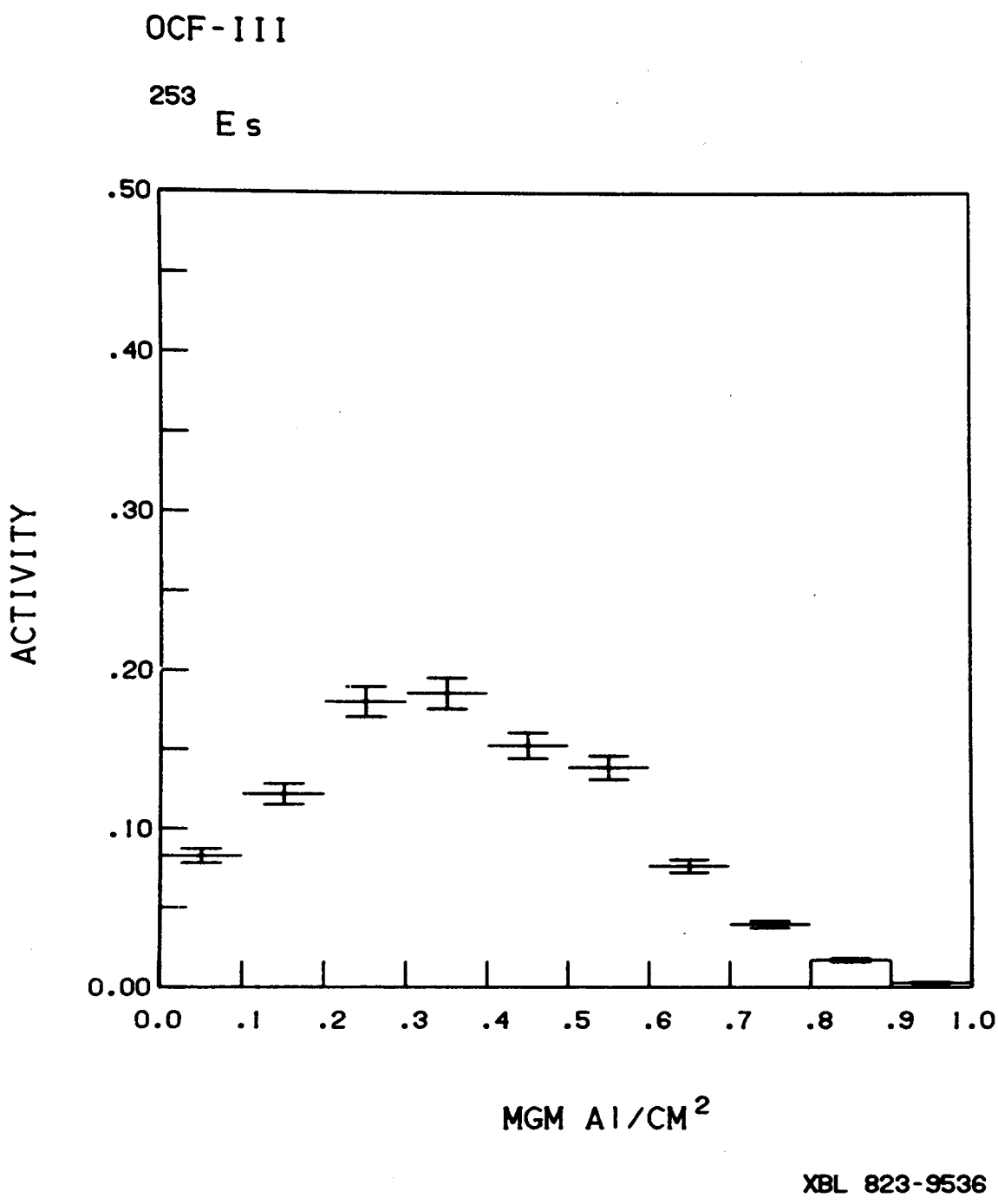
OCF-III
253
Es
ACTIVITY
.50
.40
.30
.20
.10
0.00
0.0
.1
.2
.3
.4
.5
.6
.7
.8
.9
1.0
MGM Al/CM 2
XBL 823-9536

Fig. 6c

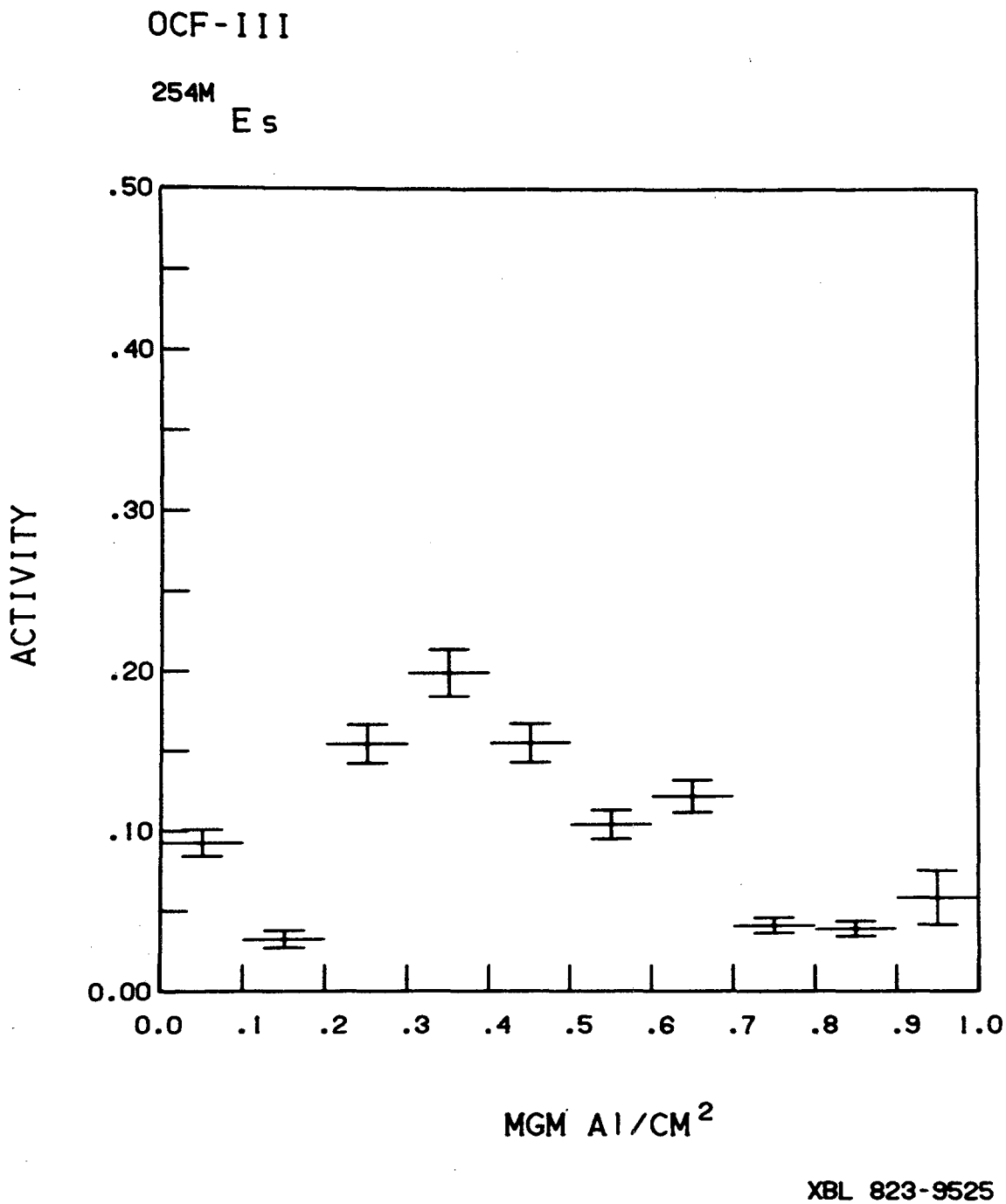
OCF-III
254M Es
ACTIVITY
.50
.40
.30
.20
.10
0.00
0.0
.1
.2
.3
.4
.5
.6
.7
.8
.9
1.0
MGM Al/CM 2
XBL 823-9525

Fig. 6d

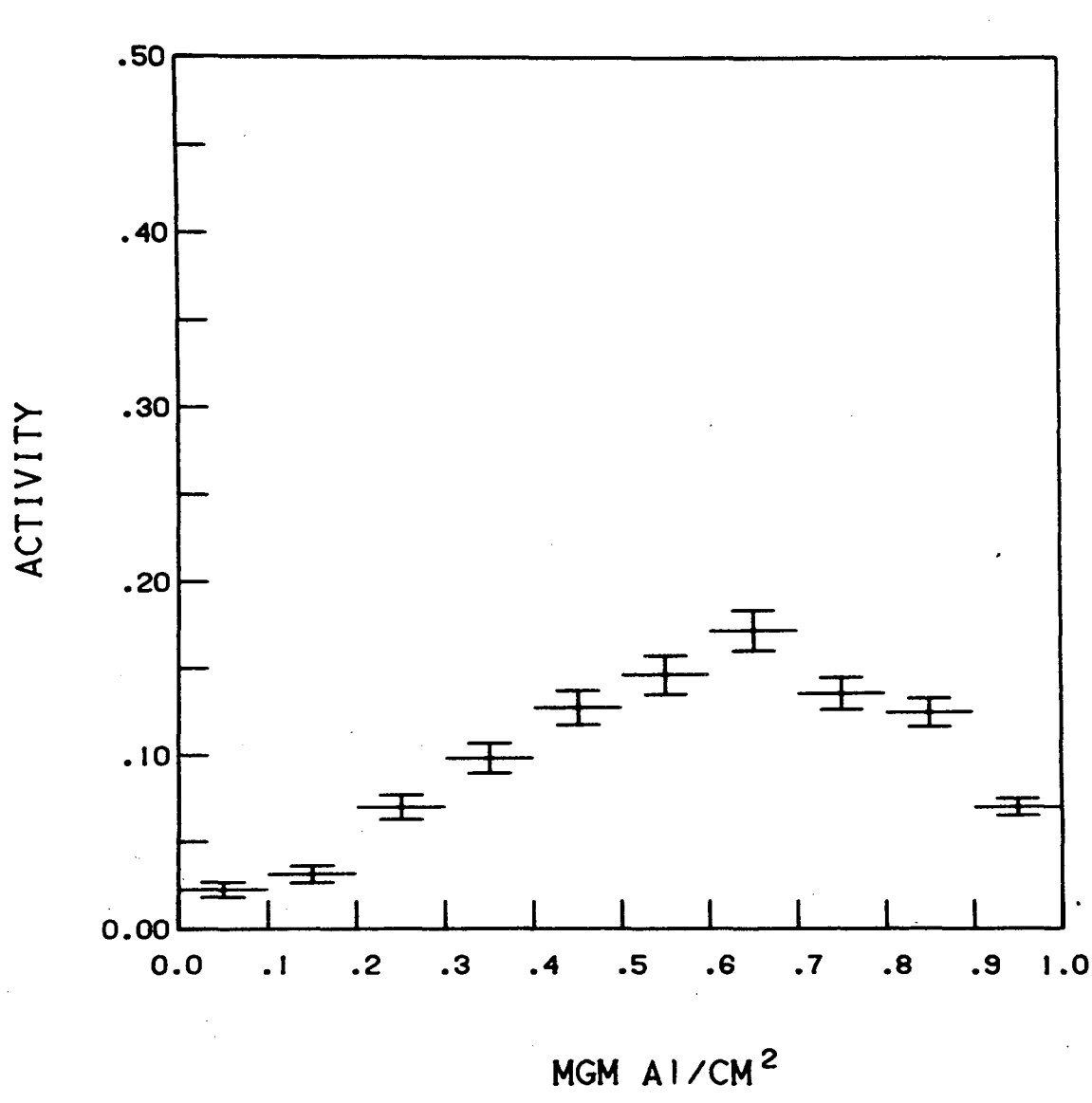
OCF-III
246 Cf
.50
.40
.30
.20
.10
0.00
ACTIVITY
0.0
.1
.2
.3
.4
.5
.6
.7
.8
.9
1.0
MGM Al/CM 2
XBL 823-9533

Fig. 7a

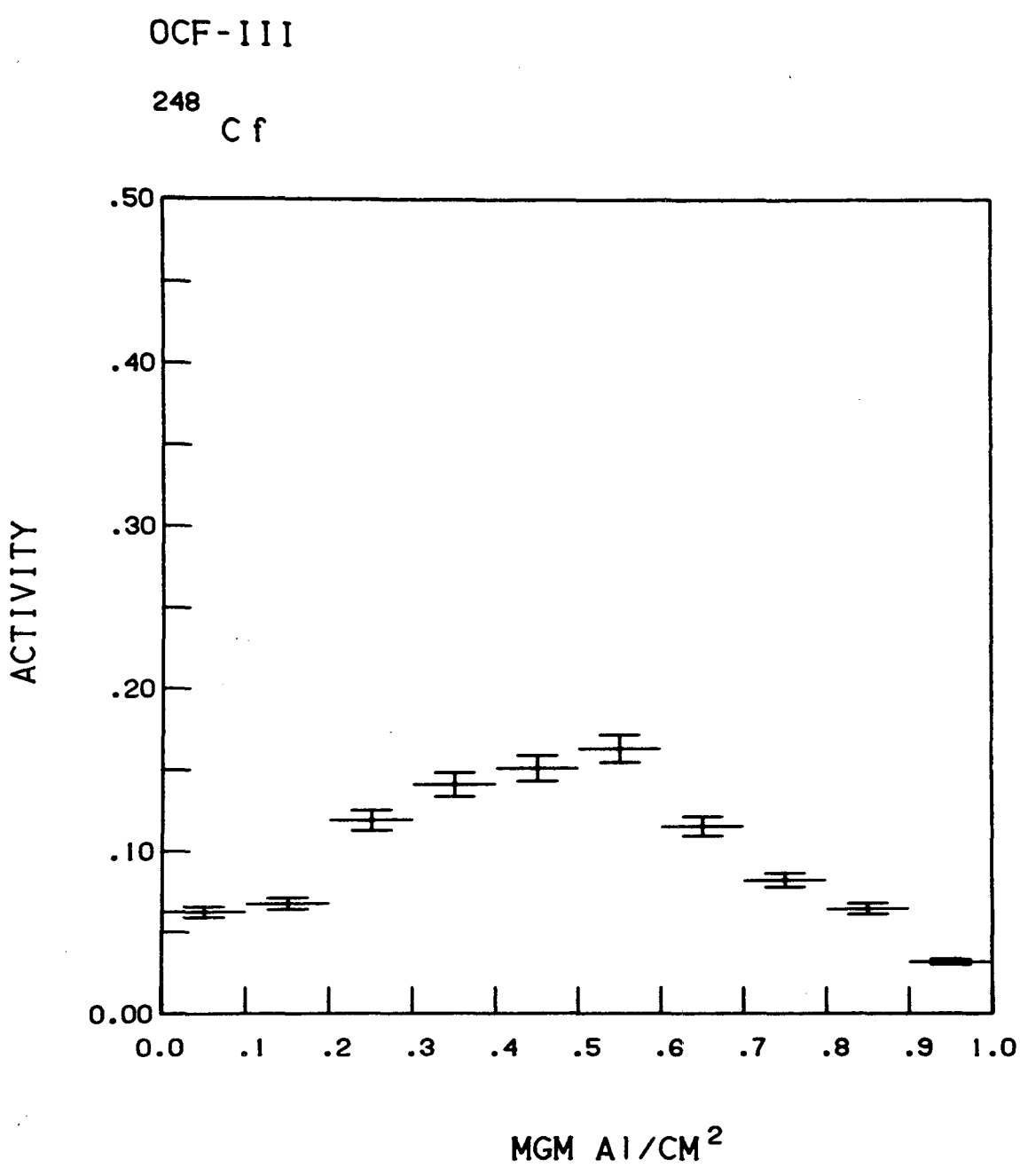
OCF-III
248 Cf
ACTIVITY
.50
.40
.30
.20
.10
0.00
0.0
.1
.2
.3
.4
.5
.6
.7
.8
.9
1.0
MGM Al/CM 2
XBL 823-9530

Fig. 7b

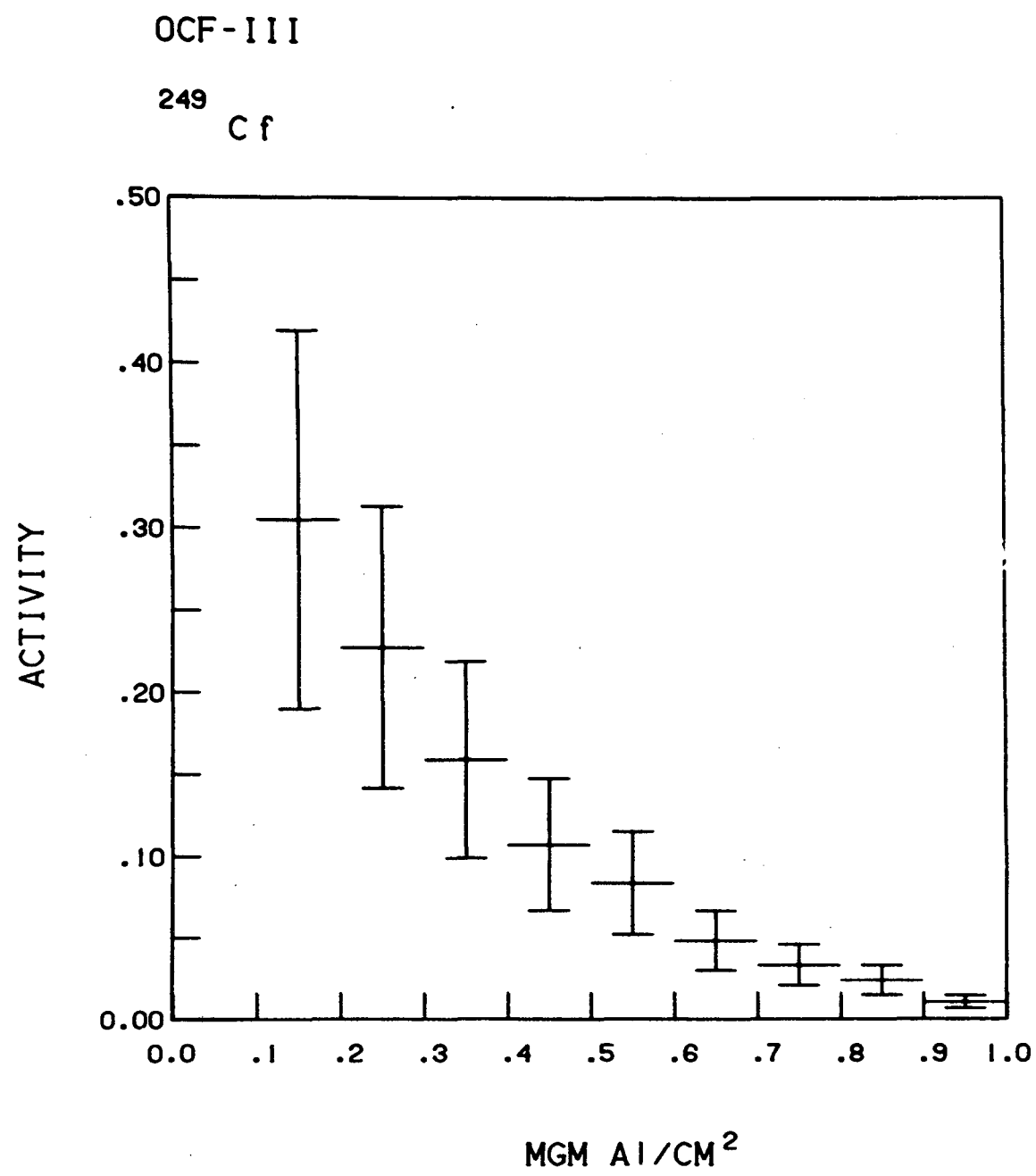
OCF-III
249
Cf
.50
.40
.30
.20
.10
0.00
ACTIVITY
0.0
.1
.2
.3
.4
.5
.6
.7
.8
.9
1.0
MGM Al/CM 2
XBL 823-9534

Fig. 7c

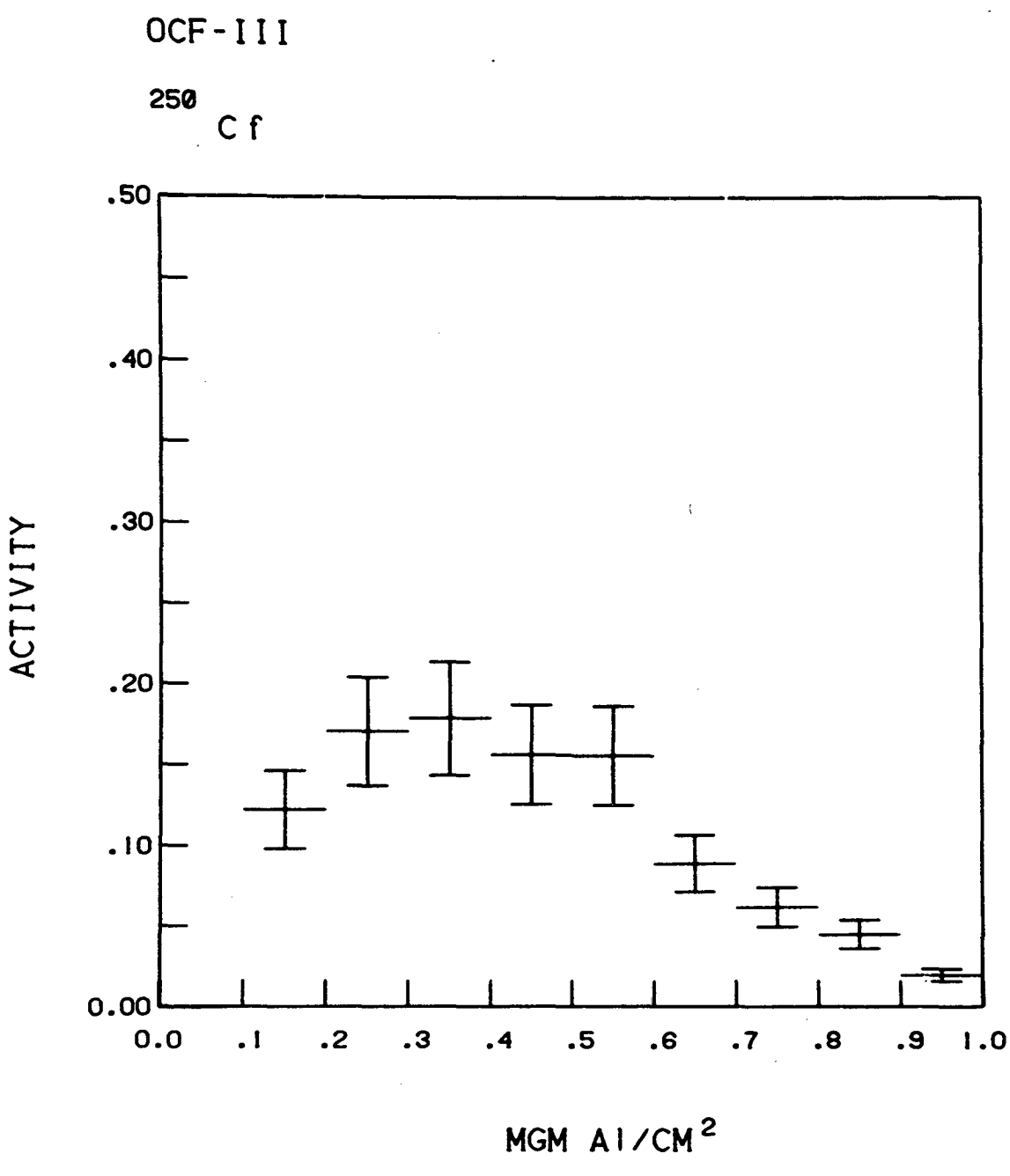
OCF-III
250 Cf
ACTIVITY
.50
.40
.30
.20
.10
0.00
0.0
.1
.2
.3
.4
.5
.6
.7
.8
.9
1.0
MGM Al/CM 2
XBL 823-9535

Fig. 7d

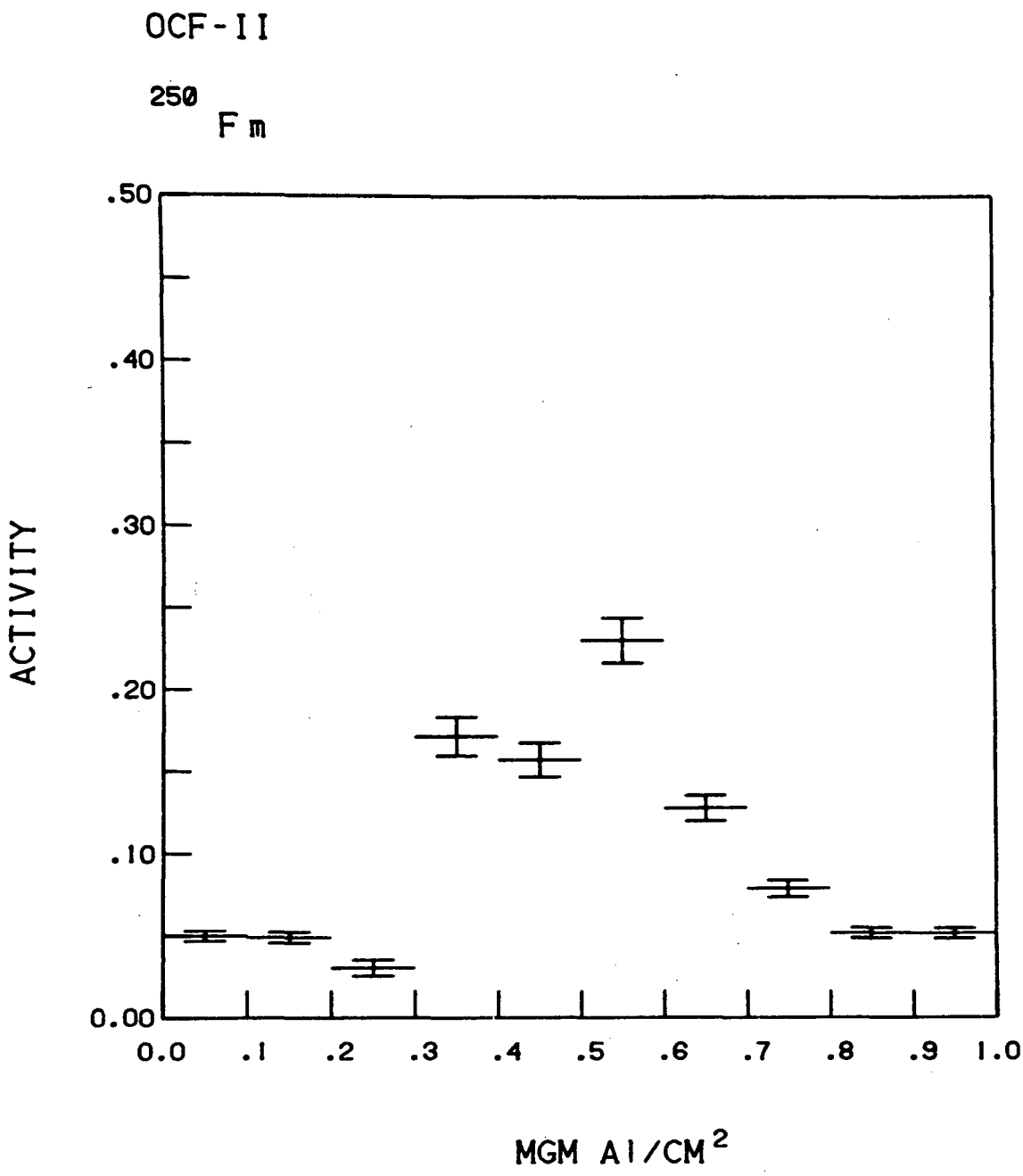
OCF-II
250
Fm
ACTIVITY
.50
.40
.30
.20
.10
0.00
0.0
.1
.2
.3
.4
.5
.6
.7
.8
.9
1.0
MGM Al/CM 2
XBL 823-9513

Fig. 8a

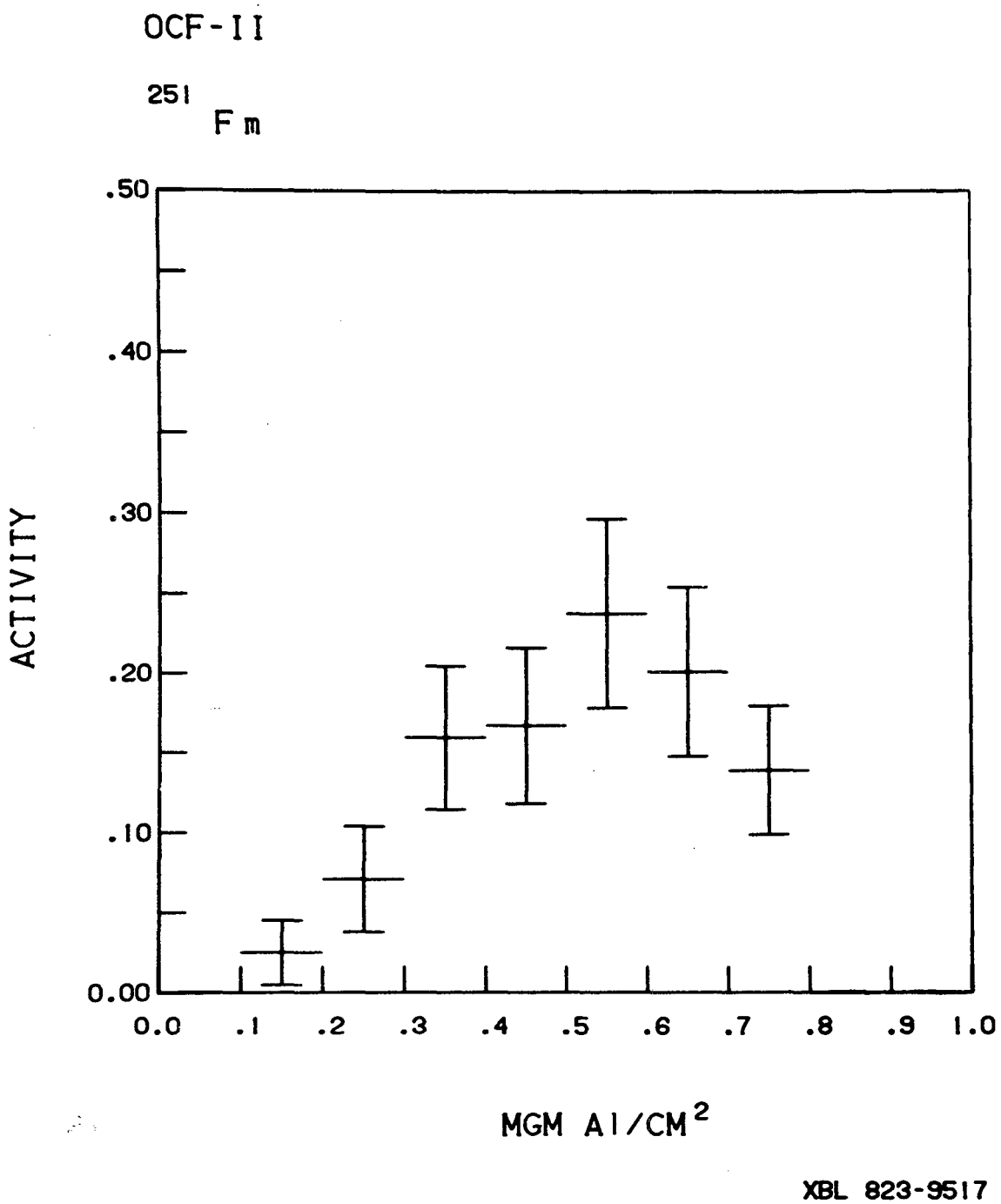
OCF-II
251 Fm
.50
.40
.30
.20
.10
0.00
ACTIVITY
0.0
.1
.2
.3
.4
.5
.6
.7
.8
.9
1.0
MGM Al/CM 2
XBL 823-9517

Fig. 8b

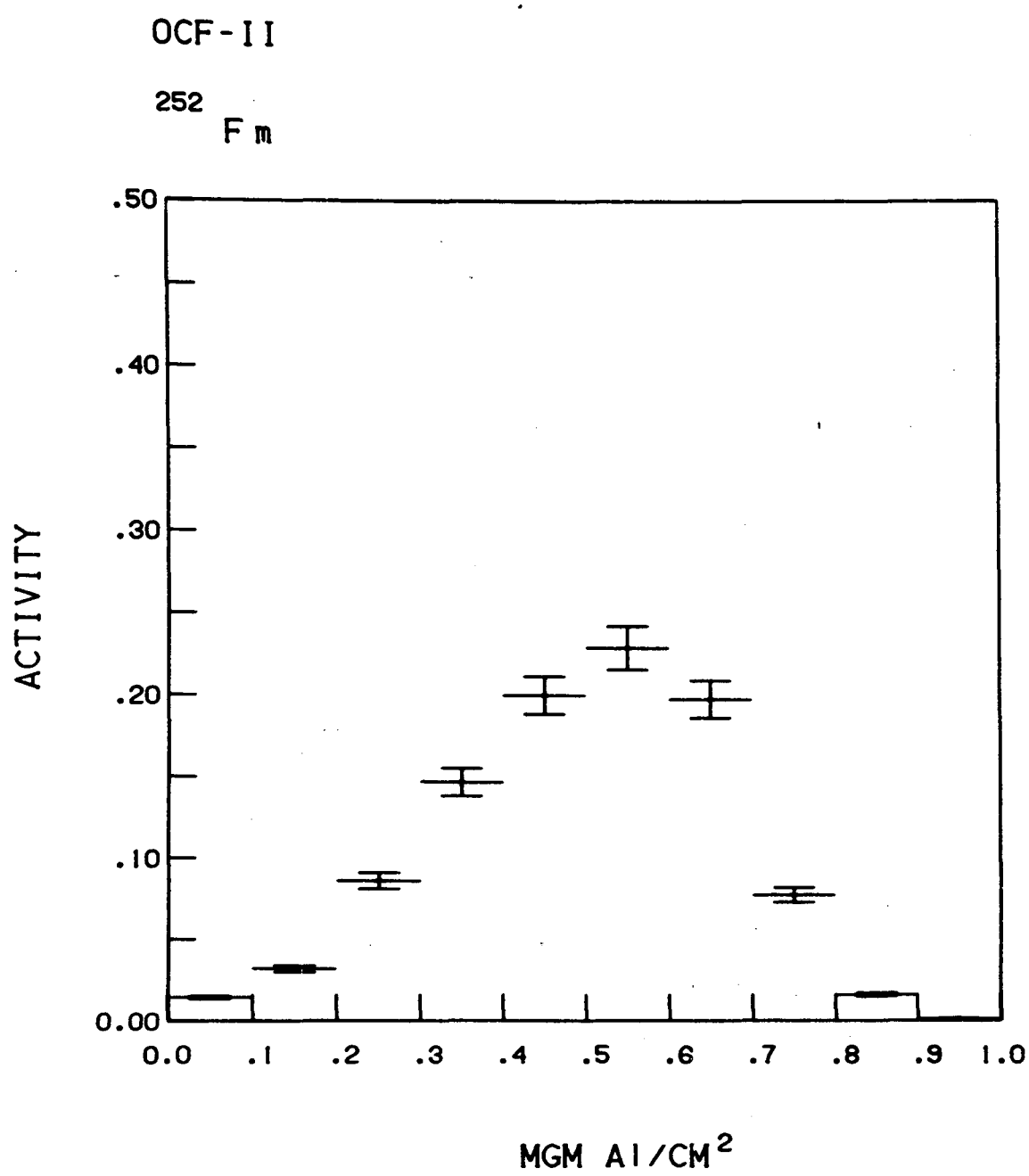
OCF-II
252
Fm
ACTIVITY
.50
.40
.30
.20
.10
0.00
0.0
.1
.2
.3
.4
.5
.6
.7
.8
.9
1.0
MGM Al/CM2
XBL 823-9518

Fig. 8c

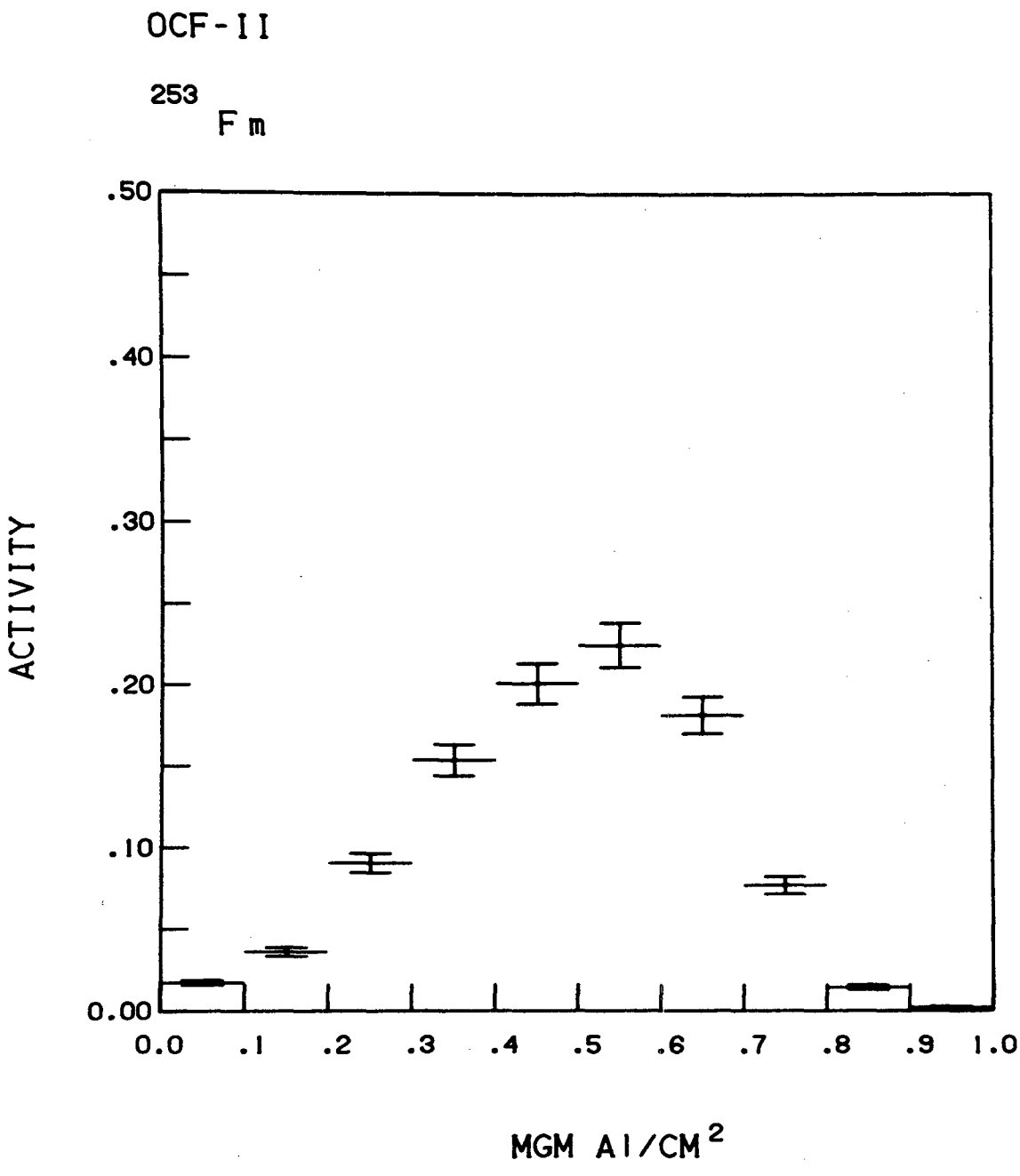
OCF-II
253
Fm
ACTIVITY
.50
.40
.30
.20
.10
0.00
0.0
.1
.2
.3
.4
.5
.6
.7
.8
.9
1.0
MGM Al/CM 2
XBL 823-9519

Fig. 8d

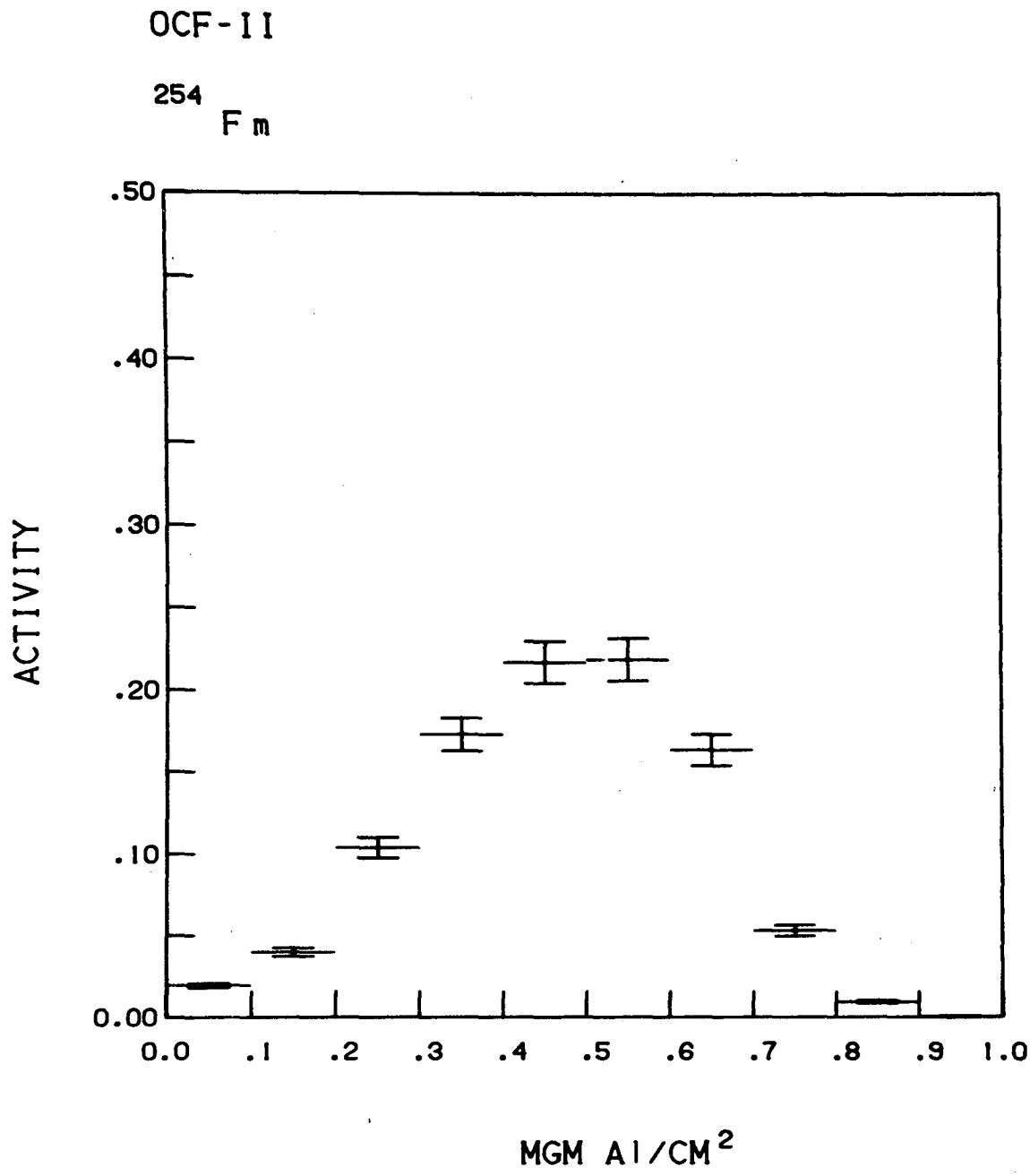
OCF-II
254
Fm
ACTIVITY
.50
.40
.30
.20
.10
0.00
0.0
.1
.2
.3
.4
.5
.6
.7
.8
.9
1.0
MGM Al/CM2
XBL 823-9515

Fig. 8e

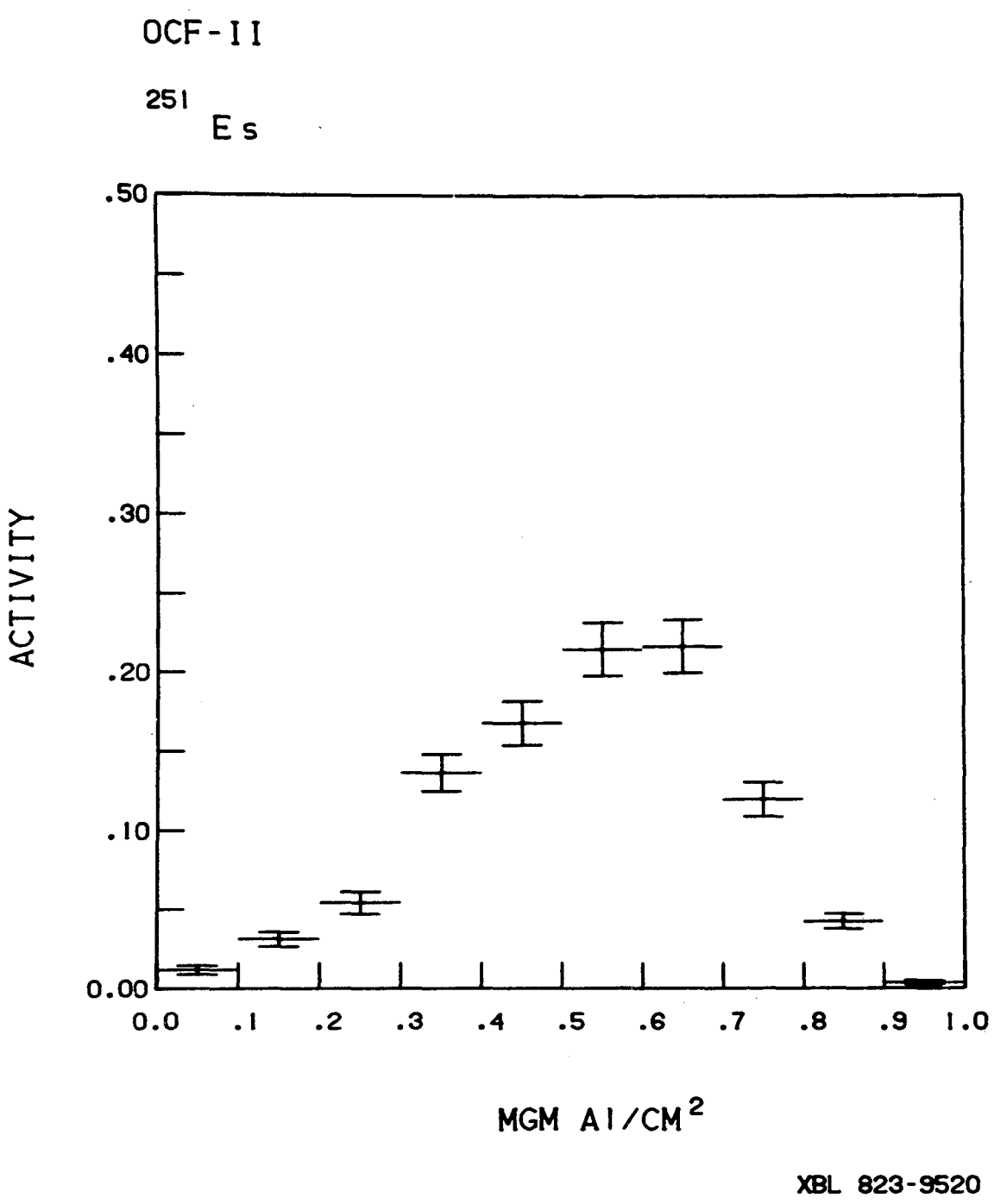
OCF-II
251
Es
ACTIVITY
.50
.40
.30
.20
.10
0.00
0.0
.1
.2
.3
.4
.5
.6
.7
.8
.9
1.0
MGM Al/CM 2
XBL 823-9520

Fig. 9a

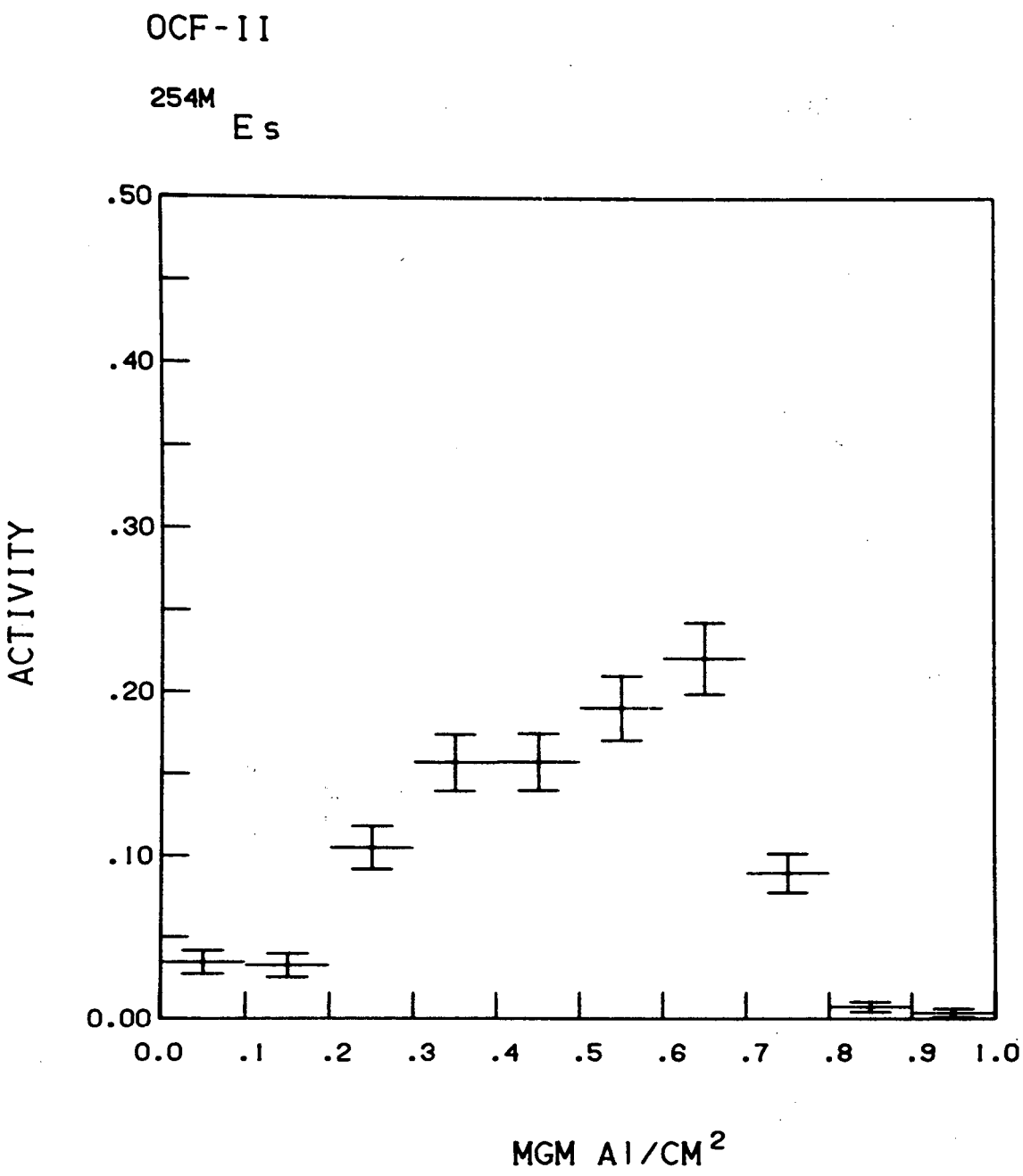
OCF-II
254M
Es
ACTIVITY
.50
.40
.30
.20
.10
0.00
0.0
.1
.2
.3
.4
.5
.6
.7
.8
.9
1.0
MGM Al/CM 2
XBL 823-9514

Fig. 9b

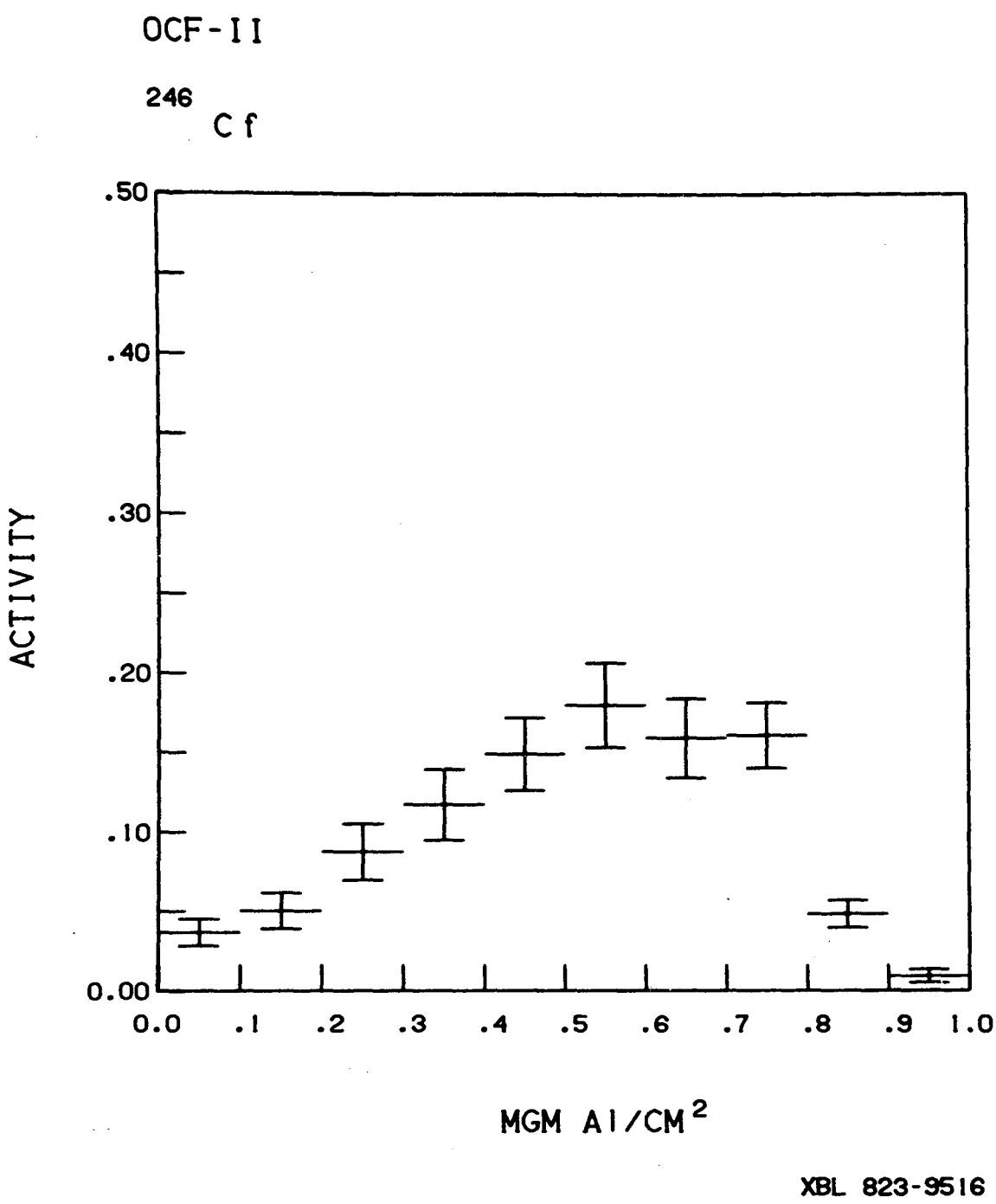
OCF-II
246 Cf
ACTIVITY
.50
.40
.30
.20
.10
0.00
0.0
.1
.2
.3
.4
.5
.6
.7
.8
.9
1.0
MGM Al/CM 2
XBL 823-9516

Fig. 10a

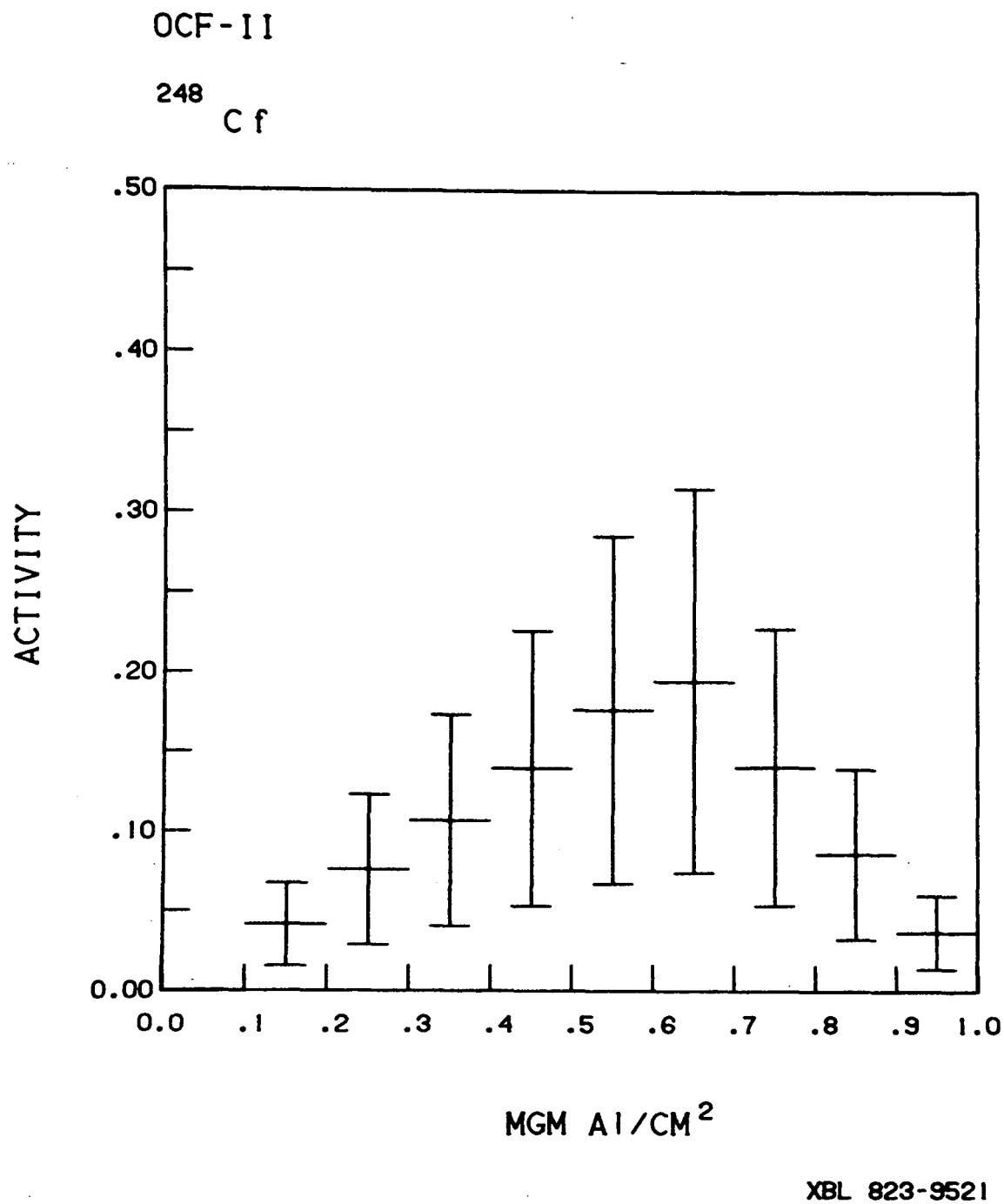
OCF-II
248 Cf
ACTIVITY
.50
.40
.30
.20
.10
0.00
0.0
.1
.2
.3
.4
.5
.6
.7
.8
.9
1.0
MGM Al/CM 2
XBL 823-9521

Fig. 10b

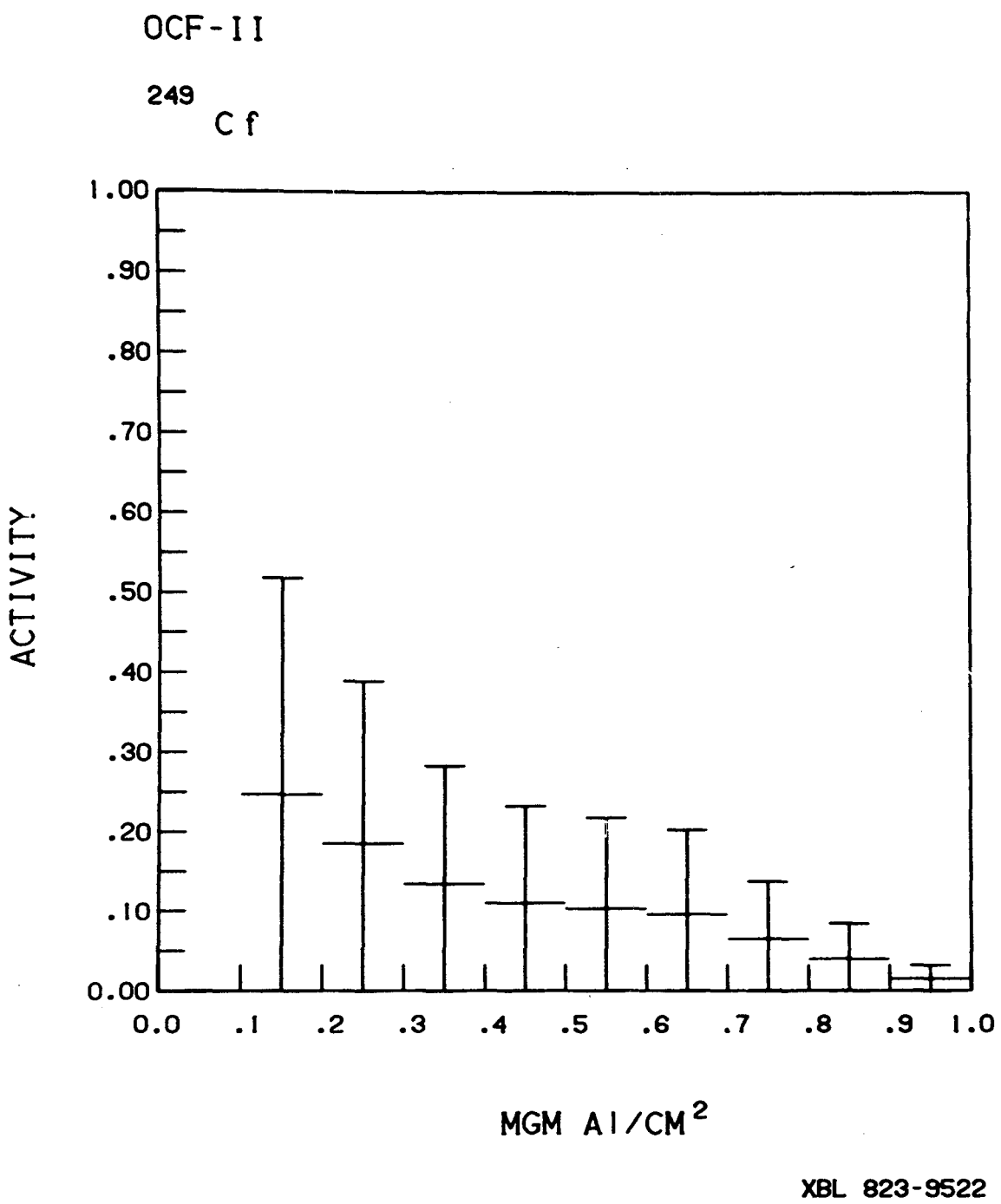
OCF-II
249
Cf
ACTIVITY
1.00
.90
.80
.70
.60
.50
.40
.30
.20
.10
0.00
0.0
.1
.2
.3
.4
.5
.6
.7
.8
.9
1.0
MGM Al/CM 2
XBL 823-9522

Fig. 10c

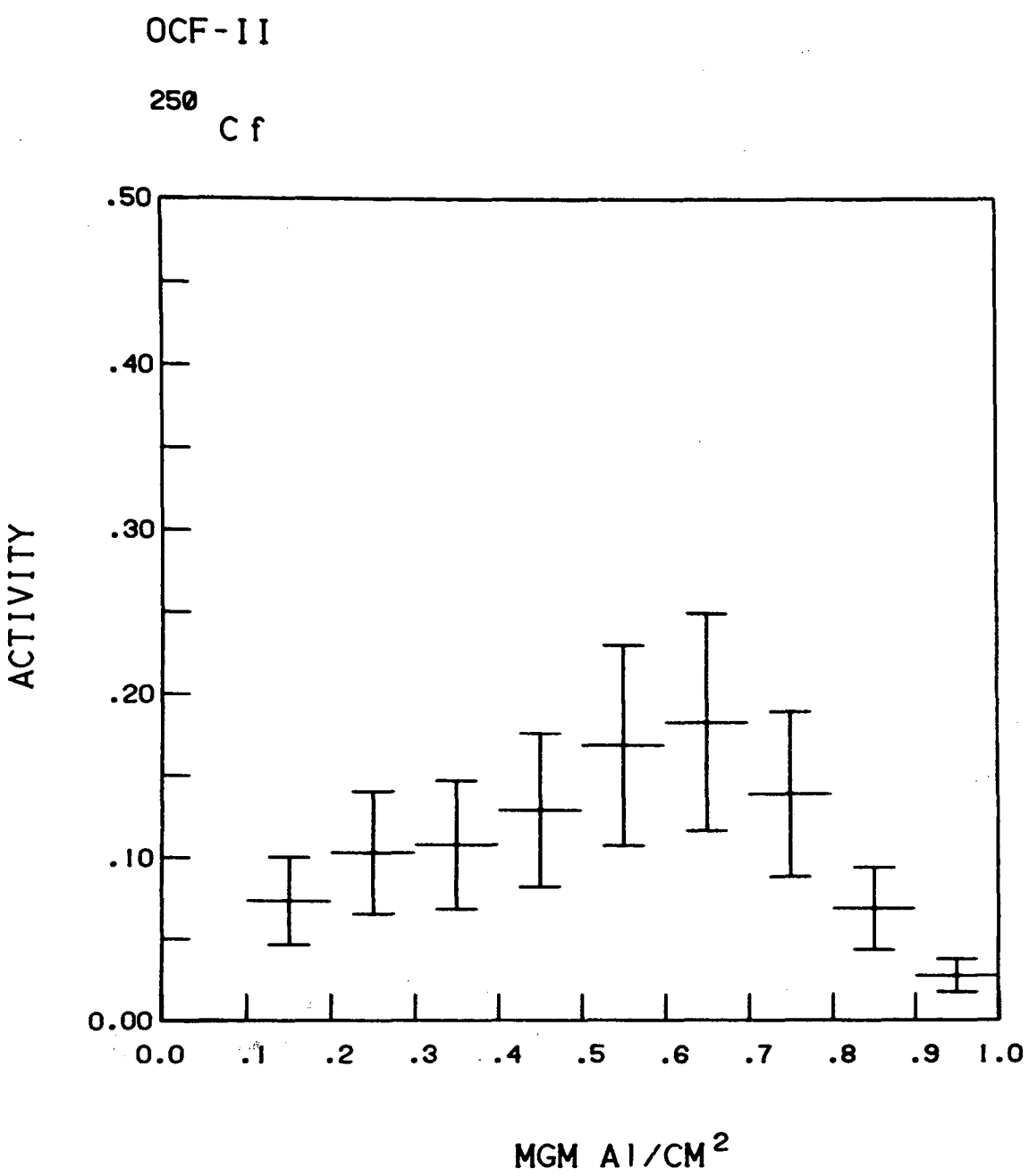
OCF-II
250 Cf
ACTIVITY
.50
.40
.30
.20
.10
0.00
0.0
.1
.2
.3
.4
.5
.6
.7
.8
.9
1.0
MGM Al/CM 2
XBL 823-9523

Fig. 10d

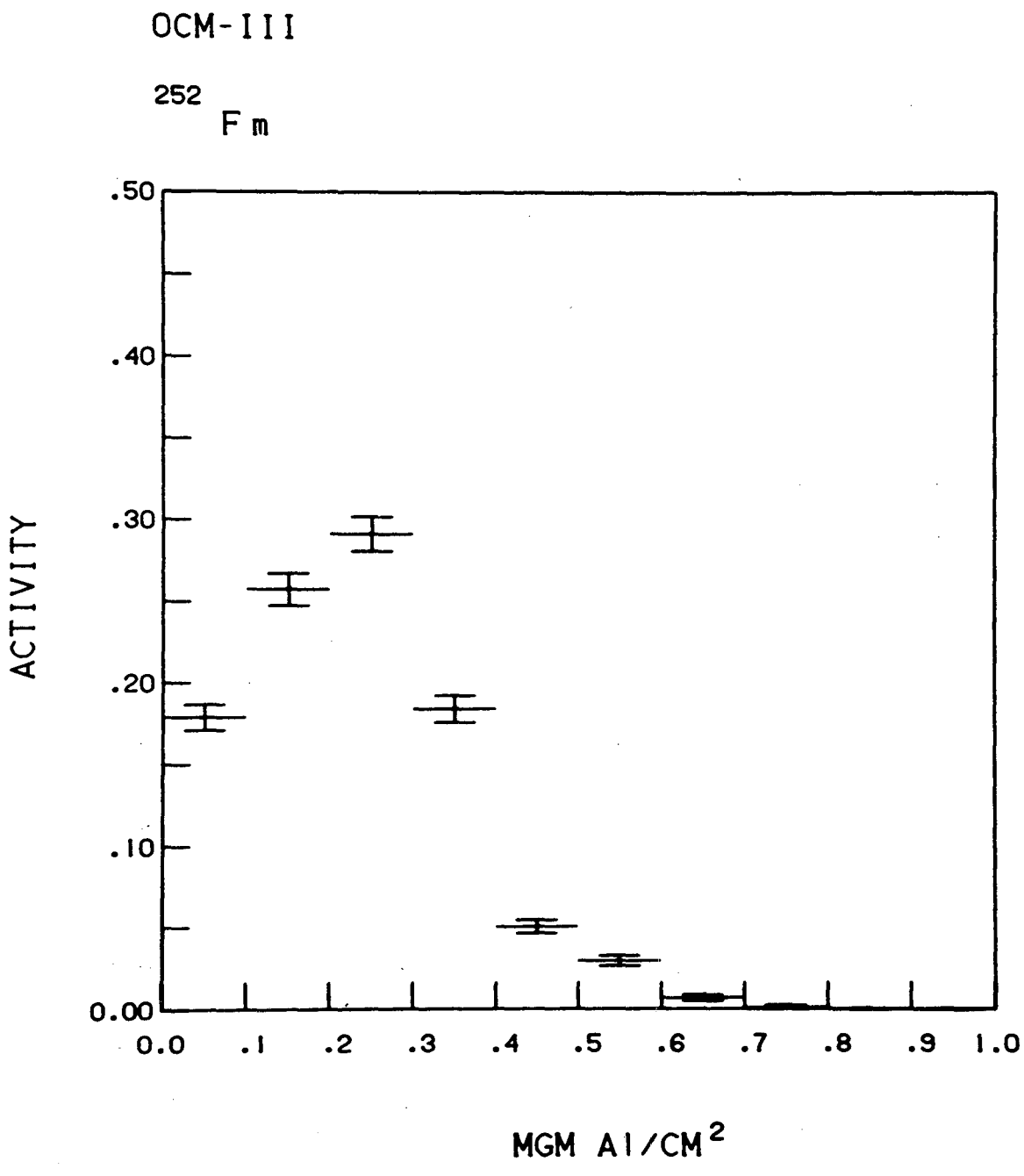
OCM-III
252
Fm
ACTIVITY
.50
.40
.30
.20
.10
0.00
0.0
.1
.2
.3
.4
.5
.6
.7
.8
.9
1.0
MGM Al/CM2
XBL 823-9554

Fig. 11

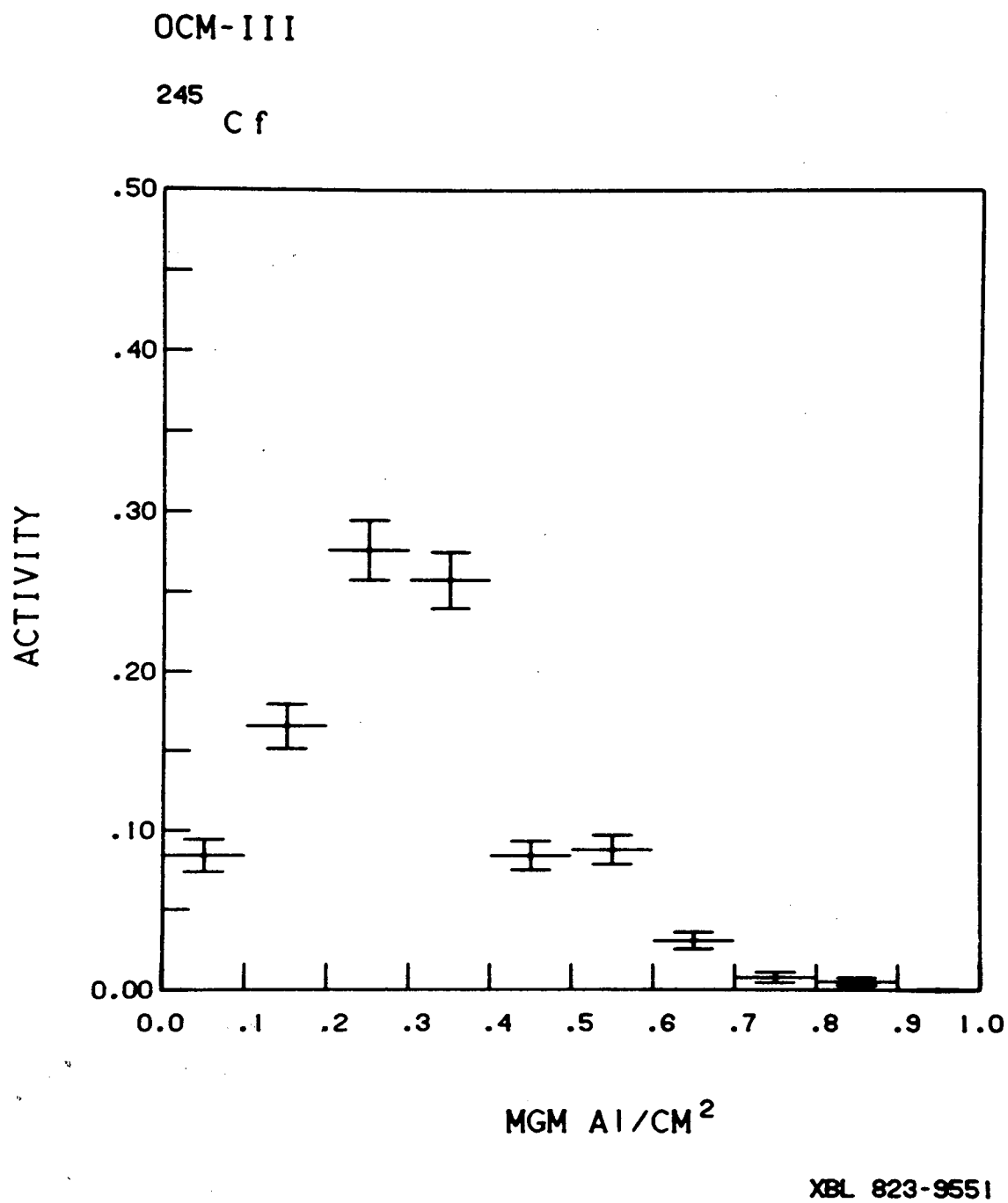
OCM-III
245
Cf
ACTIVITY
.50
.40
.30
.20
.10
0.00
0.0
.1
.2
.3
.4
.5
.6
.7
.8
.9
1.0
MGM Al/CM2
XBL 823-9551

Fig. 12a

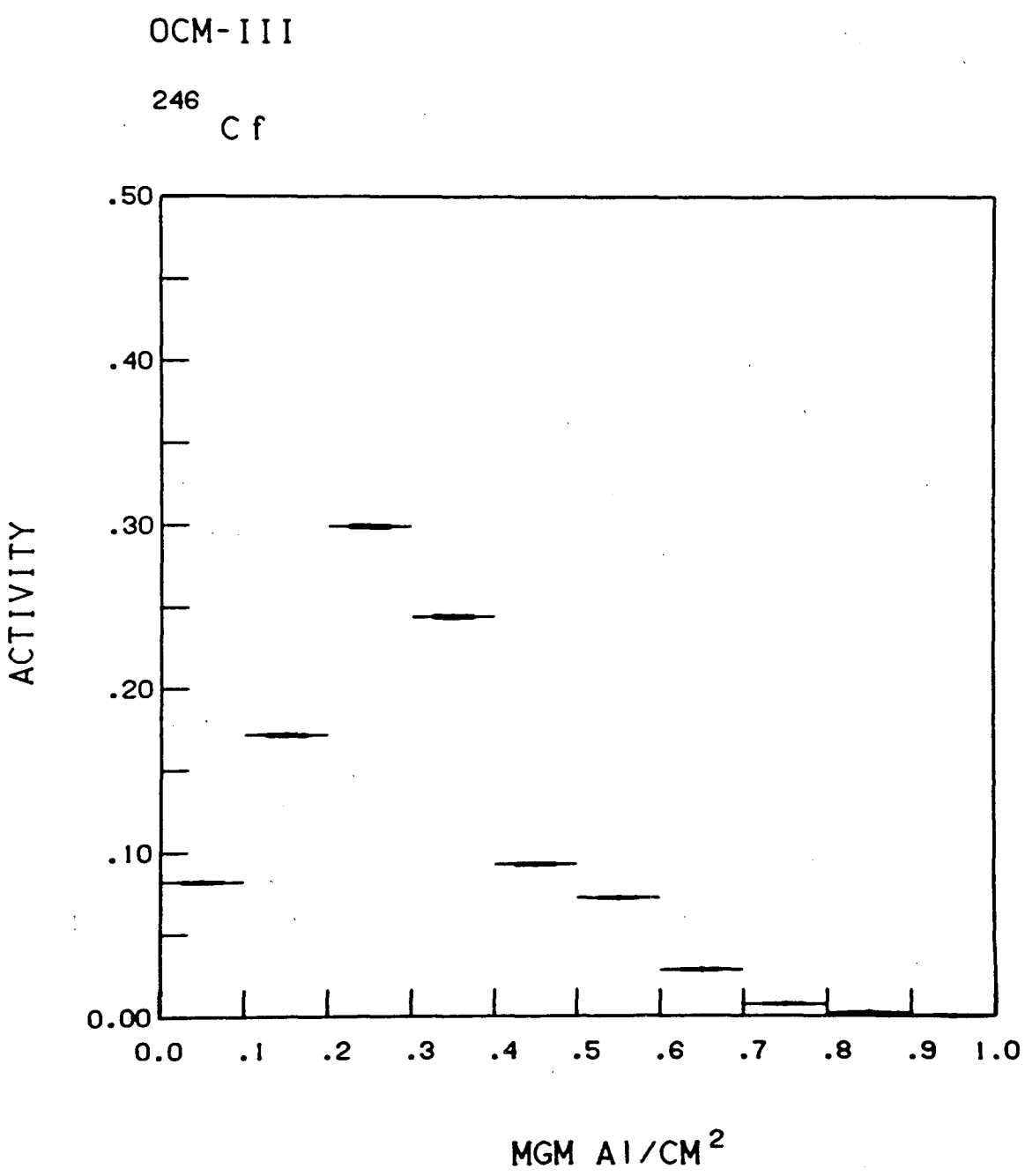
OCM-III
246 Cf
ACTIVITY
.50
.40
.30
.20
.10
0.00
0.0
.1
.2
.3
.4
.5
.6
.7
.8
.9
1.0
MGM Al/CM 2
XBL 823-9550

Fig. 12b

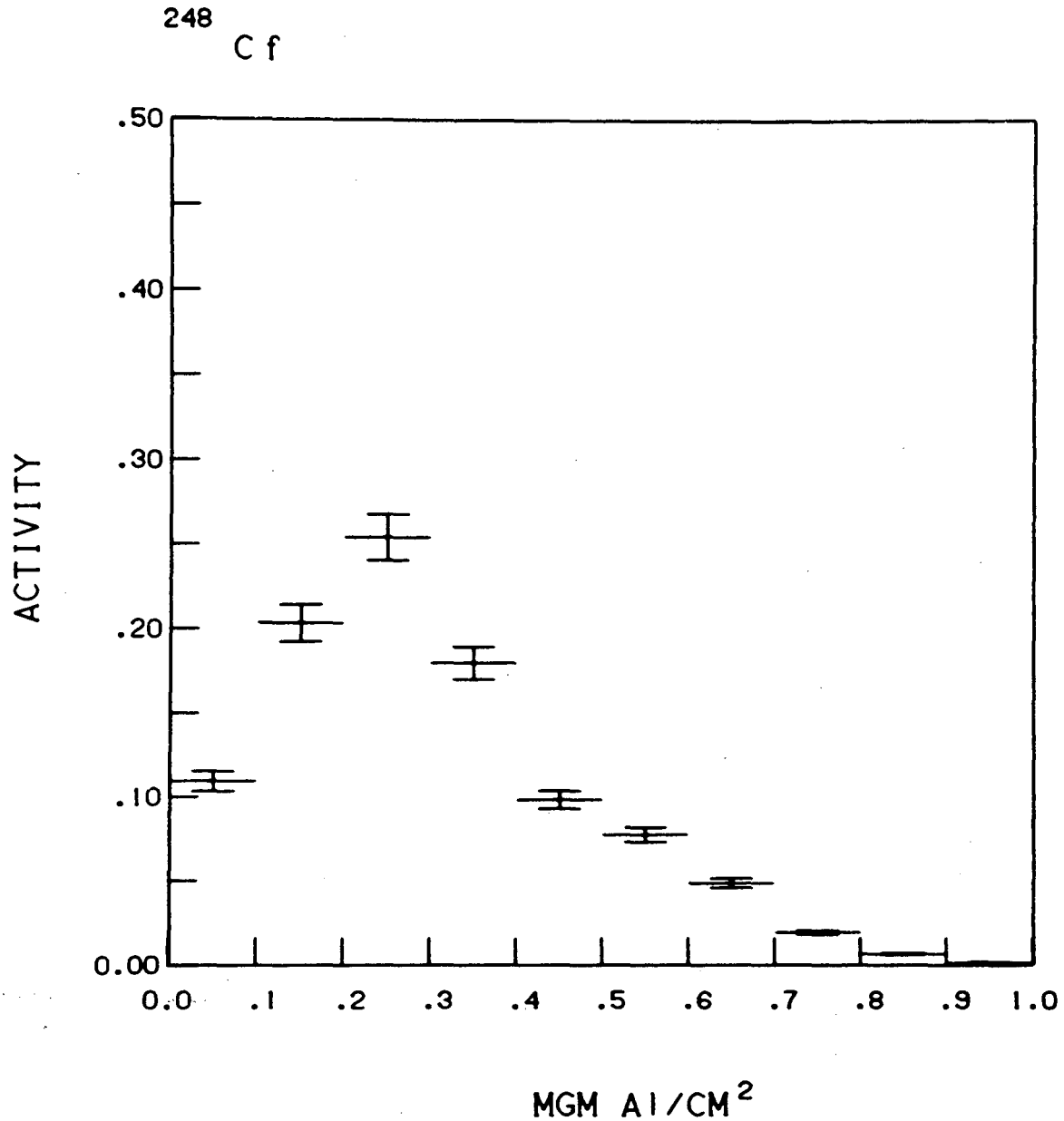
248
Cf
.50
.40
.30
.20
.10
0.00
ACTIVITY
0.0
.1
.2
.3
.4
.5
.6
.7
.8
.9
1.0
MGM Al/CM 2
XBL 823-9552

Fig. 12c

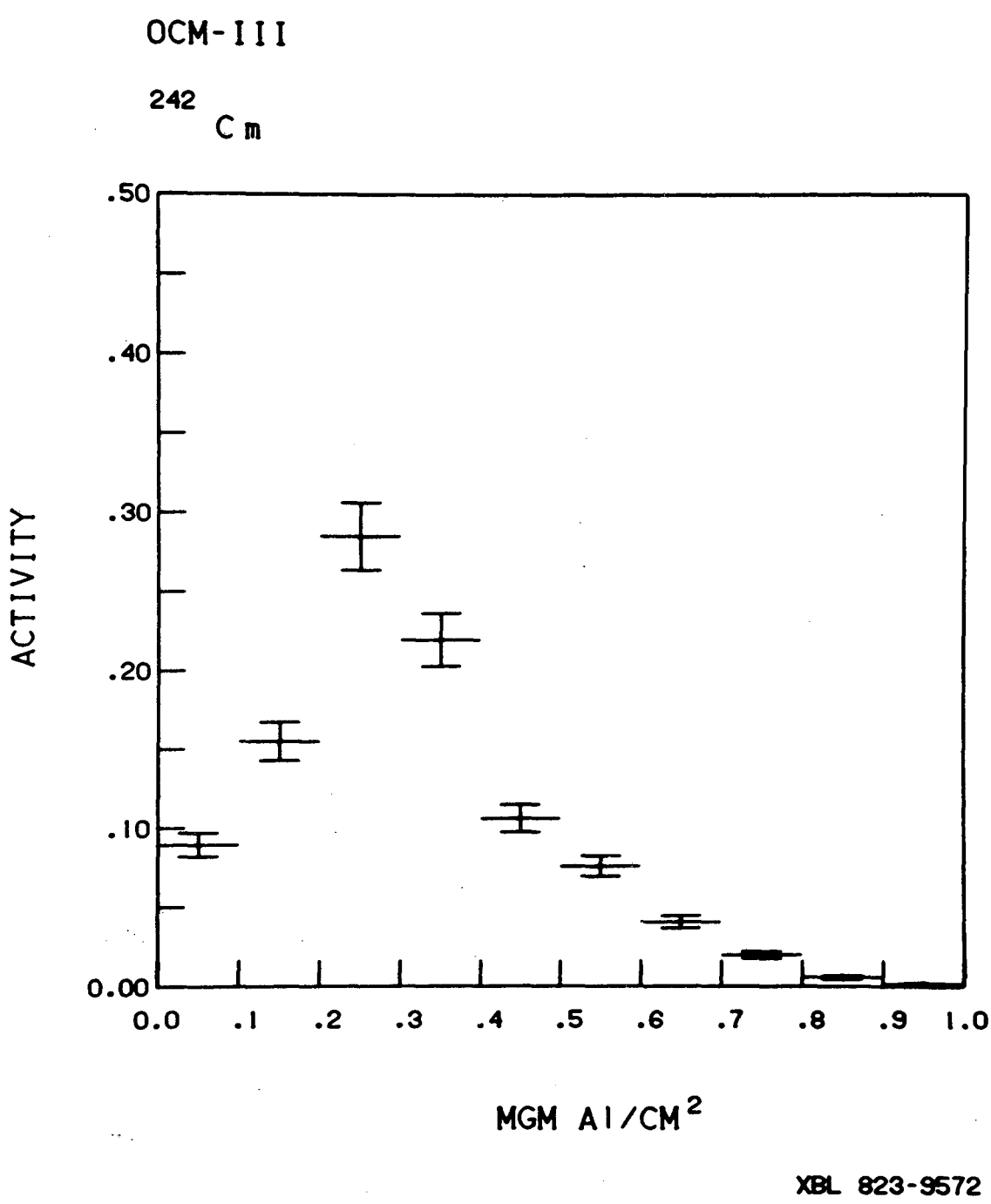
OCM-III
242 Cm
ACTIVITY
.50
.40
.30
.20
.10
0.00
0.0
.1
.2
.3
.4
.5
.6
.7
.8
.9
1.0
MGM Al/CM2
XBL 823-9572

Fig. 13a

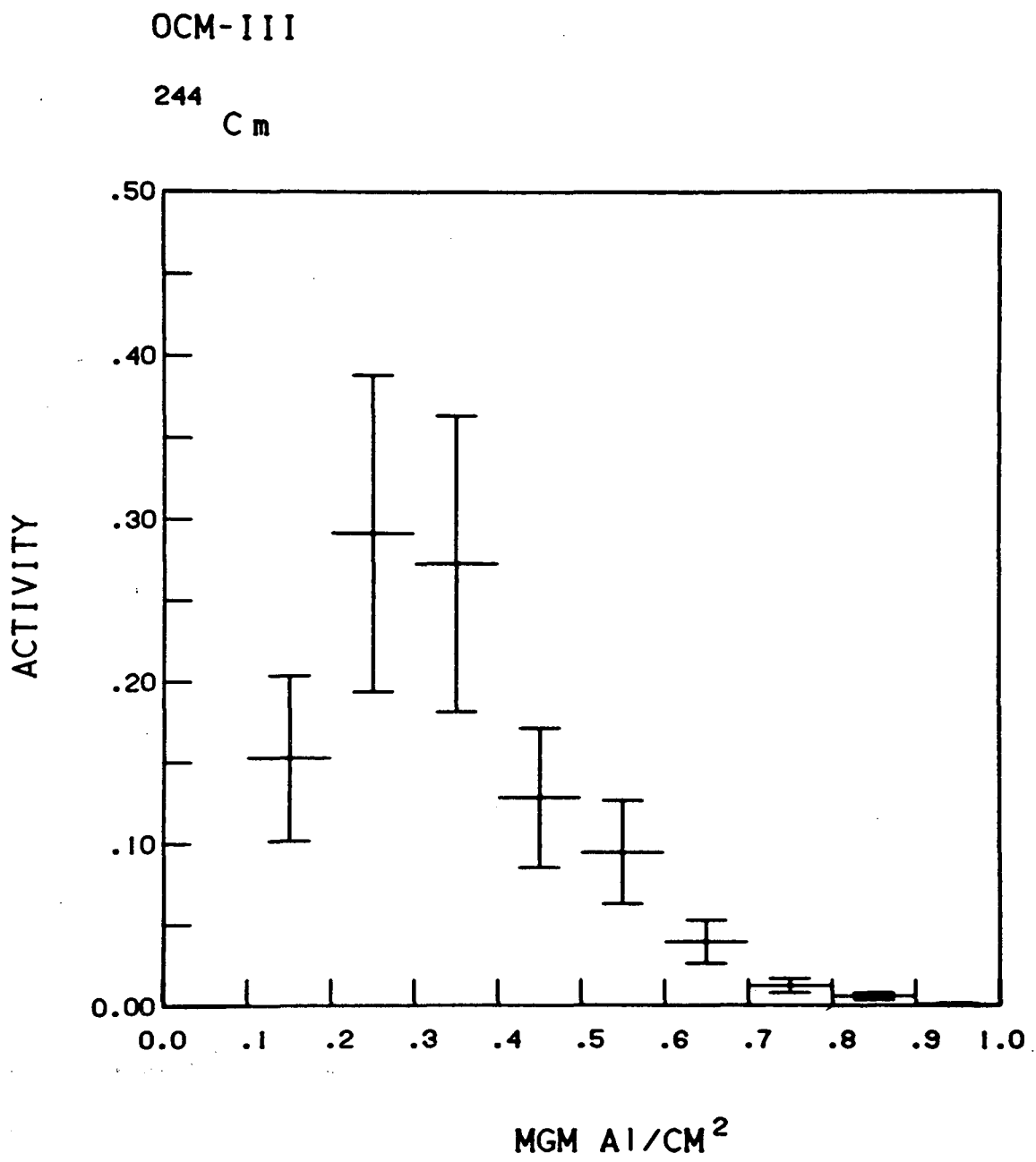
OCM-III
244 Cm
ACTIVITY
.50
.40
.30
.20
.10
0.00
0.0
.1
.2
.3
.4
.5
.6
.7
.8
.9
1.0
MGM Al/CM 2
XBL 823-9562

Fig. 13b

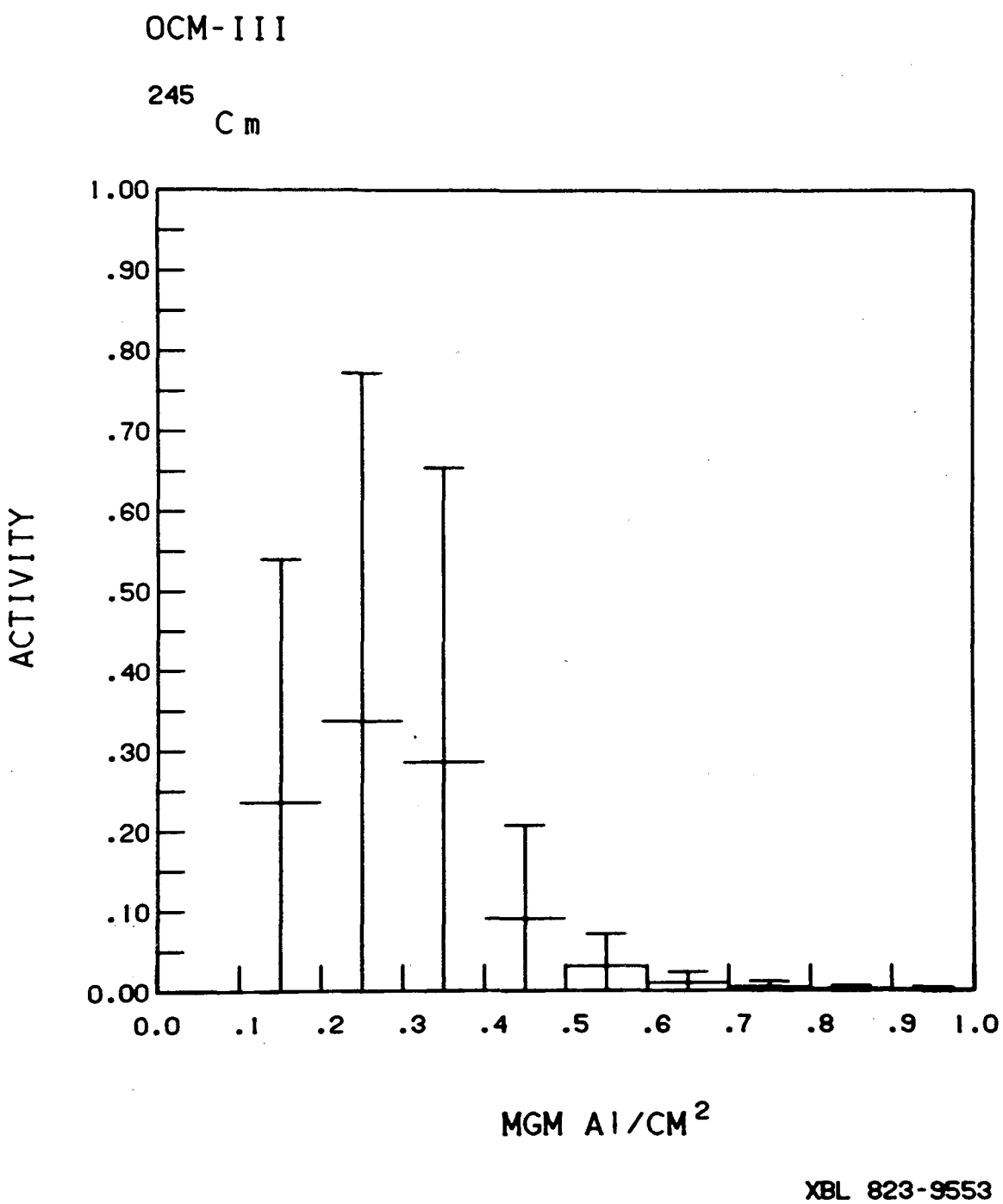
OCM-III
245
Cm
ACTIVITY
1.00
.90
.80
.70
.60
.50
.40
.30
.20
.10
0.00
0.0
.1
.2
.3
.4
.5
.6
.7
.8
.9
1.0
MGM Al/CM 2
XBL 823-9553

Fig. 13c

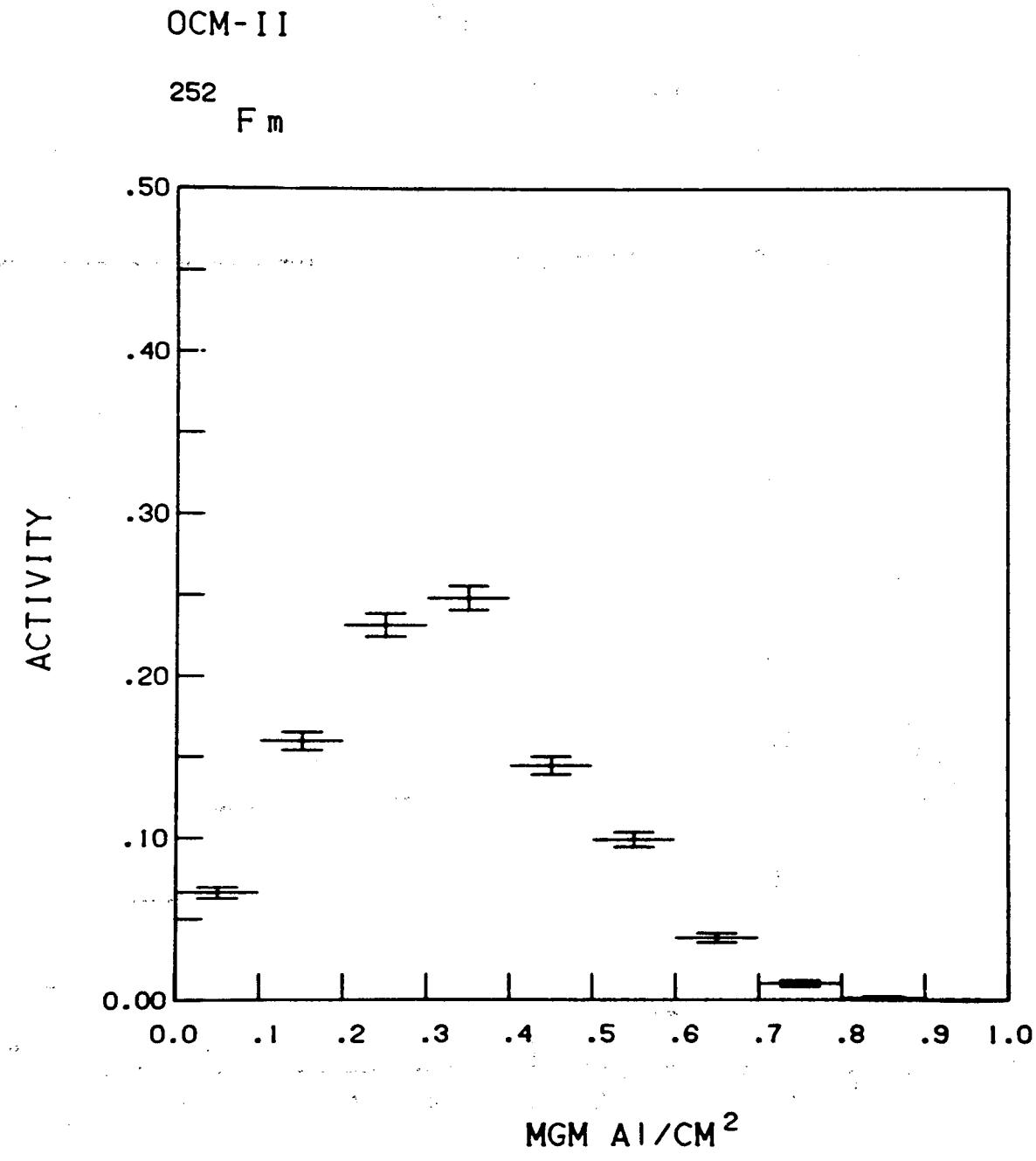
OCM-II
252 Fm
ACTIVITY
.50
.40
.30
.20
.10
0.00
0.0
.1
.2
.3
.4
.5
.6
.7
.8
.9
1.0
MGM Al/CM 2
XBL 823-9557

Fig. 14

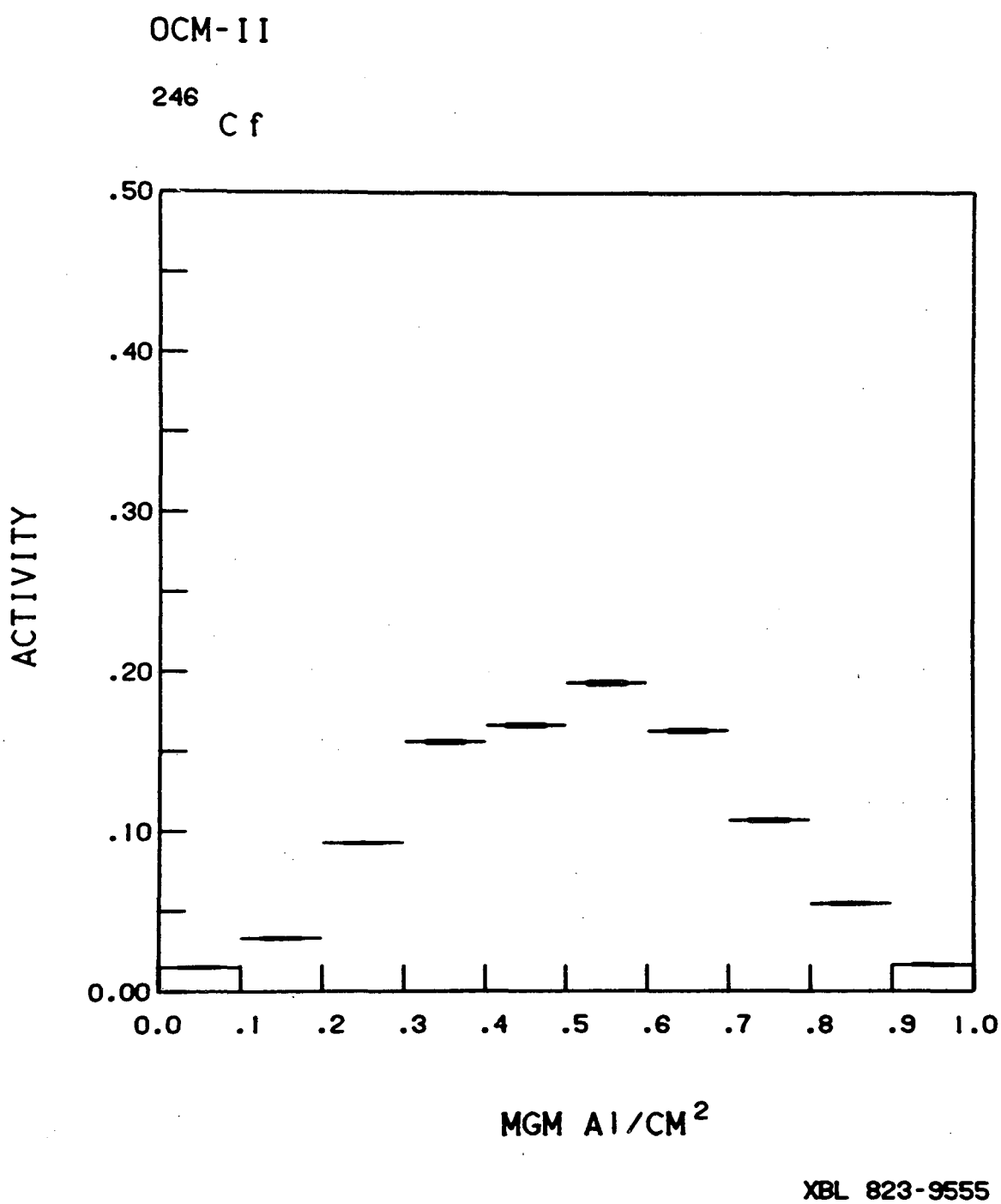
OCM-II
246
Cf
ACTIVITY
.50
.40
.30
.20
.10
0.00
0.0
.1
.2
.3
.4
.5
.6
.7
.8
.9
1.0
MGM Al/CM2
XBL 823-9555

Fig. 15a

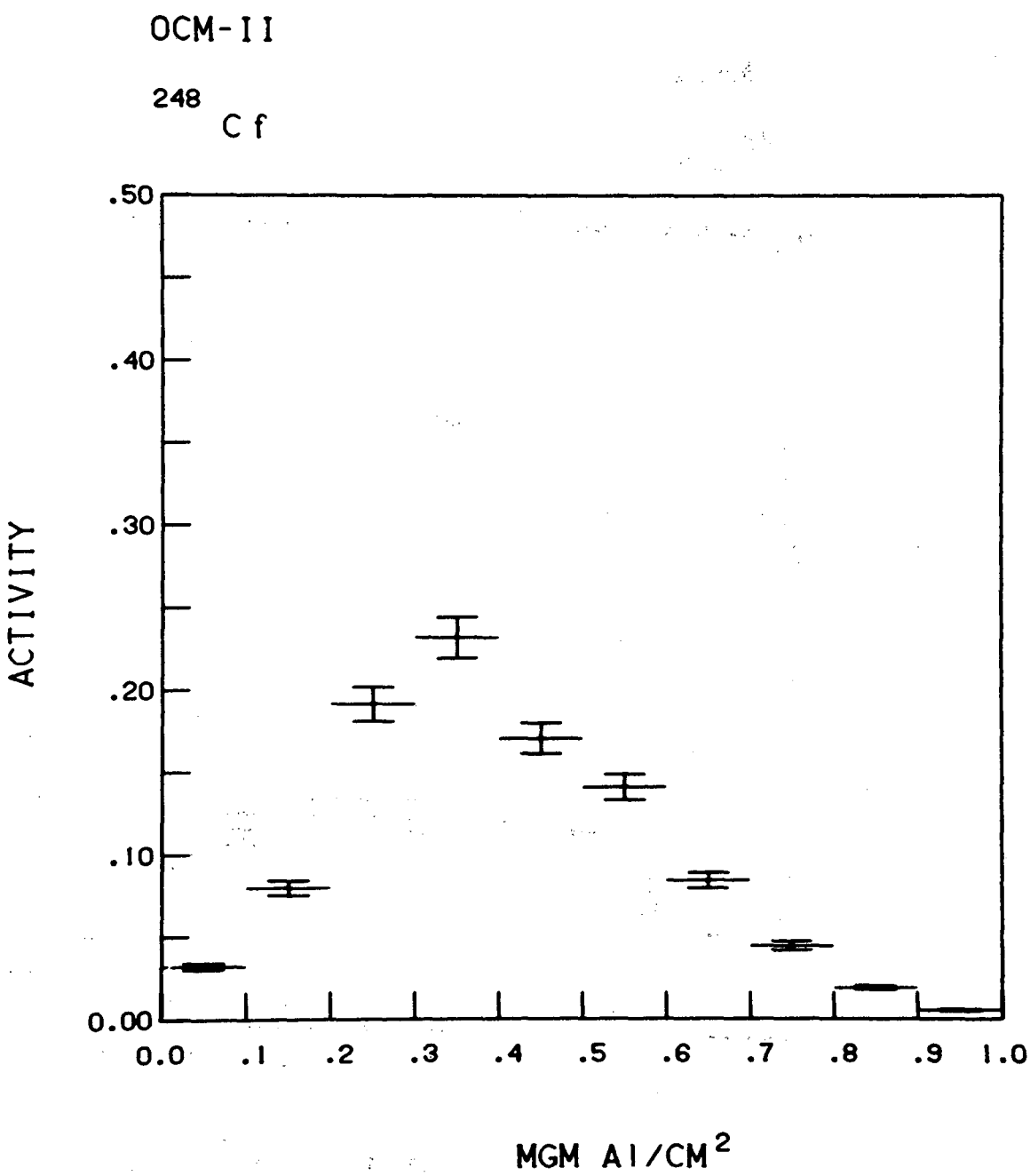
OCM-II
248 Cf
ACTIVITY
.50
.40
.30
.20
.10
0.00
0.0
.1
.2
.3
.4
.5
.6
.7
.8
.9
1.0
MGM Al/CM 2
XBL 823-9556

Fig. 15b

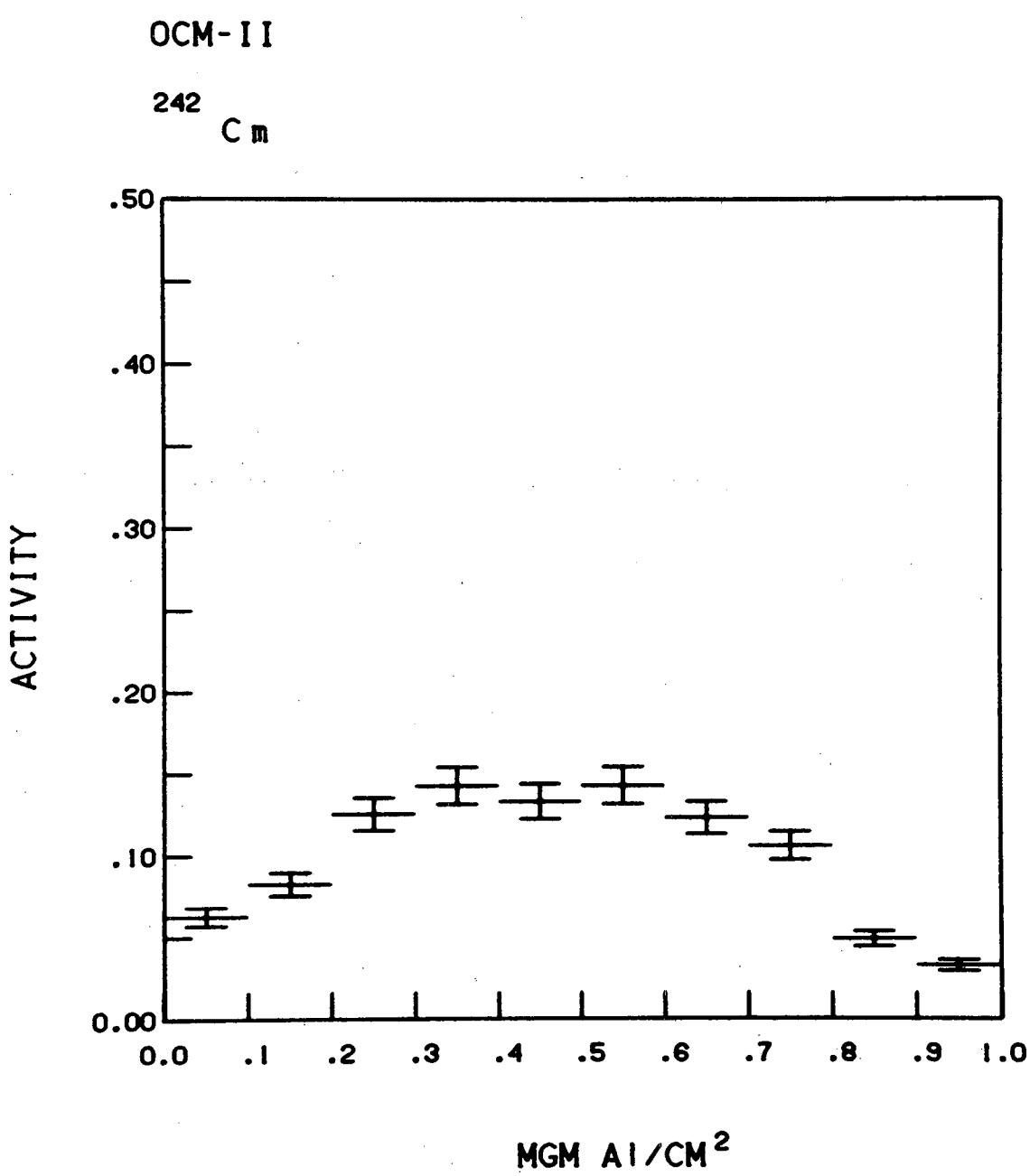
OCM-II
242 Cm
ACTIVITY
.50
.40
.30
.20
.10
0.00
0.0
.1
.2
.3
.4
.5
.6
.7
.8
.9
1.0
MGM Al/CM2
XBL 823-9573

Fig. 16a

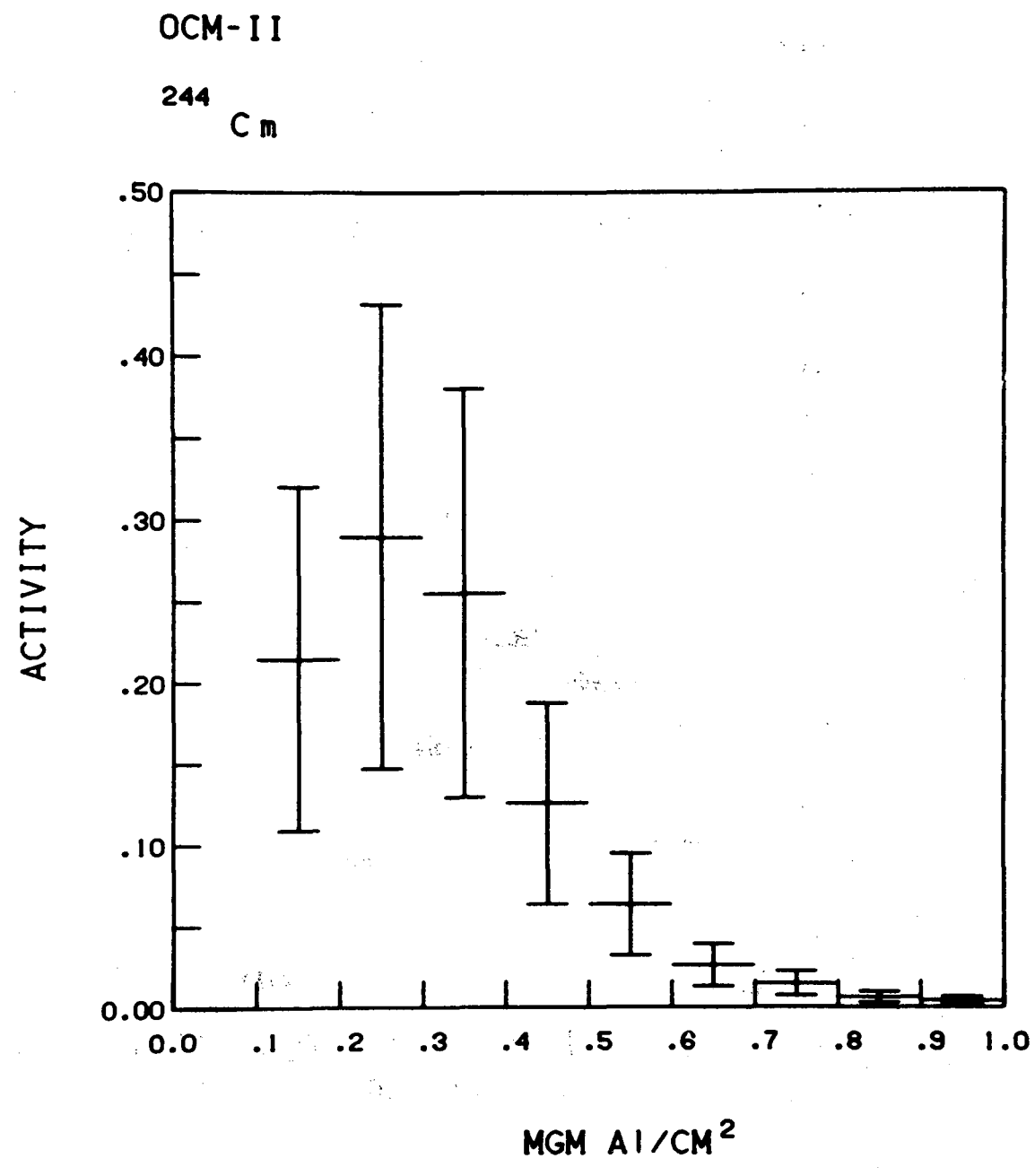
OCM-II
244 Cm
ACTIVITY
.50
.40
.30
.20
.10
0.00
0.0
.1
.2
.3
.4
.5
.6
.7
.8
.9
1.0
MGM Al/CM2
XBL 823-9571

Fig. 16b

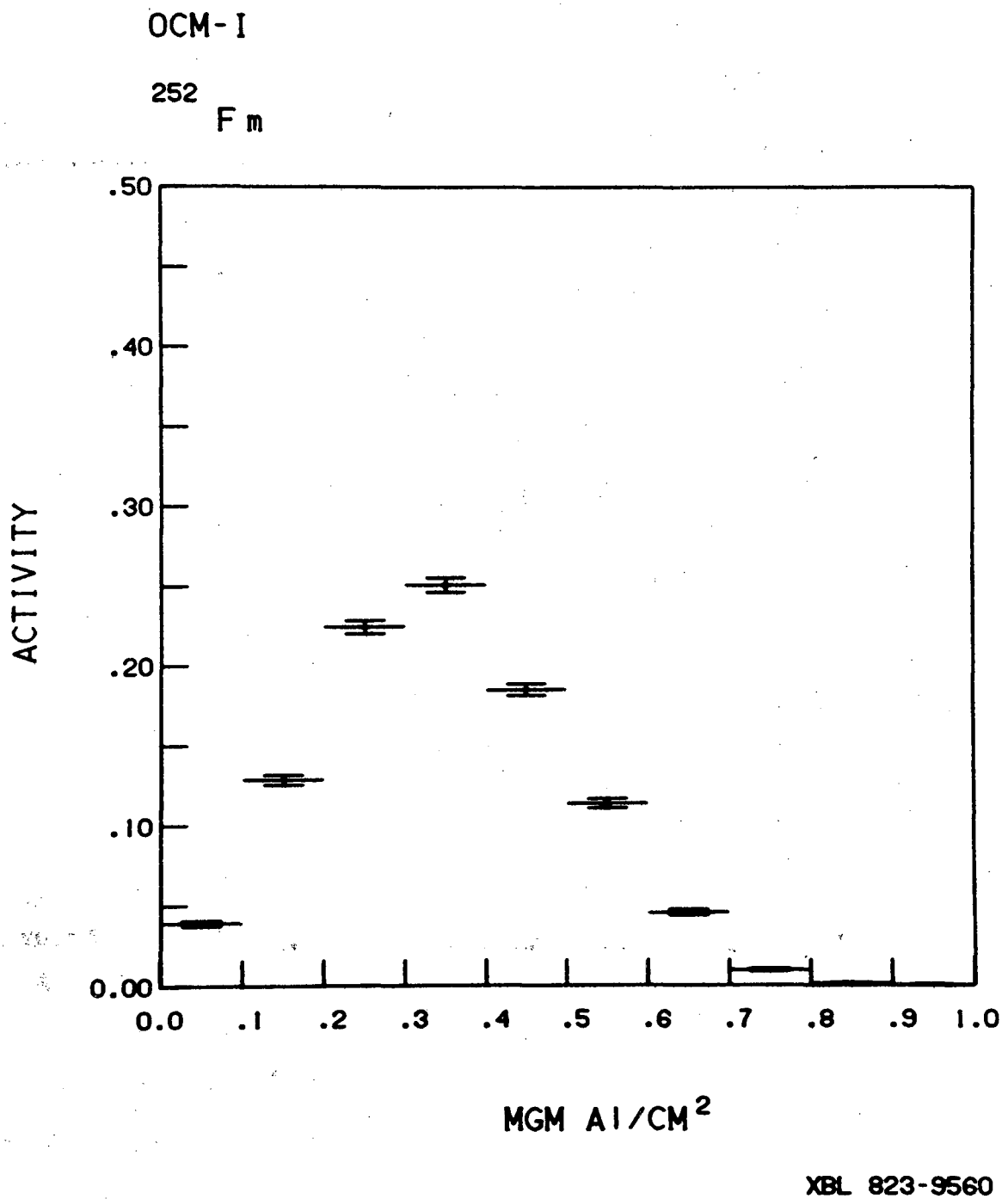
OCM-I
252 Fm
ACTIVITY
.50
.40
.30
.20
.10
0.00
0.0
.1
.2
.3
.4
.5
.6
.7
.8
.9
1.0
MGM Al/CM2
XBL 823-9560

Fig. 17

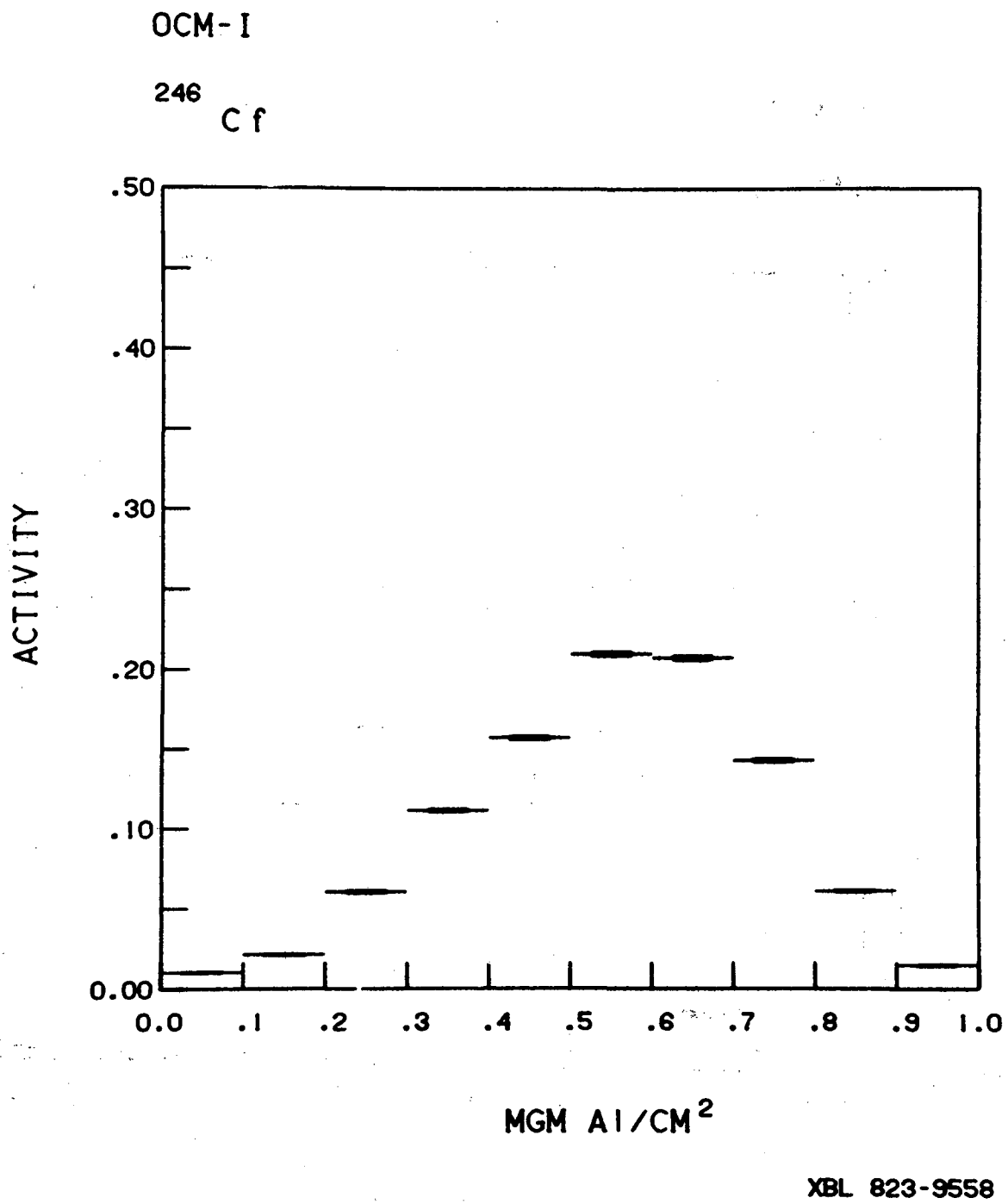
OCM-I
246 Cf
.50
.40
.30
.20
.10
0.00
ACTIVITY
0.0
.1
.2
.3
.4
.5
.6
.7
.8
.9
1.0
MGM Al/CM 2
XBL 823-9558

Fig. 18a

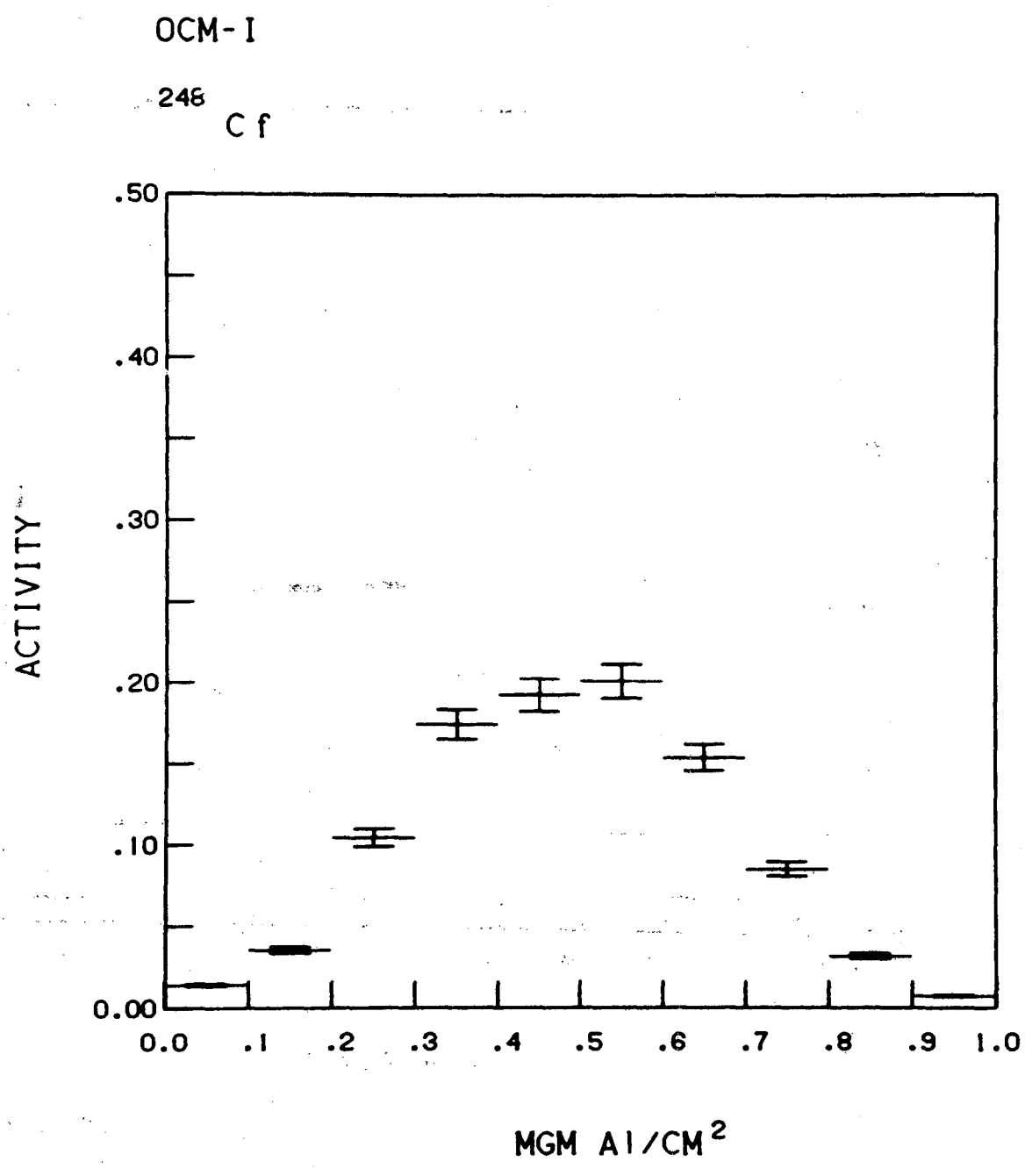
OCM-I
248
Cf
.50
.40
.30
.20
.10
0.00
ACTIVITY
0.0
.1
.2
.3
.4
.5
.6
.7
.8
.9
1.0
MGM Al/CM 2
XBL 823-9559

Fig. 18b

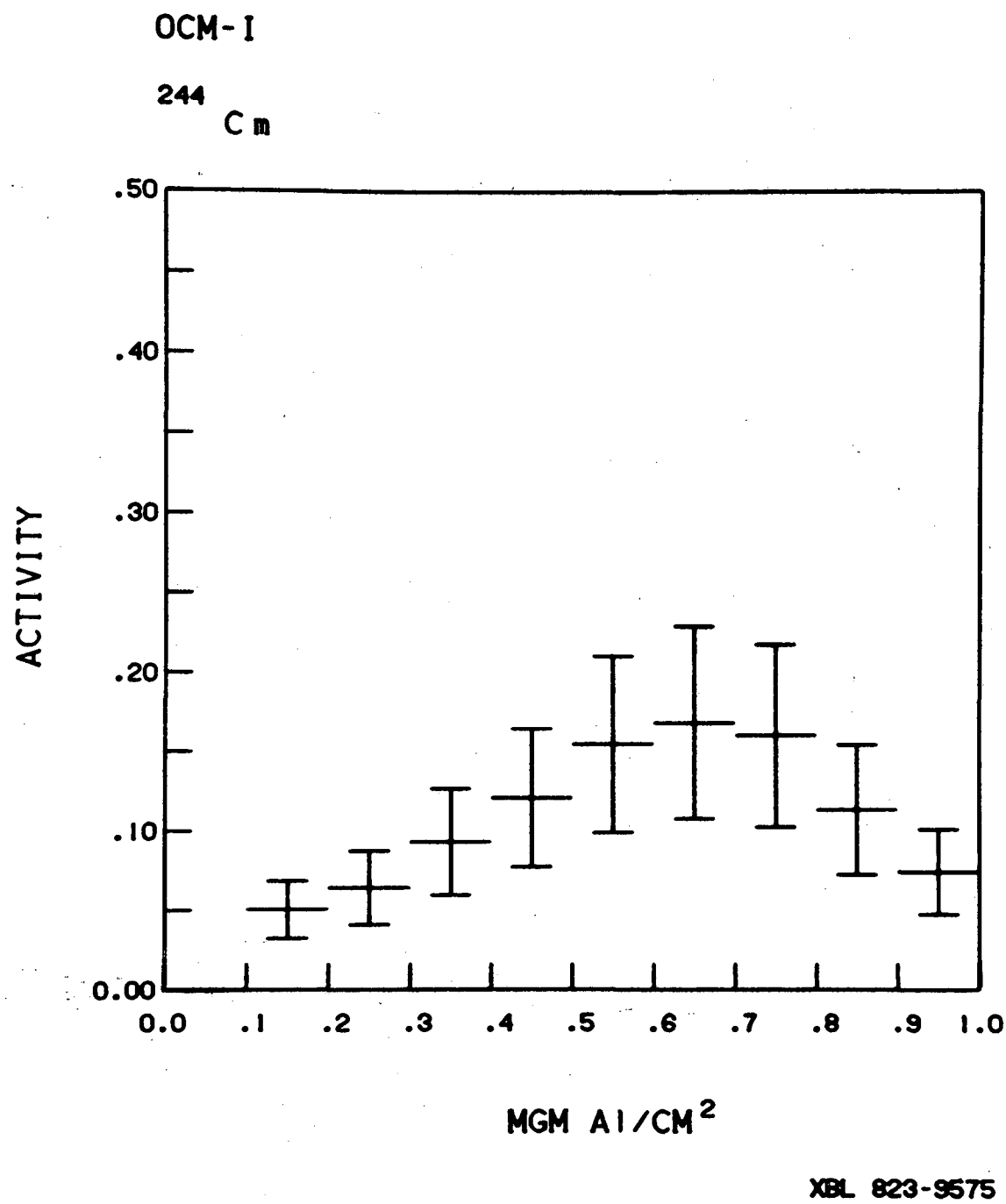
OCM-I
244 Cm
.50
.40
.30
.20
.10
0.00
ACTIVITY
0.0
.1
.2
.3
.4
.5
.6
.7
.8
.9
1.0
MGM Al/CM 2
XBL 823-9575

Fig. 19a

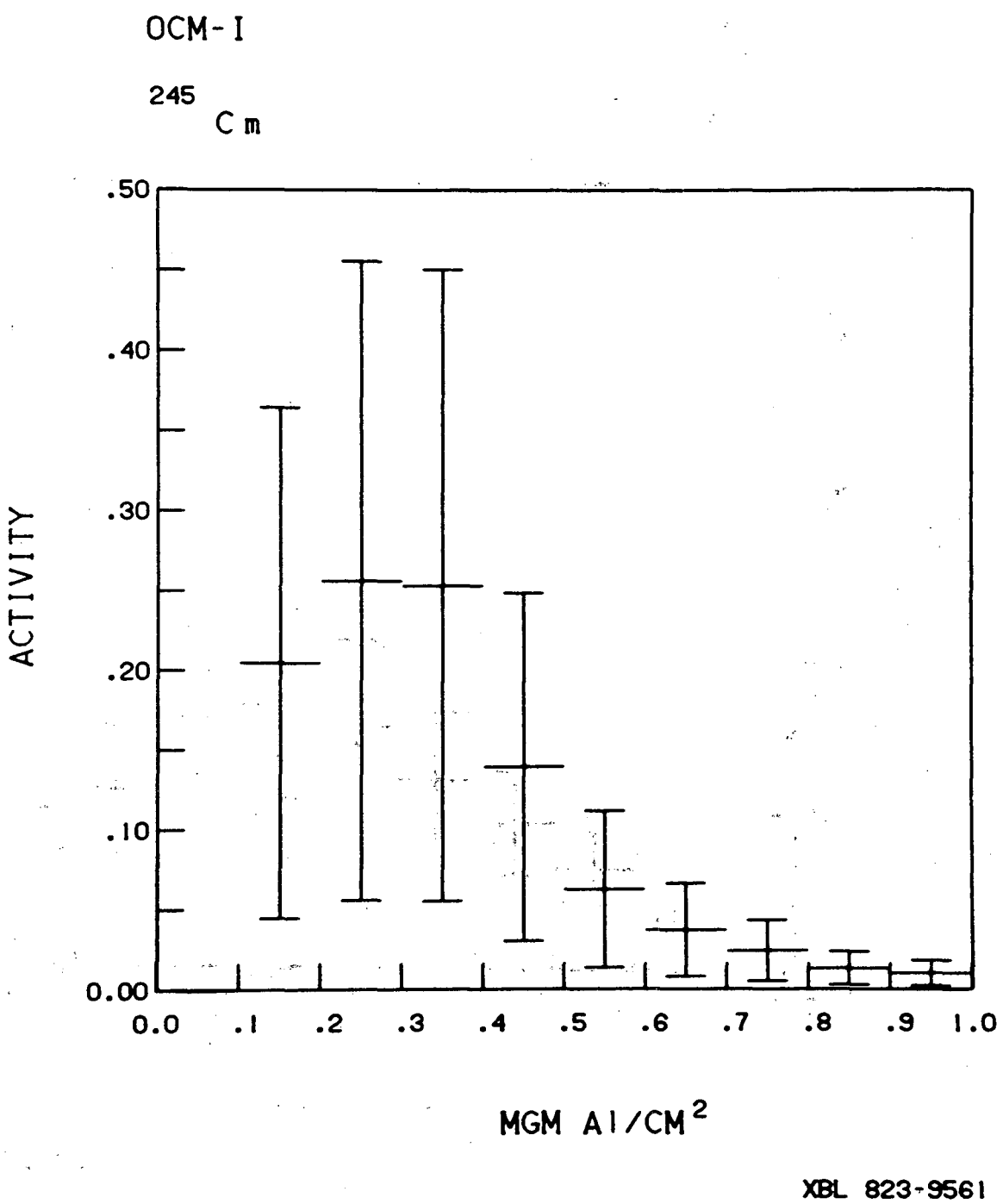
OCM-I
245
Cm
ACTIVITY
.50
.40
.30
.20
.10
0.00
0.0
.1
.2
.3
.4
.5
.6
.7
.8
.9
1.0
MGM Al/CM 2
XBL 823-9561

Fig. 19b

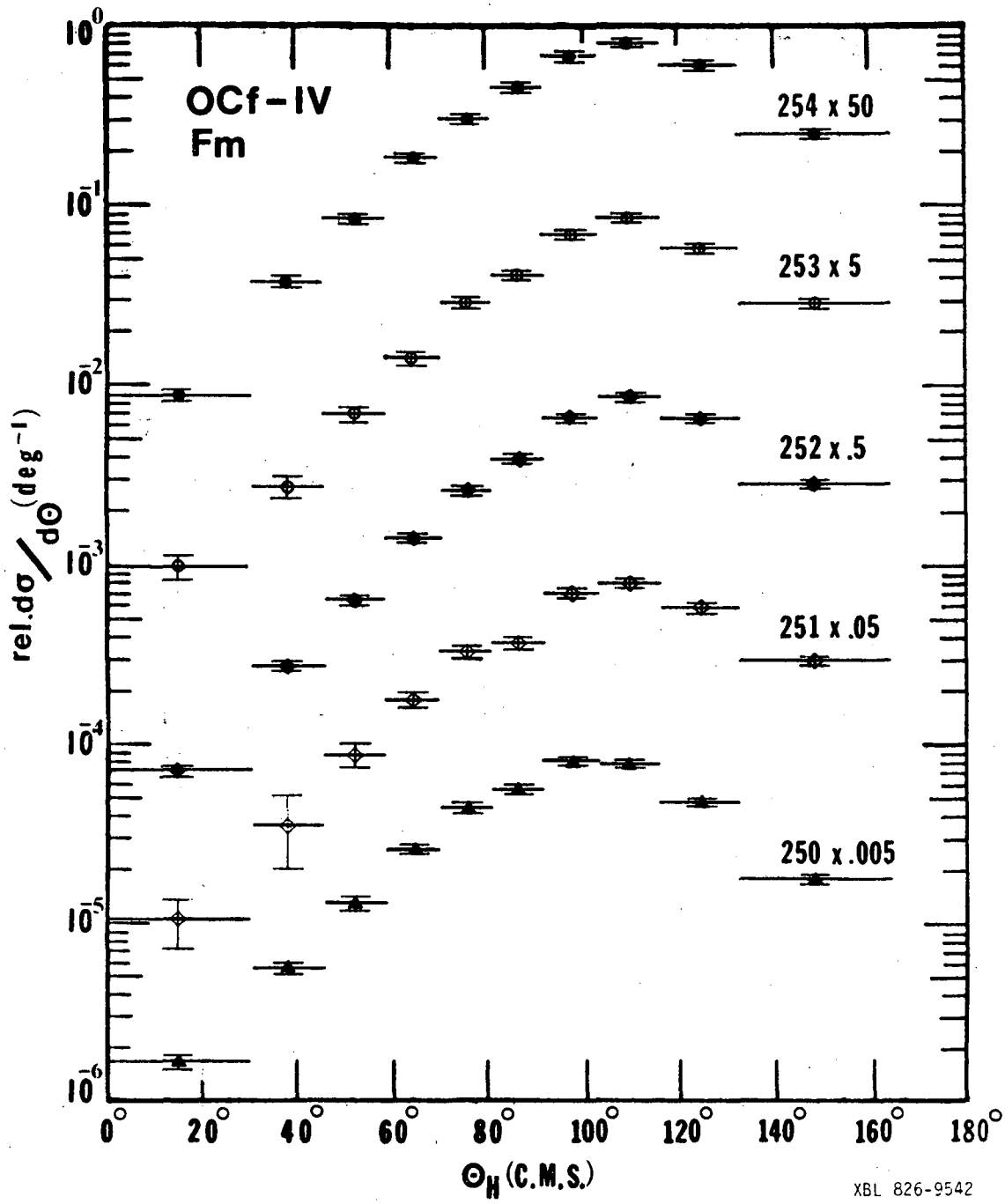
OCf-IV
Fm
254 x 50
253 x 5
252 x .5
251 x .05
250 x .005
rel.dσ/dΘ (deg⁻¹)
Θ_H (C.M.S.)
XBL 826-9542

Fig. 20

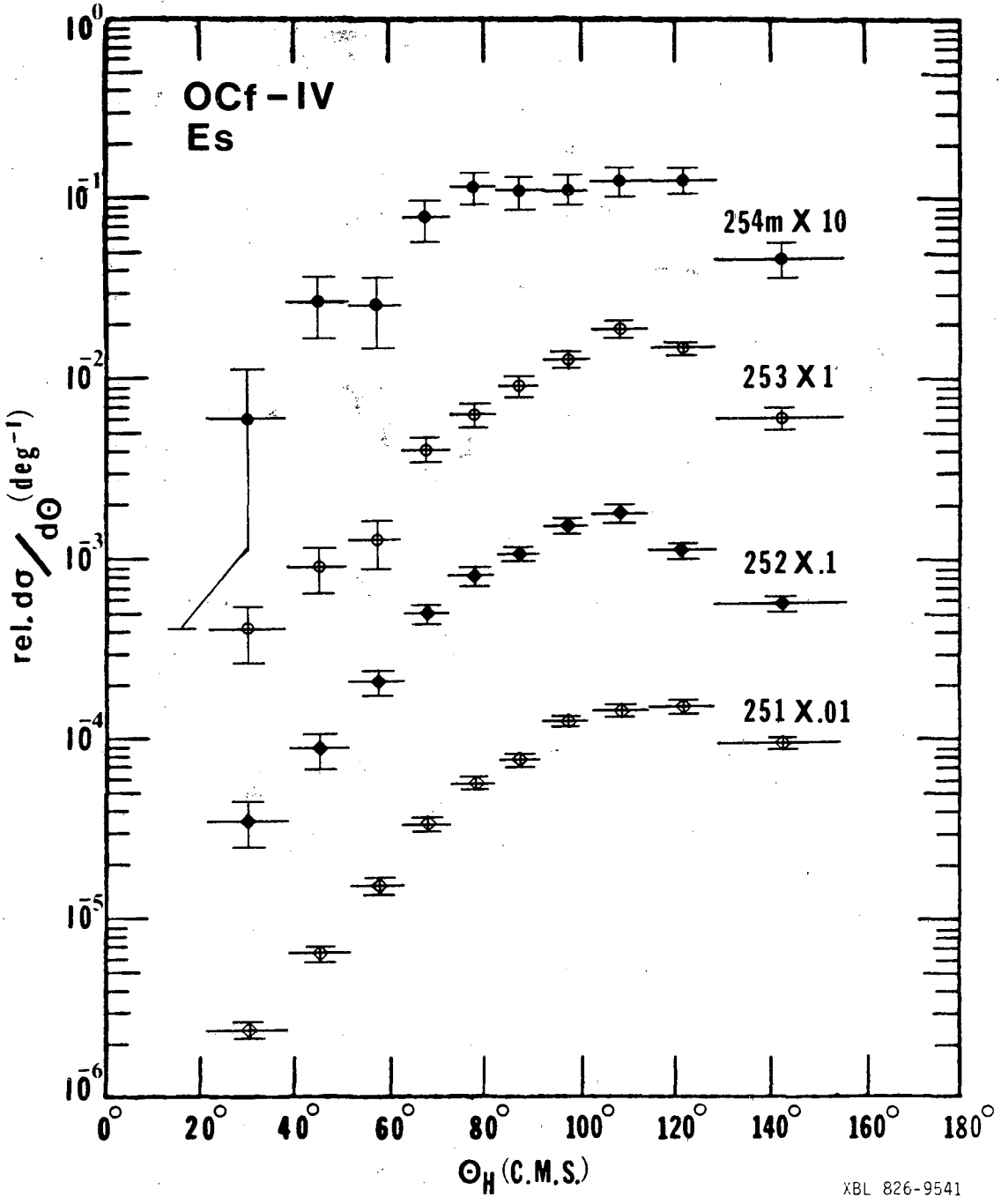
OCf - IV
Es
254m X 10
253 X 1
252 X .1
251 X .01
rel. dσ/dΘ (deg⁻¹)
Θ_H (C.M.S.)
XBL 826-9541

Fig. 21

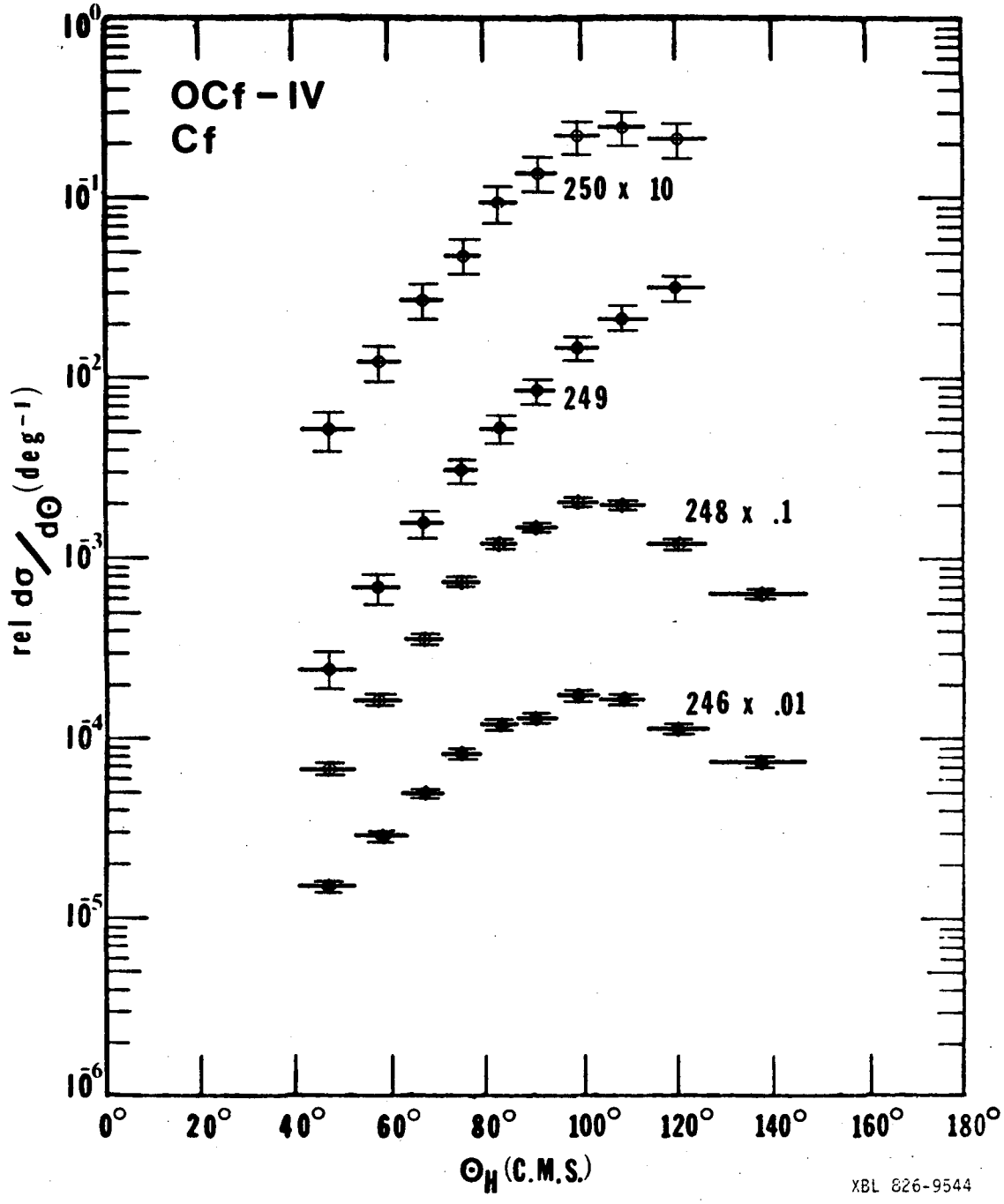
OCf - IV
Cf
250 x 10
249
248 x .1
246 x .01
rel dσ/dΘ (deg⁻¹)
Θ_H (C.M.S.)
XBL 826-9544

Fig. 22

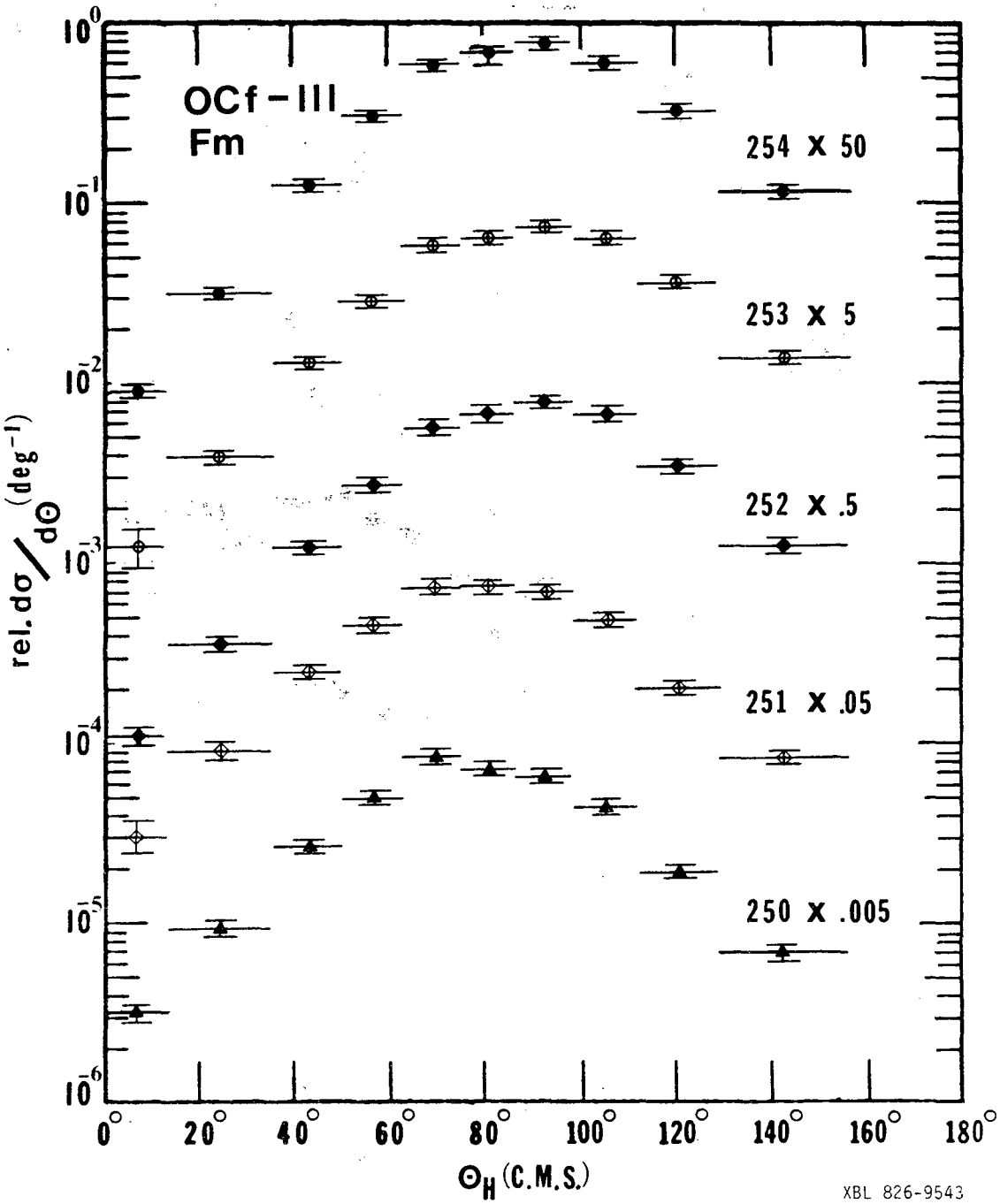
OCf-III
Fm
254 X 50
253 X 5
252 X .5
251 X .05
250 X .005
rel. dσ/dΘ (deg⁻¹)
Θ_H (C.M.S.)
XBL 826-9543

Fig. 23

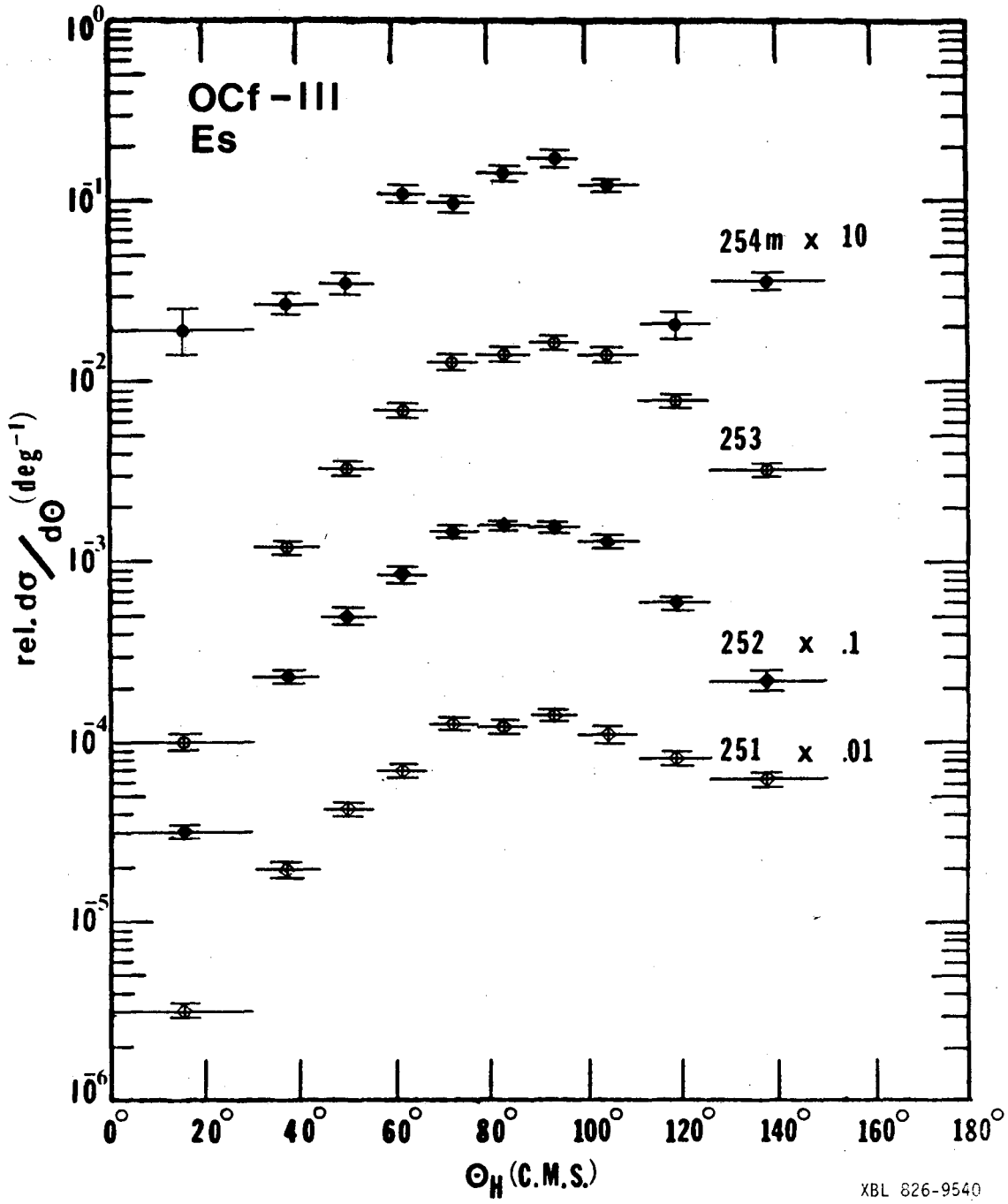
OCf - III
Es
254m x 10
253
252 x .1
251 x .01
rel. dσ/dΘ (deg⁻¹)
Θ_H (C.M.S.)
XBL 826-9540

Fig. 24

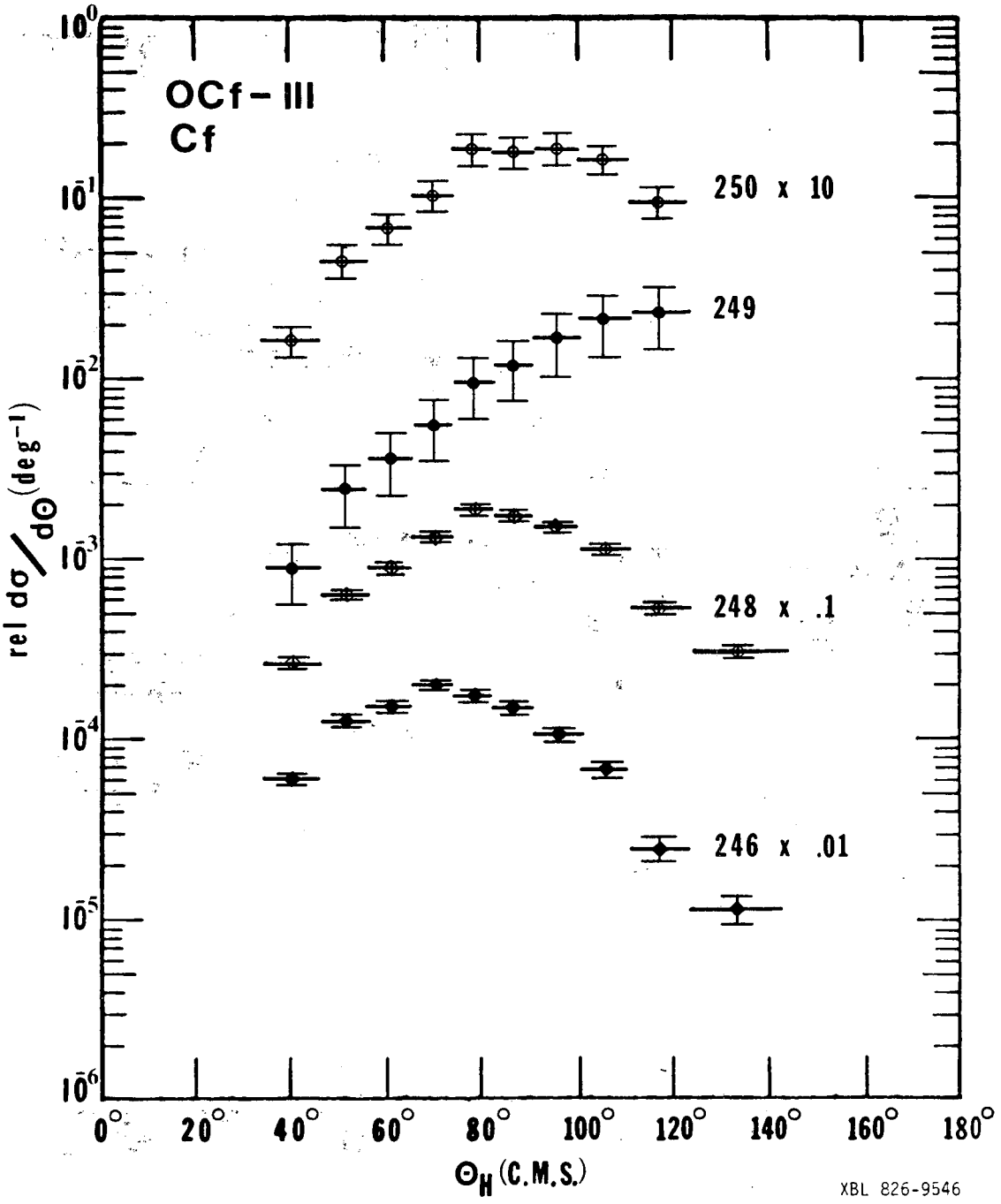
OCf-III
Cf
250 x 10
249
248 x .1
246 x .01
rel dσ/dΘ (deg⁻¹)
Θ_H (C.M.S.)
XBL 826-9546

Fig. 25

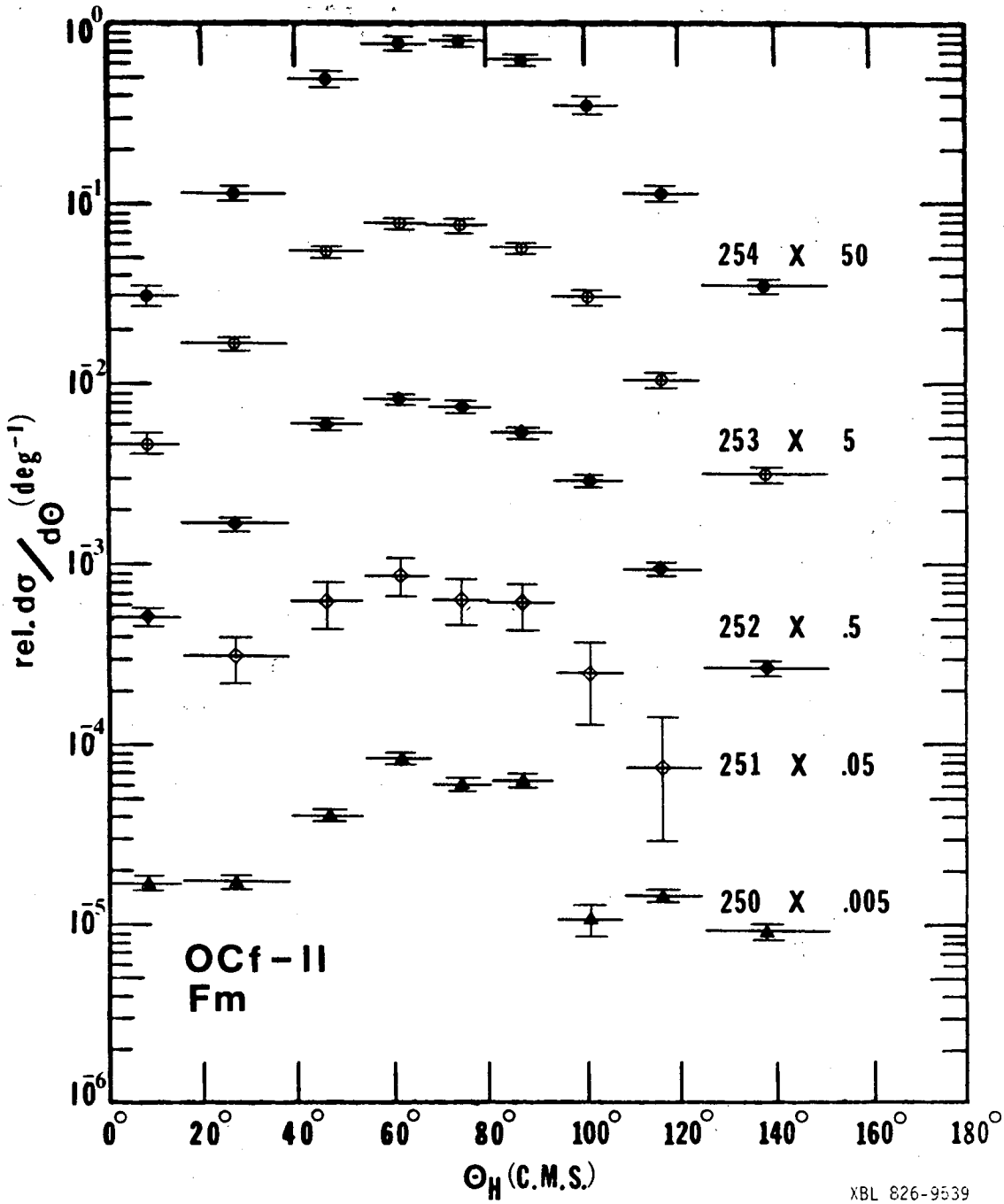
rel. dσ/dΘ (deg⁻¹)
10⁰
10⁻¹
10⁻²
10⁻³
10⁻⁴
10⁻⁵
10⁻⁶
254 X 50
253 X 5
252 X .5
251 X .05
250 X .005
OCf-II
Fm
0°
20°
40°
60°
80°
100°
120°
140°
160°
180°
Θ_H (C.M.S.)
XBL 826-9539

Fig. 26

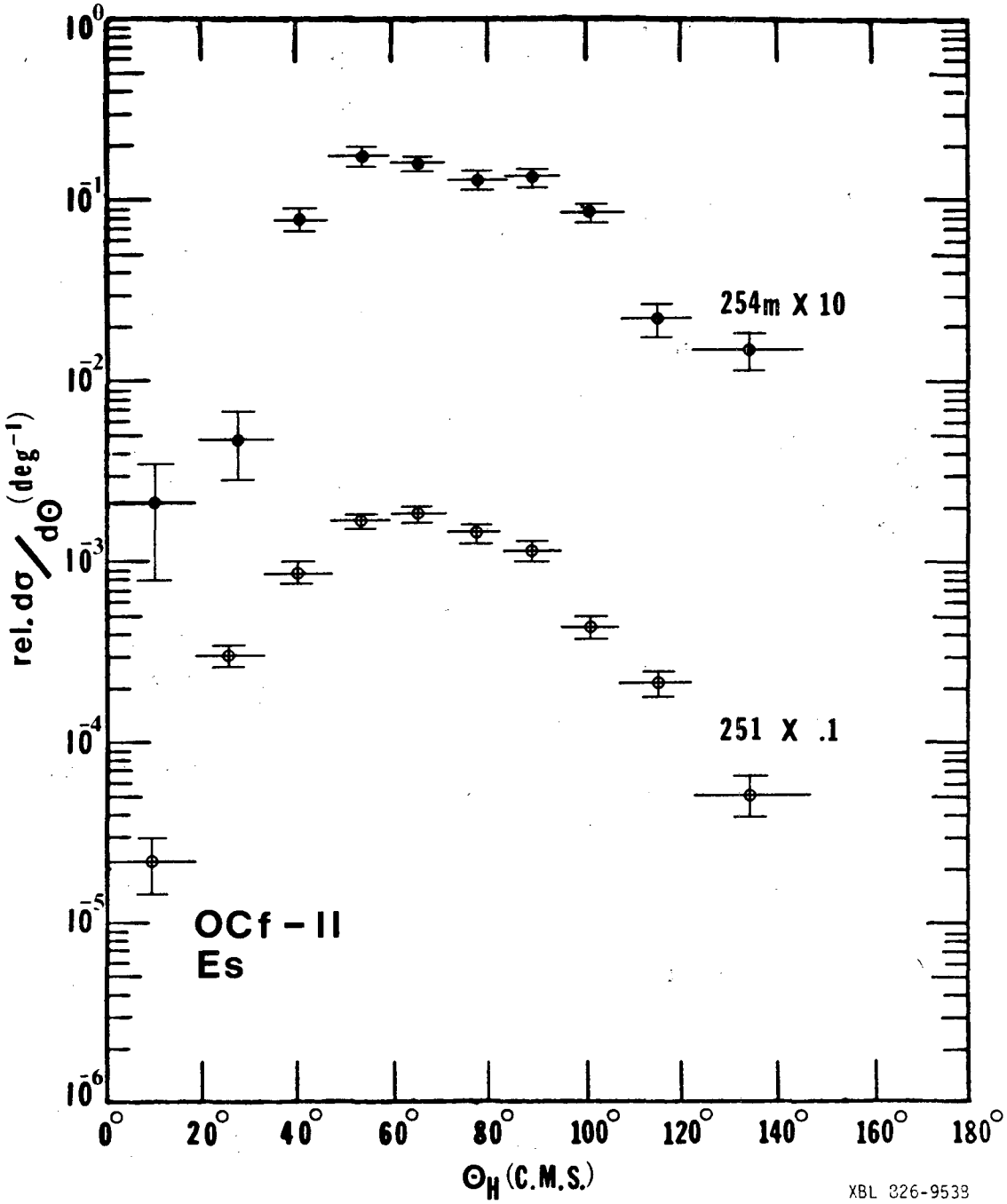

Fig. 27

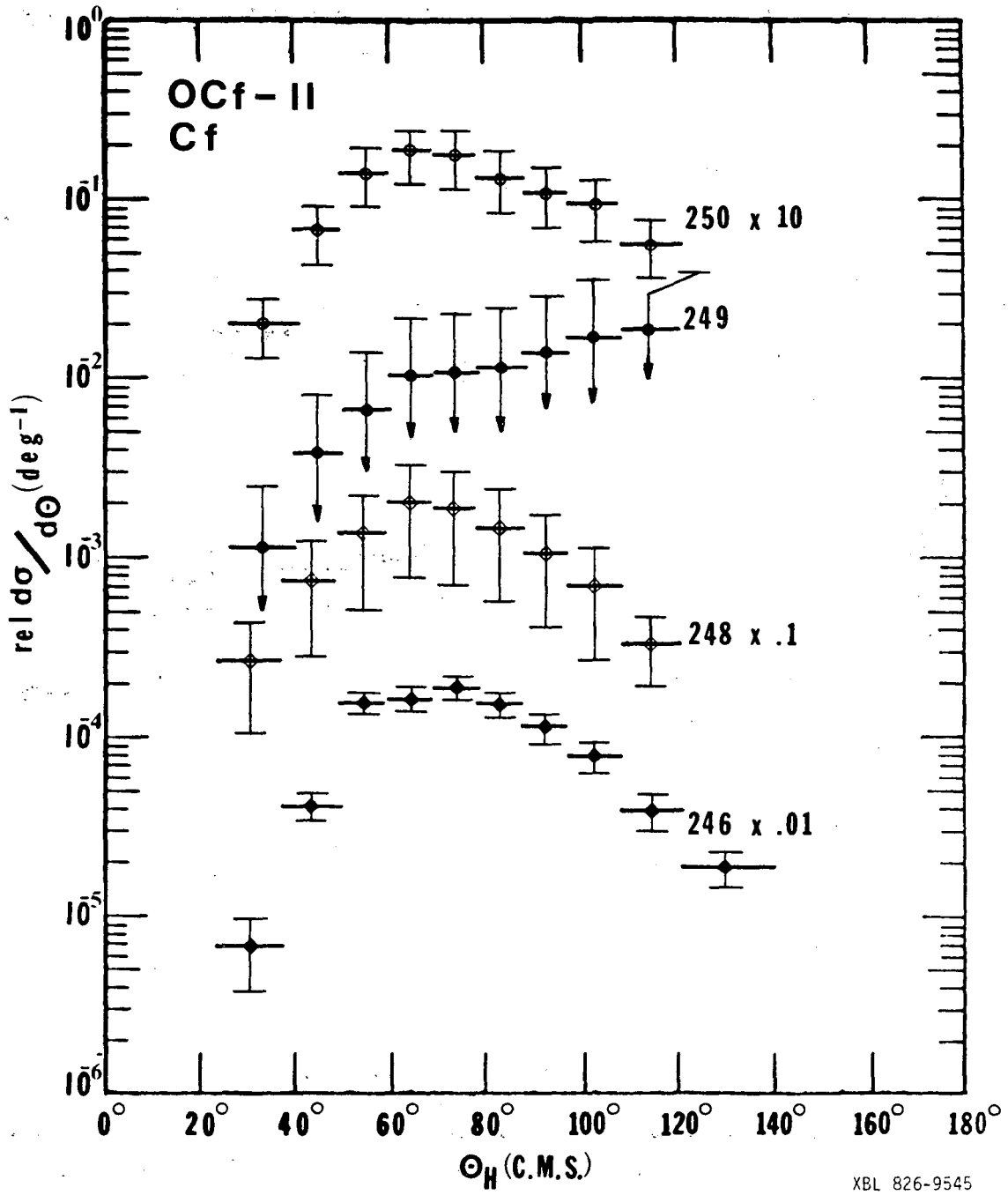
OCf - II
Cf
250 x 10
249
248 x .1
246 x .01
rel dσ/dΘ (deg⁻¹)
Θ_H (C.M.S.)
XBL 826-9545

Fig. 28

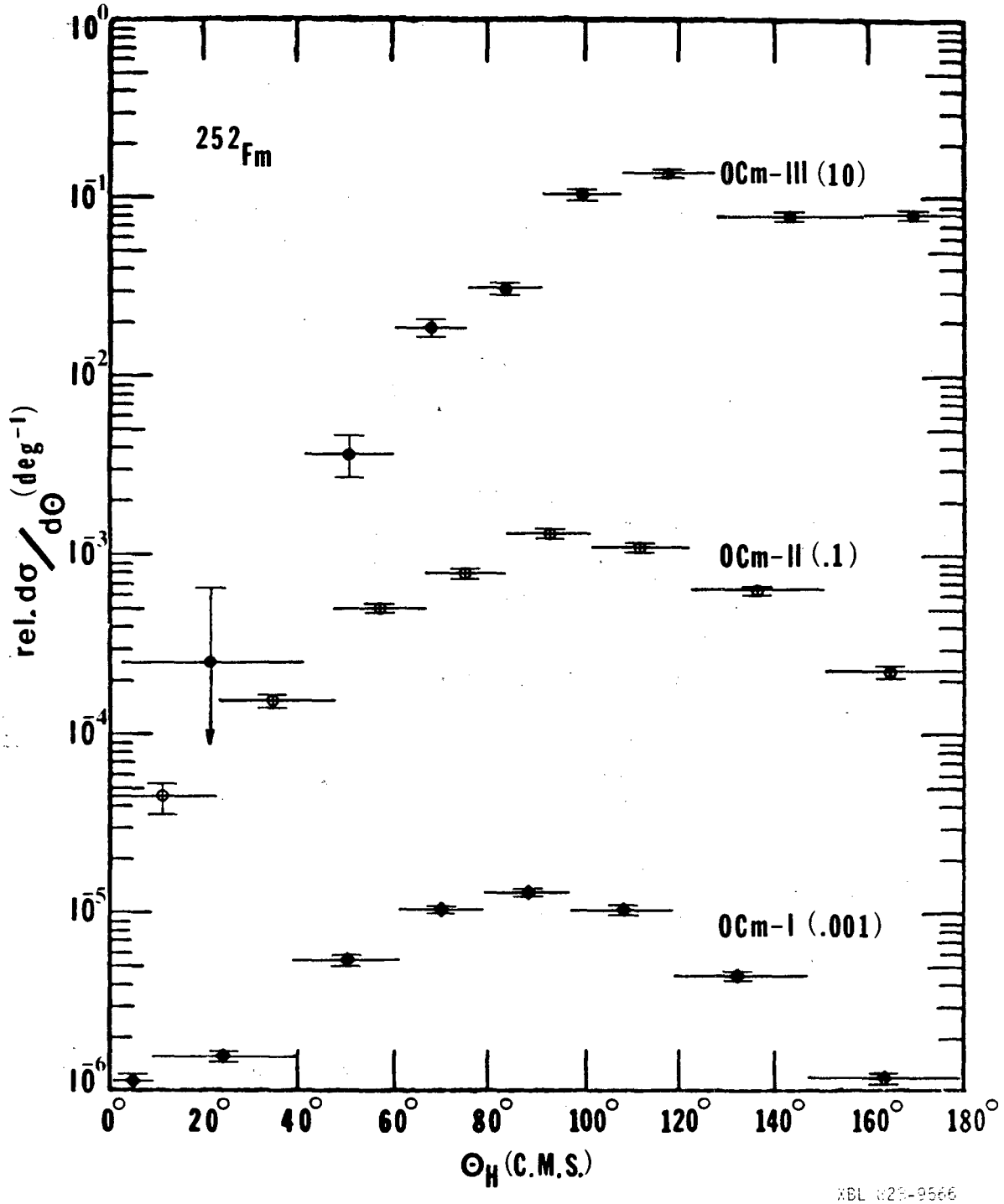
10^0
10^{-1}
10^{-2}
10^{-3}
10^{-4}
10^{-5}
10^{-6}
rel. $d\sigma/d\Theta$ (deg^{-1})
^{252}Fm
OCm-III (10)
OCm-II (.1)
OCm-I (.001)
0°
20°
40°
60°
80°
100°
120°
140°
160°
180°
Θ_H (C.M.S.)
XBL 828-9566

Fig. 29

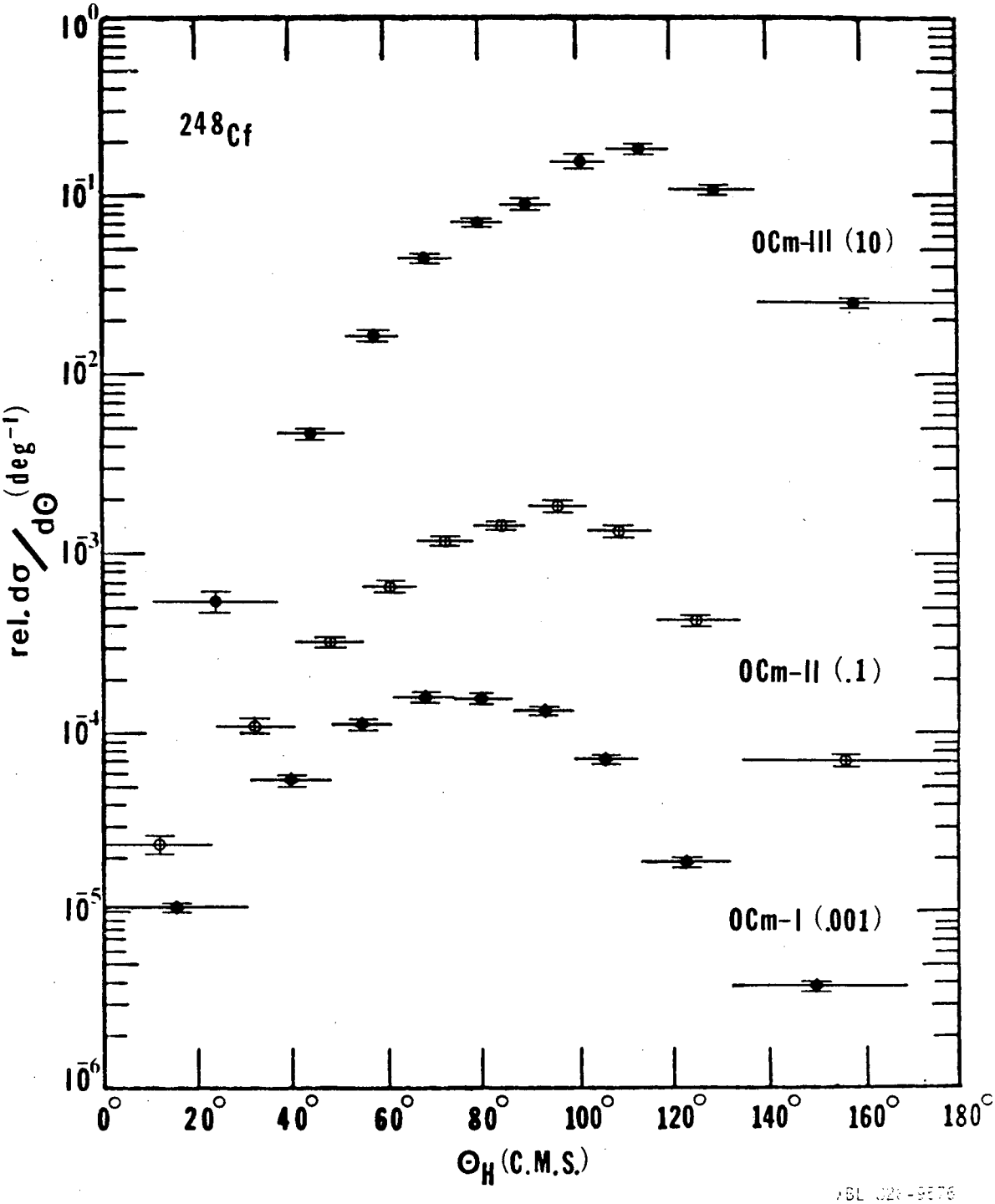
248Cf
OCm-III (10)
OCm-II (.1)
OCm-I (.001)
rel. dσ/dΘ (deg⁻¹)
ΘH (C.M.S.)
10⁰
10⁻¹
10⁻²
10⁻³
10⁻⁴
10⁻⁵
10⁻⁶
0°
20°
40°
60°
80°
100°
120°
140°
160°
180°

Fig. 30

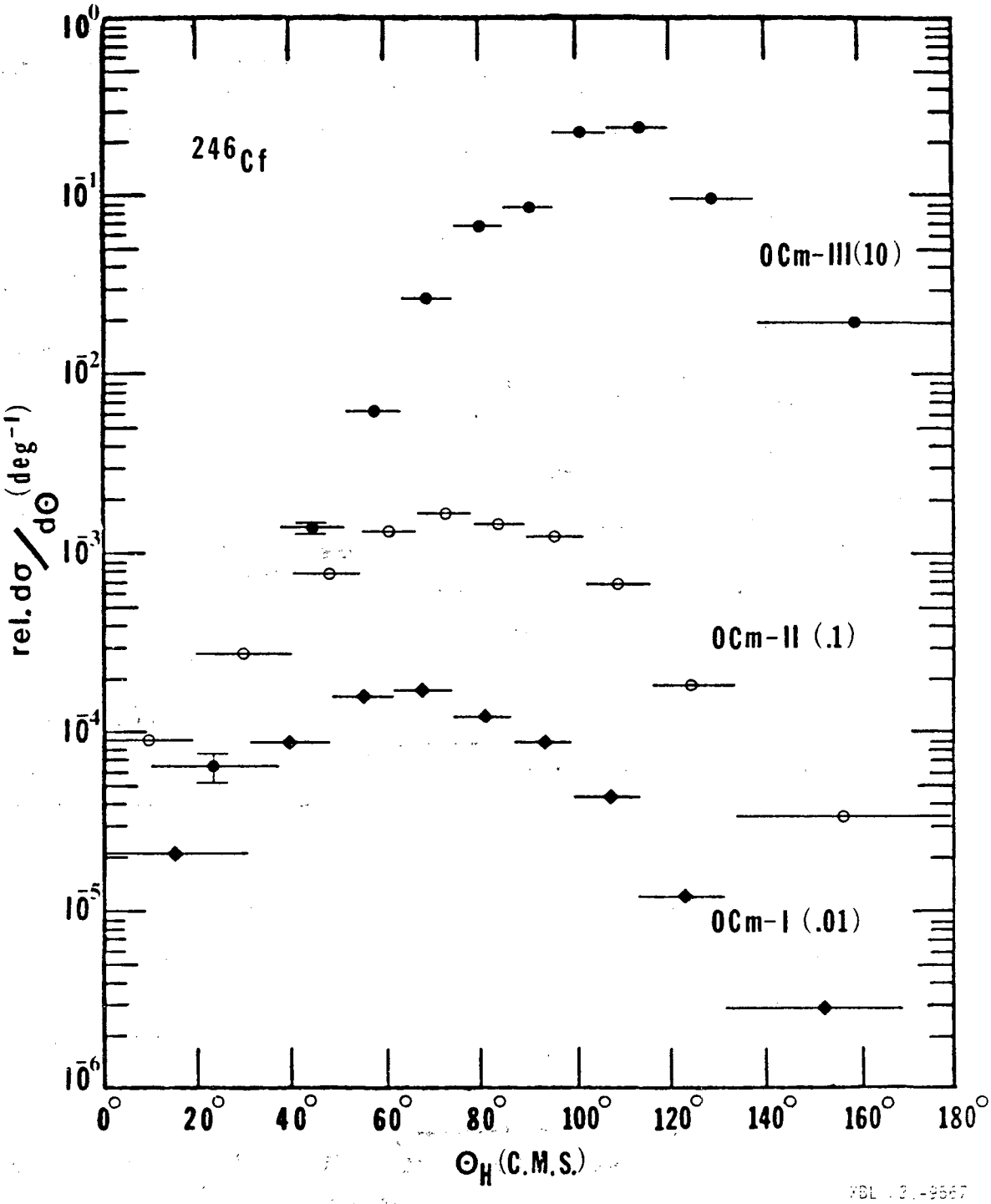
246Cf
OCm-III(10)
OCm-II (.1)
OCm-I (.01)
rel. dσ/dΘ (deg⁻¹)
ΘH (C.M.S.)
0°
20°
40°
60°
80°
100°
120°
140°
160°
180°

Fig. 31

This report was done with support from the Department of Energy. Any conclusions or opinions expressed in this report represent solely those of the author(s) and not necessarily those of The Regents of the University of California, the Lawrence Berkeley Laboratory or the Department of Energy.

Reference to a company or product name does not imply approval or recommendation of the product by the University of California or the U.S. Department of Energy to the exclusion of others that may be suitable.

TECHNICAL INFORMATION DEPARTMENT
LAWRENCE BERKELEY LABORATORY
UNIVERSITY OF CALIFORNIA
BERKELEY, CALIFORNIA 94720